Doctoral Dissertation (Shinshu university)

Study on the phase change fibrous membranes designed for personal thermal management

パーソナル熱管理に向けた相転移繊維状膜に関する研究

September 2023

WU, JIAJIA

Abstract

Personal thermal management (PTM) is an energy-saving approach for mitigating the growing energy crisis and global warming. Form-stable phase change materials (FSPCMs) are potential candidates for PTM application, owing to the reversible stimuli-responsive, no energy consumption and precise thermal regulation properties. Nowadays, most of the FSPCMs are fabricated as rigid and dense substrates, which can't be conformed to the curved surface of human body, and prevent air penetration, causing worse wearing experience. Therefore, flexible and breathable structure are desirable and attractive to realize a trade-off between thermal storage capability and wearing comfort.

It is well known that electrospinning is a versatile technique for fabricating ultrafine fibers which exhibit remarkable flexibility and possess high adaptability to the curvature change of the skin, due to its high aspect ratio. The resultant membranes feature with porous structure for air permeability, which is also favorable for wearing comfort. Therefore, phase change fibers (PCFs) by integrating PCMs into ultrafine polymer frameworks through electrospinning method behave multi-properties of superior flexibility, breathability, shape-stability, tailorability and phase change ability. Therefore, our work employed electrospinning technology to prepare flexible composite phase change membranes, including uniaxial electrospinning (chapter 2) and coaxial electrospinning (chapter 3 and 4).

In chapter 2, considering most electrospinning process were based on poisonous solvents, and pose a potential risk to the human body and natural environment, we used green electrospinning technology without toxic solvent and combined surface-crosslinking to obtain the light-weight, flexible and breathable phase change membranes. Biocompatible and biodegradable polymer PVA and PEG were employed as supporting matrix and functional component. Subsequently, glutaraldehyde vapor was grafted or crosslinked on the surface of ultrafine fibers to block hydrophilic groups. The mass ratio of PEG can reach to 55 wt% and realized an optimal melting/freezing enthalpy of 60.1/59.1 J/g, which is comparable to these of toxic solvent-based

electrospun membranes. In addition, addressed in the intrinsic low thermal conductivity of PCMs, high conductive material (CNTs) was dopped in spinning solution to promote the heat transfer rate. The thermal conductivity has been improved by 40.4% than the blank one. Besides, the phase change fibrous membranes possessed excellent tensile elongation of 262%, overcoming the intrinsic brittleness of traditional PCMs, and exhibited remarkable shape tailorability and foldability. Considering the favorable flexibility, breathability and reasonable phase change enthalpy, the resultant phase change fibrous membranes exhibit great potential for further application such as personal thermal management textile and thermal-regulated electric system.

Compared to uniaxial electrospinning technique, coaxial electrospinning is more competitive to fabricate form-stable phase change fibers, because PCMs are effectively encapsulated by core-shell structure. Since the single-mode thermal regulation based on PCMs hardly can cope with the multi-functional demand for longtime and large temperature range management, multi-mode and more precise thermal regulation textiles are more demandable. Therefore, **in chapter 3 and 4**, we integrated dual-driven heating function (solar/electric heating) with phase change property to realize the photo/electro-thermal conversion and thermal energy storage for all day, on demand and personalized thermal management.

In chapter 3, we report a fibrous membrane-based textile that was developed by designing the hierarchical core-sheath fiber structure for tri-mode thermal management. Especially, coaxial electrospinning allows an effective encapsulation of PCMs, with high heat enthalpy density (106.9 J/g), enables the membrane to buffer drastic temperature changes in the clothing microclimate. The favorable photothermal conversion performance renders the membrane with the high saturated temperature of 70.5 °C (1 sun), benefiting from the synergistic effect of multiple light-harvesters. Moreover, conductive coating endows the composite membrane with an admirable electrothermal conversion performance, reaching a saturated temperature of 73.8 °C (4.2 V). The flexible fibrous membranes with the integrated performance of reversible phase change, multi-source driven heating and energy storage present great advantages for all-day, energy-saving, and wearable individual thermal management applications.

In order to maintain the porous structure of the fiber film with higher controllability for better air permeability, we improved the functional modification method. **In chapter 4**, we applied in-situ reduction method to achieve the conformally deposition of functional materials around the individual fibers, thereby the original porous structure was better preserved.

In chapter 4, a breathable and thermoregulating fibrous membrane integrated with photo/electrothermal conversion and energy storage/release performance, was successfully prepared through coaxial electrospinning and PDA-assisted silver deposition technique. We have delicately constructed a hierarchically ordered coaxial fiber structure that assembled functional components together for a versatile platform. Interestingly, the intermediate PDA layer not only favors homogeneous loading of Ag nanoparticles (AgNPs), but also facilitates the interfacial bonding of the adjacent metal layer and the phase change fiber substrate for a seamlessly integrated system with improved structural stability and robust electrical performance. As a result, benefiting from the hierarchical coaxial structure of individual fibers and the overall well-preserved porous structure, we have fabricated an highly integrated, breathable, metalized phase change fibrous membrane with admirable heat enthalpy of 101.1 J/g, decent solar heating capability (up to 63.2 °C at 100 mW/cm^2), and low voltage-driven Joule heating performance (up to 76.8 °C at 3.5 V), which exhibited a broad application prospect in next-generation wearable personal thermal management.

CONTENTS

Chapter 1
General introduction

Chapter 1: General introduction

1.1 The introduction of phase change materials (PCMs)

PCMs are capable of absorbing and releasing thermal energy during phase transitions. When PCMs undergo the process of melting and freezing, their temperature remains constant. As the environment temperature reach the melting point of the PCM, it changes from solid to liquid and simultaneously absorb heat from the surrounding. Conversely, it releases heat when the environmental temperature goes down to the freezing point. [1-2] Therefore, PCMs can play a heating or cooling effect in a certain time, and it always be used in thermal energy storage (TES) field, because of its high laten heat density and reversible energy storage and release capability. The TES technology based on PCMs showed a promising prospect in solving the mismatch between the thermal energy supply and demand in terms of time, space and intensity, and can maximize the energy utilization efficiency [3,4].

Based on chemical composition, PCMs are mainly divided into inorganic and organic materials [5]. The inorganic PCMs, such as salt hydrate [6-8], possess a high volumetric energy storage density, flame retardancy and relatively high thermal conductivity, but it suffers from the high supercooling and phase separation. The organic PCMs, such as paraffin wax (PW) [9,10] and polyethylene glycol (PEG) [11,12], have negligible supercooling but low thermal conductivity. For both inorganic and organic PCMs, the solid rigidity and liquid leakage are the universal problems restricting their application. Flexible and form-stable phase change materials (FFSPCMs) are designed to overcome the aforementioned issues. Currently, different preparation methods of FFSPCMs are developed and presented.

1.2 The preparation methods of FFSPCMs

It is necessary to get the trade-off between the thermal storage capability and the mechanical properties of the flexible and form-stable phase change materials according

to different applications, such as thermal management of advanced electronic device, personal thermal management and heat therapy. In regarding of this, enormous methods have been applied to fabricate flexible phase change materials. These methods can be divided into (1) hybrid confinement; (2) encapsulation; and (3) polymerization [5,13].

1.2.1 Hybrid confinement

1.2.1.1 Interfacial confinement

Interfacial or layer confinement method restrict the fluidity of melted PCM by the interaction between PCM molecules and the surface of nanomaterials, such as graphene oxide (GO) [14] and $Ti_3C_2T_x$ (MXene) [15] sheet, due to their large specific surface area and high functionalization degree. Interfacial confinement results from the strong hydrogen bonding and grafting of PCM molecular chains onto supportive materials, to keep the liquid PCM packed in the layer or pores of supportive skeleton. Liu et al. [16] filled PEG in the space between the stacked MXene flackes. The interlayer capillary effect and surface tension force within the composites restrict the leakage of liquid PCM during the solid-liquid phase process. In addition, thermal conductivity of the phase change composites was promoted and were endowed with excellent EMI shielding performance.

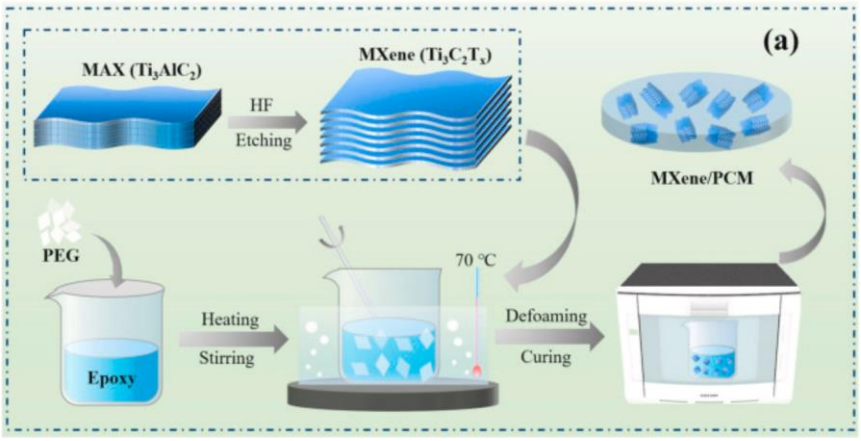

Fig. 1-1 The synthetic scheme for the PEG/Epoxy/$Ti_3C_2T_x$ composite PCMs. Reproduced with permission from ref 16. Copyright 2021, Elsevier.

1.2.1.2 Porous confinement

Porous materials have been widely used as the supporting skeletons to hold PCMs because of their high pore volume, large surface areas, and strong adsorption capability [17]. The impregnation of PCM adopts two methods: vacuum impregnation and solvent-assisted impregnation. Capillary action prevents leakage of PCM during phase transition. Beside the confinement effect on PCMs, additional properties can also be imparted to the composite PCMs, such as sunlight absorption, electrical and thermal conductivity, flame retardance etc., ascribed to the nature of employed matrix. So far, there are many methods to prepare porous scaffolds, such as ice-templated method, hydrothermal and chemical reduction, carbonization, chemical vapor deposition (CVD), chemical crosslinking, template method and so on. We summarized several porous matrices that have been employed to fabricate the form-stable phase change composites, such as carbon-based foams [18, 19], polymer sponges [20], and fibrous supporting materials [21, 22]. Due to the low density, high thermal/electrical conductivity, decent chemical and thermal stability, as well as compatible features, carbon-based scaffolds have been widely used as one of the optimal supporting matrices. Chen et al. [23] used CNT sponge as compatible supporting host, polyethylene glycol (PEG) as thermal regulating guest, and the form-stable composite PCMs was fabricated via a facile impregnation approach, it verified that the capillary action induced by the hierarchical pores can guarantee the stability of PCMs molecules. They also explored the interaction between pure PEG and CNT sponge, and induced that CNT sponge and PEG are just simple physical combination without any chemical interaction, because no new functional groups are evidently found in FTIR spectra. Yang et al. [24] utilized the flame-retardant polydopamine-aramid nanofiber (PANF) aerogel film as host, and take DES (deep eutectic solvent composed of ammonium chloride, ethylene glycol, and deionized water), a type of ionic liquid which is also noninflammable, as the phase change guest. The strong capillary confinement on DES hold them inside the pores space of the PANF aerogel films, thereby no DES leaking, and the resultant composites exhibited high phase transition enthalpy and non-inflammability

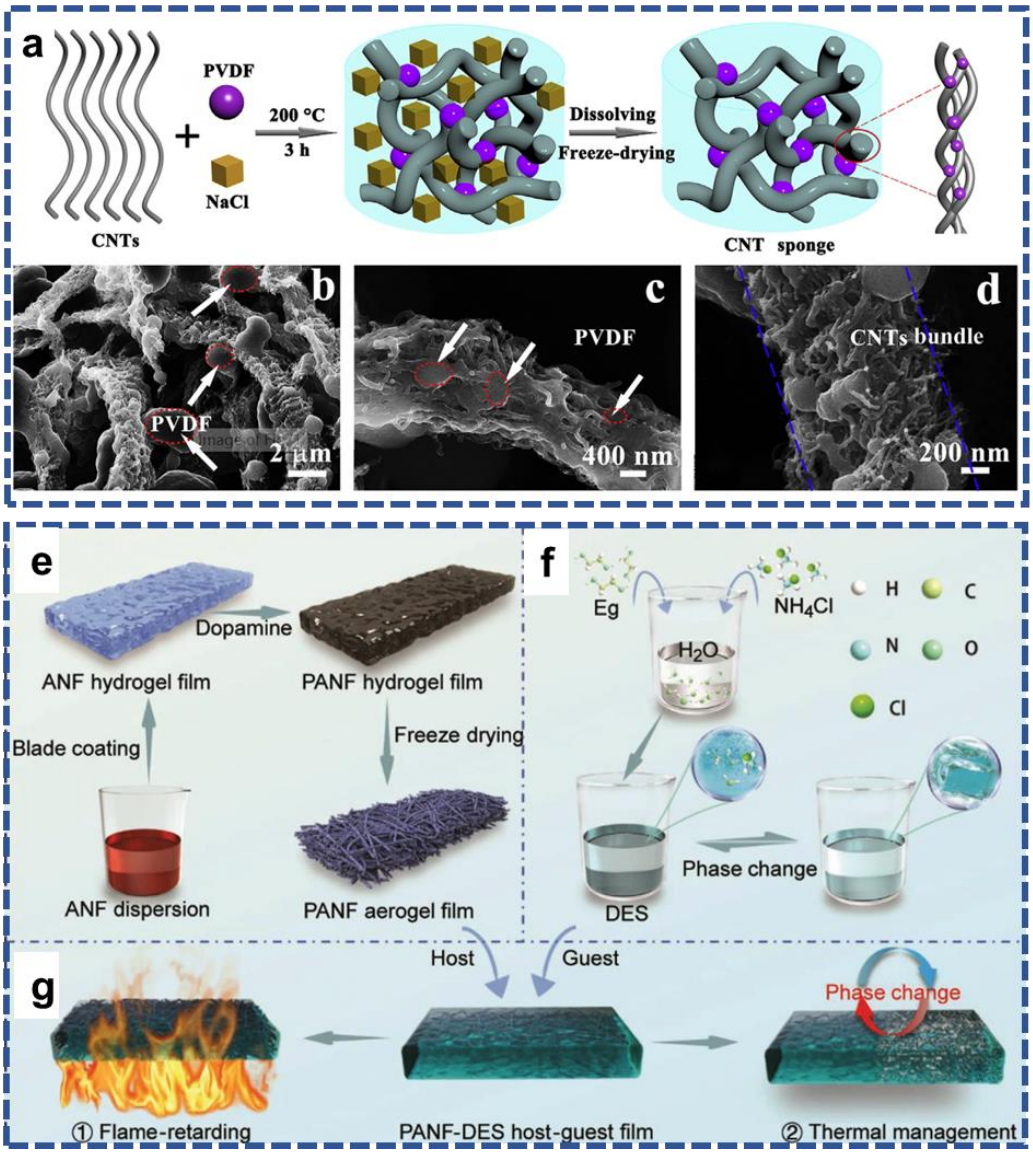

Fig. 1-2 (a) Preparation schematic illustration of 3D flexible CNT sponge. (b-d) The SEM images. Reproduced with permission from ref 23. Copyright 2020, Elsevier. (e) Schematic fabrication of the PANF host aerogel film. (f) Schematic formulation of the PCM. (g) Schematic functionality of thermal management and flame-retarding performance. Reproduced with permission from ref 24. Copyright 2021, Wiley-VCH.

In wearable applications, PCMs can be effectively confined into the interior of fibers with porous structure. Aerogel fibers are effective porous matrix to incorporate PCMs in the interconnected porous network [25, 26]. WU et al. [27] employed freeze-spinning technique to prepare aerogel fibers, and filled biocompatible PCMs into the microstructured fibers with coating of polydimethylsiloxane, the resulting textile

woven by these fibers showed good water hydrophobicity, thermoregulating capability and high mechanical robustness.

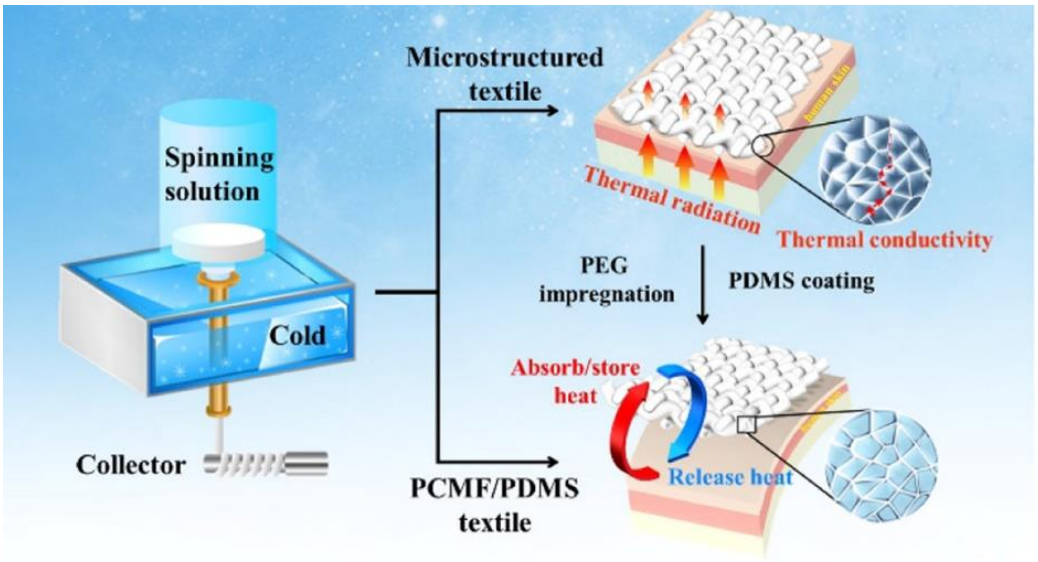

Fig. 1-3 Schematic illustration of the fabrication process of the thermal insulation and thermoregulation textiles. Reproduced with permission from ref 27. Copyright 2020, American Chemical Society.

1.2.2 Encapsulation

Encapsulation technology uses organic, inorganic, or hybrid shell materials to wrap PCMs in tiny spherical particles or hollow column structure, like tubular materials or nano-micro fibers [5, 28,29].

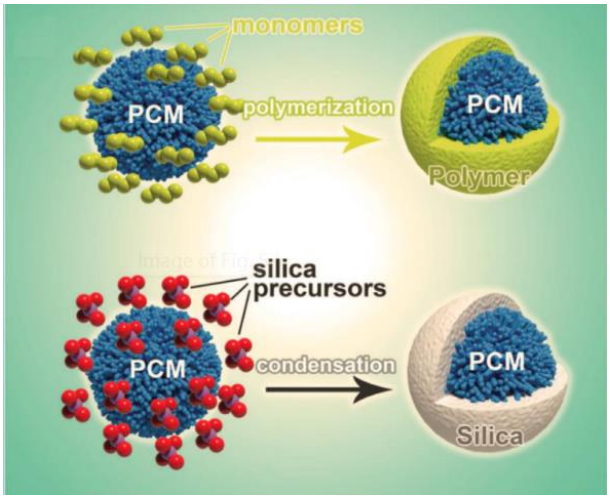

Fig. 1-4 Schematic illustration of the typical organic and inorganic shell of core-shell encapsulation. Reproduced with permission from ref 5. Copyright 2021, Elsevier.

1.2.2.1 Core-shell encapsulation (0D)

(1) Organic shell

The organic shell materials of phase change microcapsules are mainly, melamine-formaldehyde (MF) resin [30], urea-formaldehyde (UF) resin [31], poly(urea–urethane) [32], and so on. Organic shell materials endow the microcapsules with structural flexibility and excellent endurance to volume change during repetitive phase change process, but they also suffer the poor chemical stability and thermal conductivity. Zhang et al. [33] prepared phase change material microcapsules with melamine resin (MF) shell via cellulose nanocrystal (CNC) stabilized Pickering emulsion in-situ polymerization. The content of PW in microcapsules can reach as high as 87.0 wt%, and the microcapsules also possess self-extinguishing performance because of the fire-retardant properties of MF shell.

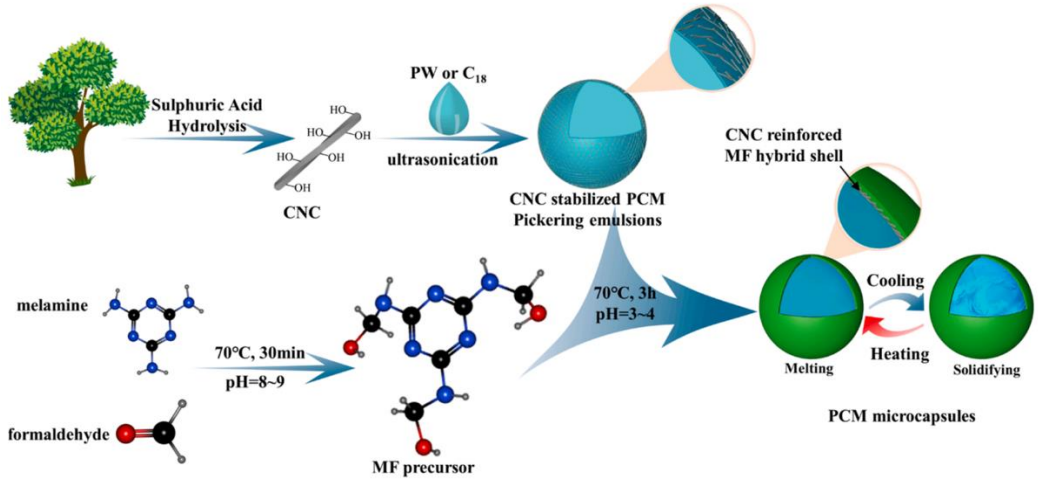

Fig. 1-5 Schematic illustration of the preparation of PCM microcapsules with CNC reinforced MF hybrid shell. Reproduced with permission from ref 33. Copyright 2022, Elsevier.

(2) Inorganic shell

The inorganic shell, including silica (SiO_2), titania (TiO_2), alumina (Al_2O_3) etc., as rigid shell forming materials, have been employed to encapsulate PCMs. Compared to organic shell, the inorganic shell exhibit higher thermal conductivity, better thermal conductivity, mechanical durability, chemical inertness and nontoxicity. Kang et al. [34]

prepared phase change microcapsules with paraffin as core and SiO_2 as inorganic shell. It is shown that the SiO_2 shell is not only conductive to avoid the leakage of the liquid paraffin undergo the phase change process, but also improve the thermal conductivity of the phase change microcapsules. The content of paraffin in the microcapsules can reach 70 wt%, resulting in a high latent heat of 126.1 J/g. The thermal conductivity of the phase change microcapsules is 0.37 W m^{-1} K^{-1}, which is 131.25% higher than that of the pure PCM.

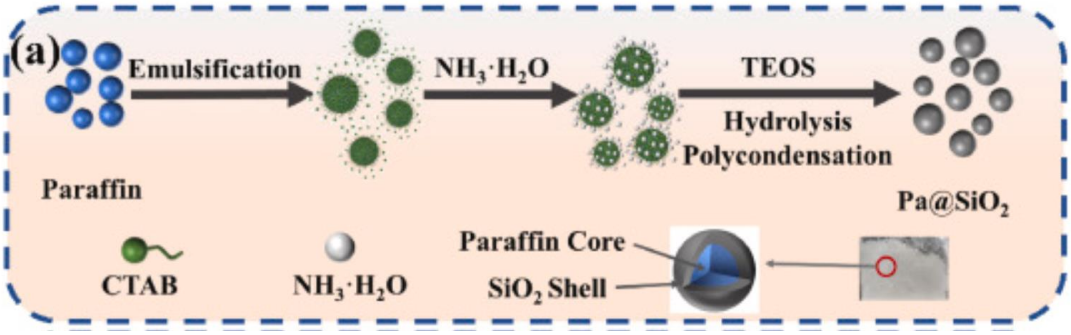

Fig. 1-6 The preparation schematic of paraffin@ SiO_2 microcapsules. Reproduced with permission from ref 34. Copyright 2022, Elsevier.

(3) Hybrid shell

Organic-inorganic hybrid shells greatly enhance the thermal and mechanical performance of phase change microcapsules. Xiong et al. [35] prepared bioelectrocatalytic phase-change microcapsules, using an emulsion-templated interfacial polycondensation technique to construct a base phase change microcapsule system and followed by surface deposition and physical adsorption to construct multilayer of shell. Specially, PCM core was encapsulated in the TiO_2 shell, forming the phase change microcapsule (TiO_2-MEPCM), and then polypyrrole (PPy) was deposited on the shell as a conductive layer. Finally, horseradish peroxidase (HRP) was immobilized on the PPy layer for additional functions.

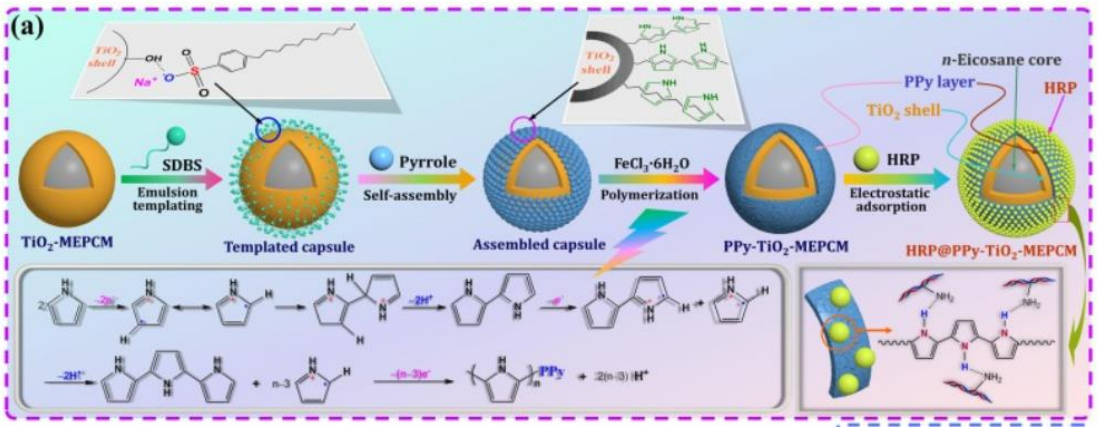

Fig. 1-7 Scheme of fabrication strategy and reaction mechanism of HRP@PPy-TiO_2-MEPCM. Reproduced with permission from ref 35. Copyright 2022, Elsevier.

1.2.2.2 Longitudinal core-shell encapsulation (1D)

The longitudinal confinement is also a kind of core-shell encapsulation, but in one dimension [13]. It is divided into tubular confinement and fibrous confinement, such as infiltrating liquid PCM into the inner cavity of CNTs and core-shell fibers.

(1) Tubular confinement

Being a hollow cylindrical structure of CNTs, PCMs can be infiltrated into the inner space of open-ended CNT. The high conductivity of CNTs is advantages to improve the thermal response. Kong et al. [36] infiltrated PCM into the polymer bamboo-like nanotubes (NTs) with PPy coating. The PPy shell layer imparts sunlight absorption property and electrical conductivity to the composite. Solar radiation can be sufficiently harvested by NTs and transferred to the internal PCMs to initiate the solid – liquid phase transition. In addition, the NTs also construct conductive path and the generated Joule heat can trigger the phase transition of the core PCMs. The integrated core-shell structure paves the way for efficient photo/electro-thermal conversion. Wang et al. [37] prepared polyethylene glycol (PEG)@modified wood powder (MW) composites by impregnating PEG into the hollow structure of wood powder, and then prepared a fire-warning aerogel composed of the carbon nanotubes, calcium alginate and PEG@MW through freeze-drying method. PEG@MW can absorb the excessive heat and store them, thus restrict heat transfer to the fire-warning aerogel, possessing the thermal

insulation effect, and PEG@MW was also served as the supportive skeleton, which is conductive to improve the mechanical properties of the aerogel.

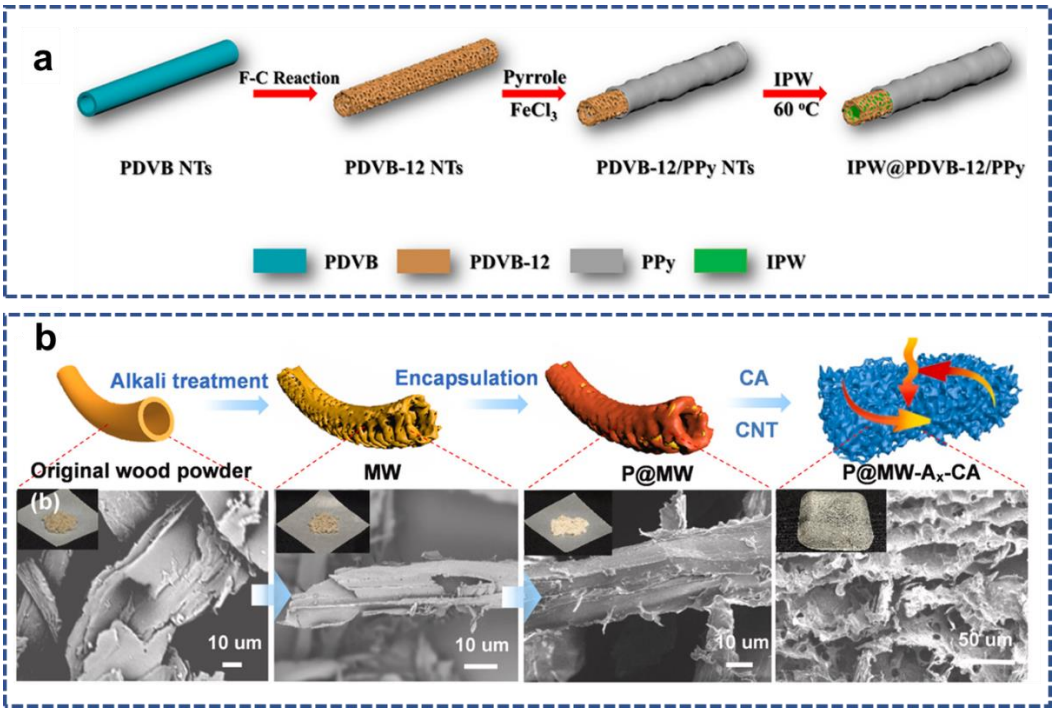

Fig. 1-8 (a) Schematic illustration of the preparation of PCM@ NTs@PPy. Reproduced with permission from ref 36. Copyright 2021, American Chemical Society. (b) Schematic illustration of the preparation of P@MW/ A-CNT/CA aerogel and SEM images. Reproduced with permission from ref 37. Copyright 2022, Elsevier.

(2) Fibrous confinement

Coaxial electrospinning is utilized to fabricate core-sheath nanofibers, where PCMs are encapsulated as core by supportive sheath materials in nanoconfined technology [38,39]. Liu et al. [40] prepared the phase-change separators PW @ PAN through coaxial electrospinning technology, the membrane-based separator was endowed with thermoregulating property, as PCM is employed as the core and PAN polymer acts as a protective sheath in a core-sheath structure.

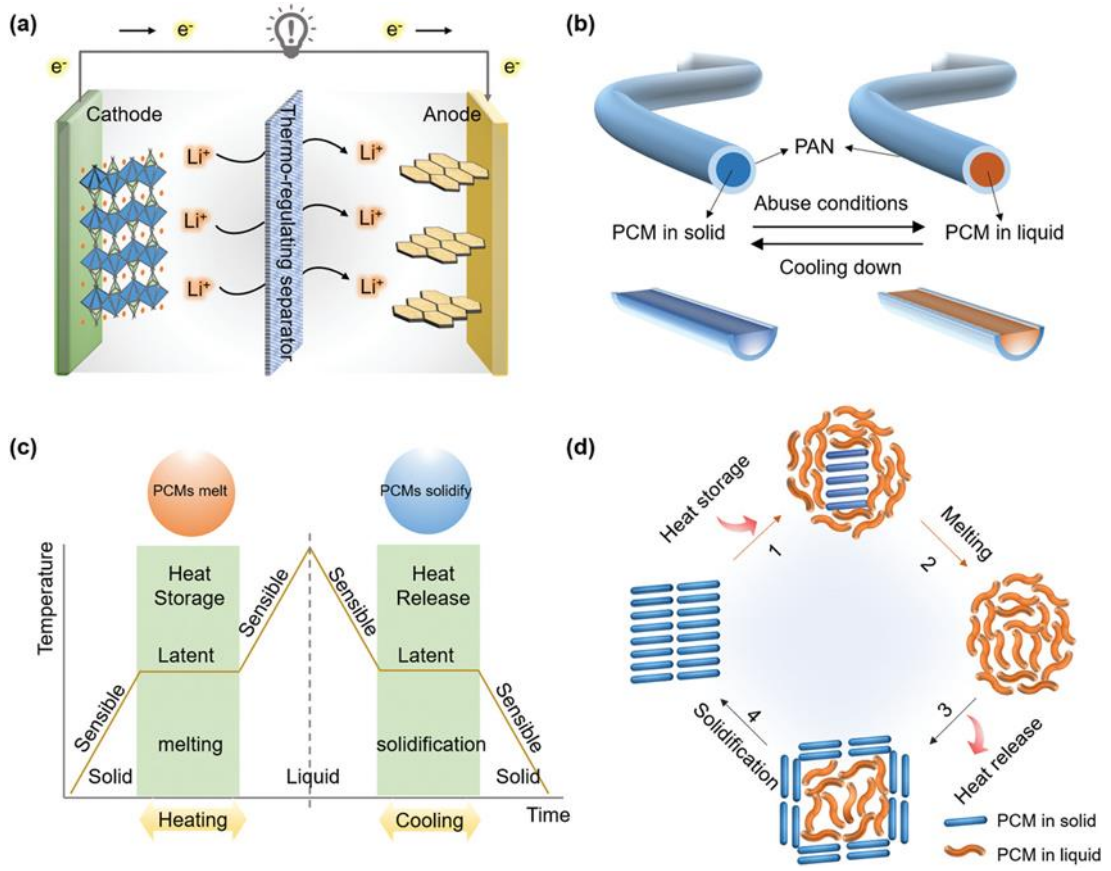

Fig. 1-9 (a) Configuration of LIBs with the thermoregulating separator. (b) Schematic structure of the thermoregulating separator. (c) Mechanism of the thermoregulating separator for alleviating the internal temperature in LIBs. (d) Specific structure change of PCMs upon heat absorption and heat release. Reproduced with permission from ref 40. Copyright 2021, Wiley-VCH.

Moreover, vacuum injection strategy is also a facile method to encapsulate PCMs in hollow tubes [41]. Wang et al. [42] fabricated flexible phase change fibers (PCFs) by injecting PCM and thermochromic agent (TA) into polydimethylsiloxane (PDMS) hollow tubes via a vacuum injection method, then PCFs were woven into textiles for intelligent thermal regulating application. The encapsulated PCM can store the heat energy to maintain the temperature around a constant level, thus improve thermal comfort for wearer. Ning et al. [43] fabricated multifunctional smart fibers using hollow silicone rubber fibers filled with liquid metal (LM), and the rubber shell was added with phase change microcapsules. The fibers exhibit spontaneous heating or cooling effect, according to the surrounding temperature fluctuation, through heat energy storage and release by phase transition of PCMs. It creates a more comfortable microenvironment

between clothing and human skin, which is attributed to the admirable bidirectionally and automatically thermal adjustment.

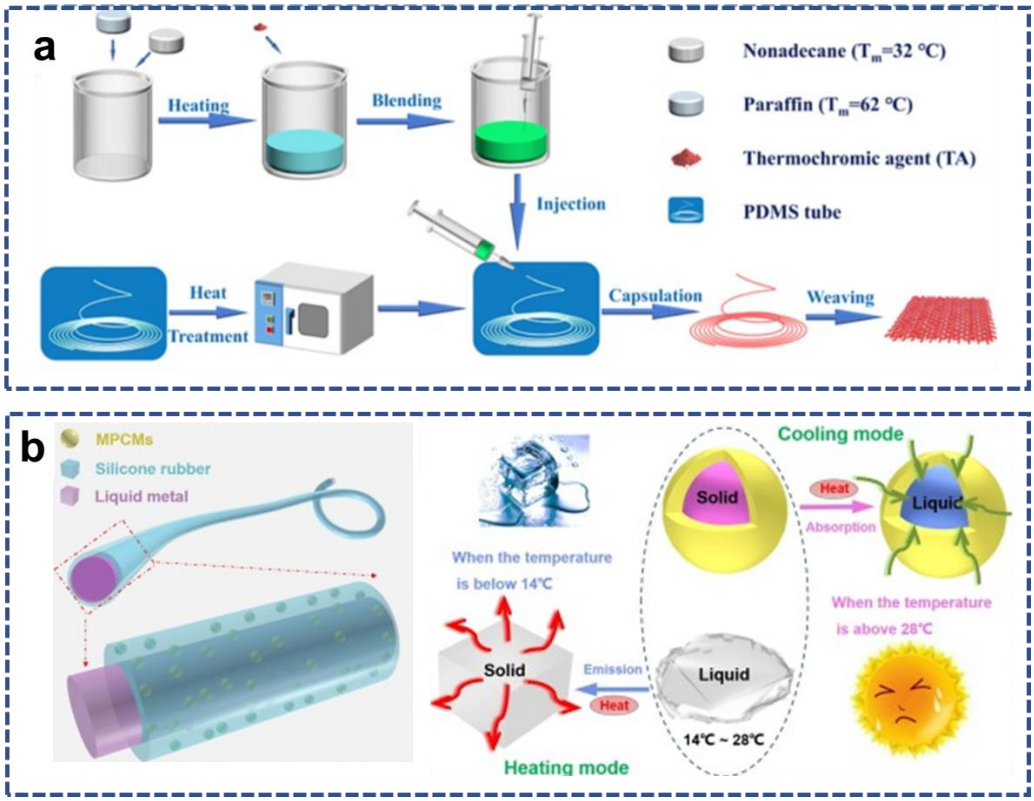

Fig. 1-10 (a) Schematic diagram of the preparation of PCFs. Reproduced with permission from ref 42. Copyright 2023, Elsevier. (b) Schematic diagram of the structure and the thermal-regulating mechanism of the multifunction fibers. Reproduced with permission from ref 43. Copyright 2021, Elsevier.

1.2.3 Polymerization

Polymerization is also a universal strategy to fabricate flexible and form-stable phase change composites. It was constructed by blending PCMs into the molecular skeleton of elastic polymer, as well as bonding PCM chains to polymeric skeleton. The products fabricated through the former method is belonged to the Polymer/PCM blending composites. The later one that develops the phase change polymer with cross-linked molecular structure is categorized to the crosslinked polymeric PCMs.

1.2.3.1 Polymer/PCM blending composites

Polymer/PCM blending composites are usually prepared by melt blending or blending with organic solvents. Elastic polymers are intensive used as polymer skeleton to improve the flexibility, including thermoplastic elastomers and macromolecular polymers. The former one is represented by styrene–butadienestyrene (SBS), olefin block copolymer (OBC) and polyurethane (PU). The later one is represented by high-density polyethylene (HDPE), polyvinyl alcohol (PVA), polymethyl methacrylate (PMMA) and polydimethylsiloxane (PDMS). The macroscopic mechanical properties of the phase change composites are dominated by the intrinsic features of supporting polymer matrix, because the molecular chains of the supporting polymer are larger than pure PCMs. Therefore, the physically blending between PCMs and elastic thermoplastic polymers paves the ways for PCM composites with adjustable flexibility.

As the remarkable multiblock thermoplastic elastomers, OBC and SBS are widely used as a polymer matrix for the development of the flexible PCMs with temperature-varying mechanical properties. They consist of three-block molecular structures, where the part of hard segments remains unchanged and provide supportive effect, while the soft segments can slide freely, affording tensile and tear resistance. The crystalline structure of PCM in the solid phase will restrict the free movement and stretching of the soft chain segment after mixing with the block copolymer, which shows the rigidity characteristics. During the phase transition, the crystal structure gradually disappears, and the soft segment exhibits good flexibility upon debonding. Hu et al. [44] fabricate flexible phase change composite through loading paraffin into interpenetrating network formed by SBS and CNTs for thermal management and thermal storage. The intrinsically flexibility of the phase change composites results from the 3-D network formed by the chemical cross-linking between SBS and CNTs.

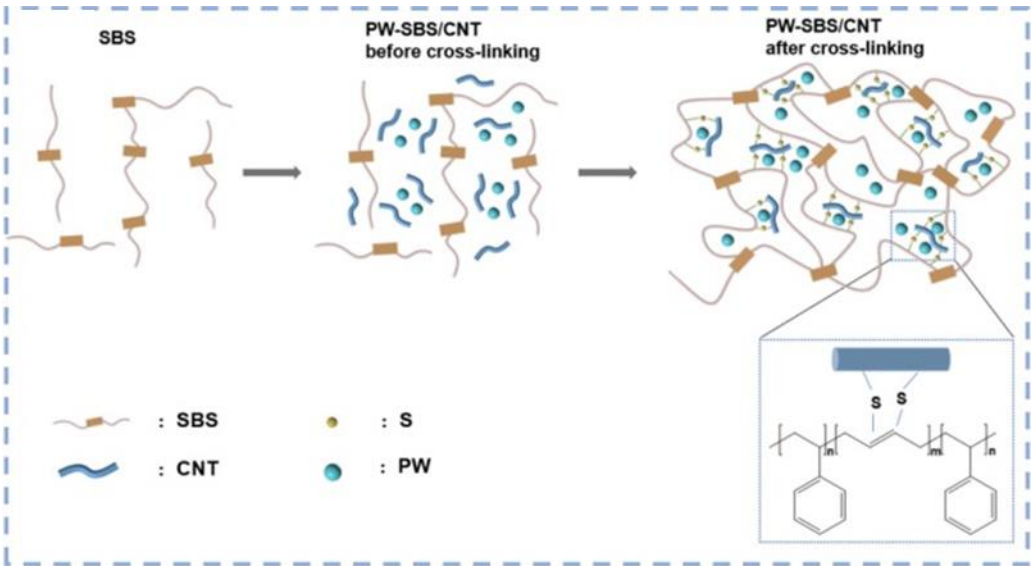

Fig. 1-11 Schematic diagram of the preparation of PW-SBS/CNT composites. Reproduced with permission from ref 44. Copyright 2022, Elsevier.

1.2.3.2 Crosslinked polymeric PCMs

Cross-linked structures are designed to improve mechanical and chemical stability by linking PCM molecular segments with a backbone. PEG is widely used in this method, because of the dual-terminal hydroxyl groups that are prone to be chemical modified. For example, PEG can be crosslinked with isocyanate in polymer skeleton to construct polymeric network, thus the phase change composites exhibit solid-solid phase change performance and realized an excellent shape stability [45]. The crystallinity of PCMs can be tuned through control the crosslinking density of the polymeric network. Therefore, it is possible to adjust the thermal storage density and mechanical properties as desired or for a trade-off, which is promising for developing intrinsic flexible PCM composites. Kou et al. [46] synthesized intrinsic flexible and form-stable PCMs through two step polymerization process. They crosslinked PEG crosslinked with melamine and TDI, and consequently prepared the PCM film by casting. They investigate the thermal performance of the phase change film with PEG with different molecular weight. The resulting phase change film also exhibited admirable intrinsic flexibility, excellent conformability and intersting tailorability and foldability.

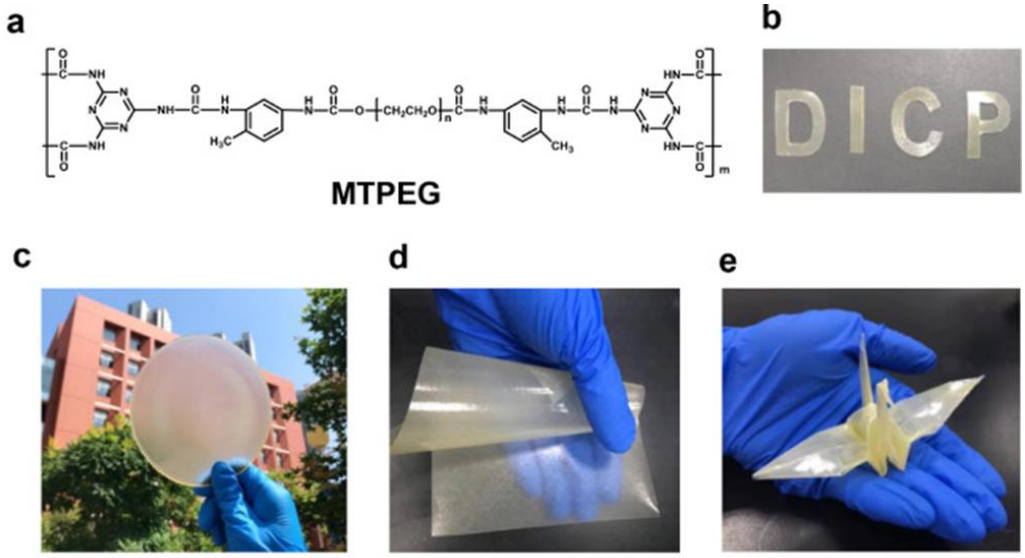

Fig.1-12 (a) Schematic representation of intrinsic PCM synthesized with PEG, melamine and TDI. (b-e) The photographs of the intrinsic flexible PCM films. Reproduced with permission from ref 46. Copyright 2021, Elsevier.

1.3. Thermal energy conversion mechanisms

1.3.1 Photo-thermal energy conversion

The Effective conversion and utilization of abundant solar energy is a necessary condition to meet the global demand for inexhaustible energy. Therefore, photo-thermal energy conversion is an indispensable and promising research topic. However, most of PCMs have inferior solar absorptance in the visible light region, so rendering solar absorptivity to PCMs is promising for clean and renewable energy utilization [47,48]. Solar-thermal materials are capable of harvesting solar energy, which has been widely used in power generation, thermal energy storage, water purification, and sterilization systems over the past decades. A facile and universal method to fabricate solar-thermal composite phase change materials is cooperating solar-thermal materials with PCMs, thereby the generated thermal energy could be stored by PCMs, which realize effective use of solar energy as well as energy storage to solve the mismatch between energy supply and demand [49]. Therefore, solar-thermal energy conversion and storage exhibit great potential for utilization of intermittent solar energy. This process contains two steps, firstly, the sunlight is first converted into heat energy, then the generated heat

is stored as latent heat through the phase change process of PCMs. Solar-thermal materials are able to effectively absorb solar irradiation in a broad band across the entire solar spectrum, and exhibit high photo-thermal conversion efficiency. Various nanostructured materials can excite solar-thermal effect, including carbon-based materials, metallic materials, semiconductors, and some conjugated polymers, etc. These materials mainly have three kind of solar-thermal conversion mechanisms, including conjugate effect and hyperconjugate effect, surface plasmon resonance (SPR) effect, and localized SPR (LSPR) effect, and nonradiative relaxation effect. The photothermal conversion on carbon-based materials and some conjugated polymers are belonged to the conjugate effect and hyperconjugate effect. The photothermal conversion on metallic materials ascribed to the SPR effect and LSPR effect. The typical semiconductors, such as MoS_2 and CuS, are widely used in photothermal conversion, attributed by the nonradiative relaxation effect.

The solar-thermal conversion efficiency of PCM composites is calculated by the following equation [50]:

$$\eta PT(\%) = \frac{m \cdot \Delta H}{A \cdot p \cdot t}$$

Where m is the mass of PCM, ΔH is the heat enthalpy of PCM, p is the irradiation intensity of the solar, A is the area of sample, and t is the phase change time.

1.3.2 Electric-thermal energy conversion

Different from the intermittent and uncontrollability of solar energy, electric power supply is continuous and stable, thus the electric-thermal conversion technology has better continuity and stability than photo-thermal conversion technology. The conversion device has the advantages of compact, fast and portable, which exhibit great potential in thermal management fields, such as power vehicles, electronic devices, and off-peak electric storage systems. Pure PCMs have very low electrical conductivity, and it is hard for PCMs to trigger the electrical-thermal conversion. Therefore, it is necessary to cooperate PCMs with supporting materials with high electrical conductivity. These conductive materials determine the conversion from electric energy

to heat energy, and PCMs act as an energy accumulator for the generated thermal energy. Various electrically and thermally conductive fillers including metal materials (Cu, Ag, Au, Al, Ni), carbon materials (CNTs, graphene), and conductive polymers (PANI, PPy, PEDOT) have been integrated into the PCM system [51,52]. The generated joule heat could be stored as the latent heat of PCMs.

The electric-thermal conversion efficiency of PCM composites is calculated by the following equation:

$$\eta ET(\%) = \frac{m \cdot \Delta H}{U \cdot I \cdot t}$$

Where m is the mass of PCM, ΔH is the heat enthalpy of PCM, U is the applied voltage, I is the input current, and t is the phase change time.

1.3.3 Photo-thermoelectric energy conversion

Photo-thermoelectric energy conversion are composed of photo-thermal conversion and thermoelectric conversion. Firstly, solar-thermal materials convert solar energy to heat energy. Secondly, the generated energy was reproduced to be electric energy by a thermoelectric generator. Between these two steps, PCMs store the heat energy as the latent heat, maintain a higher temperature different in longer time for generating electric energy. Therefore, PCMs serve as a long-lasting heat source for a thermoelectric generator, providing dispatchable power generation abilities [53, 54]. The photo-thermoelectric energy conversion efficiency of PCM composites is calculated by the following equation:

$$\eta PET(\%) = \frac{U \cdot I}{A \cdot p}$$

Where U is the output voltage, I is the output current, p is the irradiation intensity of the solar, A is the area of sample.

1.4. Applications of the flexible PCMs

1.4.1 Thermal management of electronic devices

As people's needs increase and technology develops, high integration of electronic

devices is an inevitable trend, such as the development of high-energy battery packs and high-performance chips. As a result, a large amount of heat can easily accumulate in the device and lead to the failure of the circuit. With its high thermal energy storage density and tremendous heat absorption capacity, PCM can effectively help buffer temperature rise when assembled with electronic components. Compared to traditional thermal management methods, PCM consumes no energy and requires no additional components. However, in many cases, the complex shape of electronic devices makes it difficult for PCMs to fit snugly into the device and thus not achieve full effectiveness. In such cases, flexible PCMs can solve the fit problem by greatly improving the adaptability. It is well known that the performance of power batteries is greatly affected by temperature. An efficient thermal management system facilitates the battery to operate in a reasonable temperature range. Battery thermal management systems (BTMs) based on phase change materials (PCM) are a passive thermal management approach, and they exhibit the merits of low operating costs and good temperature uniformity [55].

At present, organic PCMs are the main PCMs used in most research of BTMs, due to the advantages of low cost, good stability, low toxicity, non-corrosiveness, no supercooling and phase separation. However, they have the drawbacks of inferior thermal conductivity and high flammability. To address these problems, researchers have tried to add fillers with high thermal conductivity and flame retardancy, which is a hot issue in the field of battery thermal management.

Due to the inevitable flammability of organic PCM, inorganic materials with flame retardant properties have become a hot research topic in the future. The research on inorganic PCM is important to solve the thermal runaway problem of power batteries. Due to the limitation of phase transition temperature, most of the inorganic PCMs available for BTMS are hydrated salts, which have unstable thermophysical properties. However, inorganic PCMs are completely nonflammable and cost much less than organic PCMs. The main obstacle to the application of inorganic PCM is the inferior thermal conductivity and stability caused by phase separation, dehydration or supercooling. To buffer the thermal runaway while maintaining the electrochemical

performance of the cell, a thermally regulated hydrogel electrolyte was designed by Meng et al. The phase change chain PEG is incorporated into the agarose backbone (AGr) by hydrogen bonding. When the internal temperature of the cell reaches the melting point, the PEG in TRHE changes from a crystalline state to an amorphous state and absorbs heat, thus achieving thermal buffering and preventing overheating and explosion of the zinc-ion battery [56].

With the development of technology, high-rate charging and discharging technologies began to appear. Especially, the emergence of fast charging and discharging technology tends to cause excessive heat accumulation and local temperature rise in the battery pack. However, the low thermal conductivity of pure PCM is unfavorable for heat dissipation, so improving the thermal conductivity of PCM is the focus of many scholars' research at present. At present, the basic methods to achieve high thermal conductivity of PCM can be roughly divided into two categories: increasing high thermal conductivity on carbon-based materials and increasing high thermal conductivity on metal-based materials. However, there is still a problem that cannot be ignored. Metal particles, expanded graphite and other heat transfer enhancing materials are commonly used in PCM, but these additional materials are highly conductive and therefore cannot guarantee the safety of power cells. Therefore, future research will focus on electrically insulating and highly thermally conductive fillers. Boron Nitride (BN), featuring electrical insulation and high thermal conductivity, is a good choice to improve the safety of power batteries [57]. Guo et al. [58] reported a PCM for lithium-ion batteries capable of dual-mode thermal management by liquid metal (LM) modified polyethylene glycol/LM/boron nitride (BN) for photothermal effects and passive heat transfer. Typically, the soft, deformable LM is modified on the BN surface to act as a thermal bridge to decrease the contact thermal resistance between adjacent fillers to achieve high thermal conductivity. In addition, the LM with excellent photothermal properties provides efficient cell heating capability for PCM. As a dual-mode cell thermal regulator, it is also endowed with manufacturing tunability, electrical insulation, shape stability, corrosion resistance, and flame retardancy.

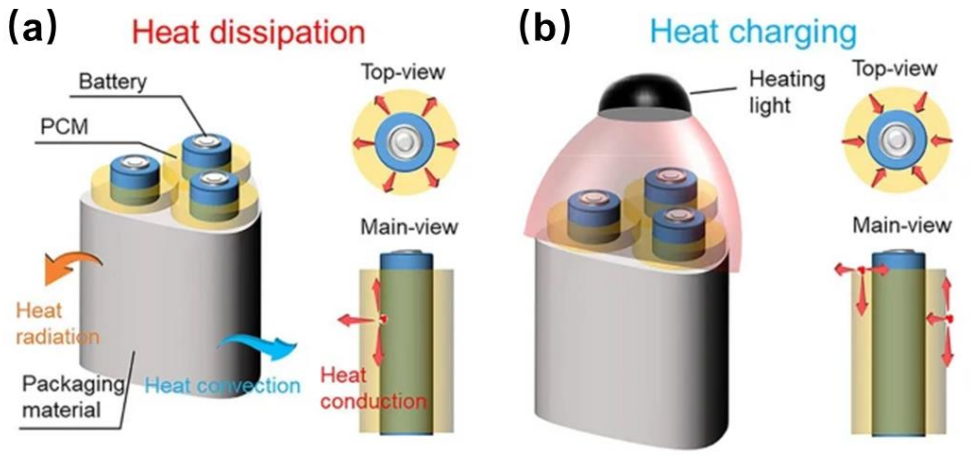

Fig. 1-13 (a) Working principle of passive battery thermal management at high temperature using PCM thermal regulator. (b) Working principle of heating of battery in a cold environment through light-to-heat conversion. Reproduced with permission from ref 58. Copyright 2022, Springer Nature.

1.4.2 Personal thermal management

It is crucial to maintain the temperature within an appropriate range for the human body. The reversible absorption and release of latent heat by PCM can serve as a responsive thermal control medium to adjust the local temperature in the microclimate under clothing. When the temperature rises above the melting point, PCMs absorb the heat through solid to liquid phase transition, buffering heat conduction to skin. When the temperature decreases below the crystallization point, PCMs release the stored latent heat, preventing temperature from sudden dropping. More efficient thermal management requires PCM to be flexible and able to conform to the curvature changes of skin [59, 60]. In order to adapt to the thermal comfort of the human body, the PCMs with a phase change temperature in the range of 18-36 °C is appropriate for wearing application, such as n-nonadecane, n-heptadecane, n-eicosane, n-octadecane, etc. Addressing on the leakage issue, coaxial electrospinning and microencapsulation technology have been employed to fabricate the form-stable PCM composites with long-term durability. For phase change microcapsules, they have been incorporated into textiles by mature methods in the textile industry, such as as coating, padding, laminating, printing, etc.

It is notable that the work properties of PCMs are dependent on many factors, such as filling rate, material class, and distribution. Therefore, there may sometimes be a trade-off between working performance and wearing comfort. Li et al. [61] prepared phase change composite films by continuous electrospinning. The synthesized core-shell PCM was used as the phase change medium, and then Janus-type structures were formed by a spraying process. The versatile composite films with Janus-structure possess favorable properties of phase change thermoregulating, radiative cooling, Joule heating, photothermal conversion, thermal camouflage, and EMI shielding capabilities.

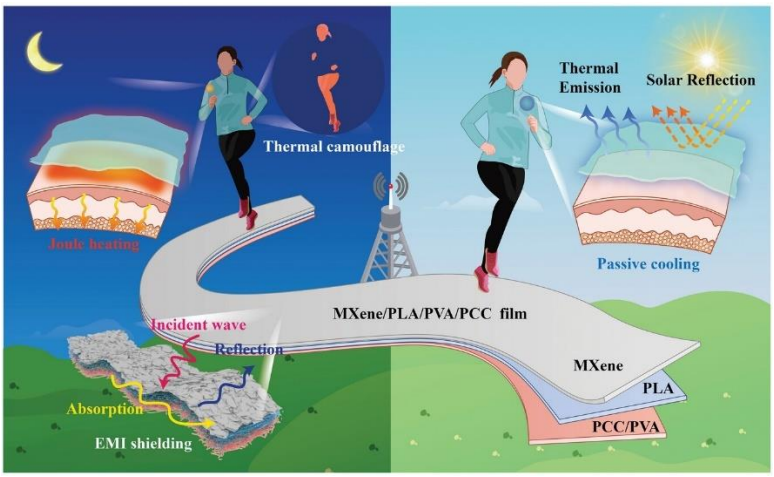

Fig. 1-14 Schematic of the application of the Janus phase change composite film. Reproduced with permission from ref 61. Copyright 2023, Wiley-VCH.

1.4.3 Thermal management for building

As living standards continue to rise, so does the demand for thermal comfort in buildings, causing an increase in energy consumption. Heating and cooling applications account for 32–33% of a building's total energy cost. For global energy demand and reduce environmental pollution, even a small improvement in energy savings in building heating and cooling system is significant and meaningful [62, 63]. On this regard, it is effective to incorporate PCMs with melting points of 18 to 30 °C into wallboards, floors, ceilings, and other structures of buildings in buffering the interior temperature fluctuations and reducing energy consumption.

Besides wallboards and roofs, other building structures, like floors, ceilings, and

windows, have also been incorporated with PCM for building thermal management. Currently, considerable efforts have been contributed to develop PCM-based radiant heating system for building thermal regulation on floors. Yang et al. [64] constructed a bilayer structure for temperature management in building. They cooperate a room-temperature PCM system with a passive radiation cooling (PRC) function. PCM was introduced to regulate the cooling performance of the bilayer structure, because their energy storing capability facilitate the cooling effect by the PRC.

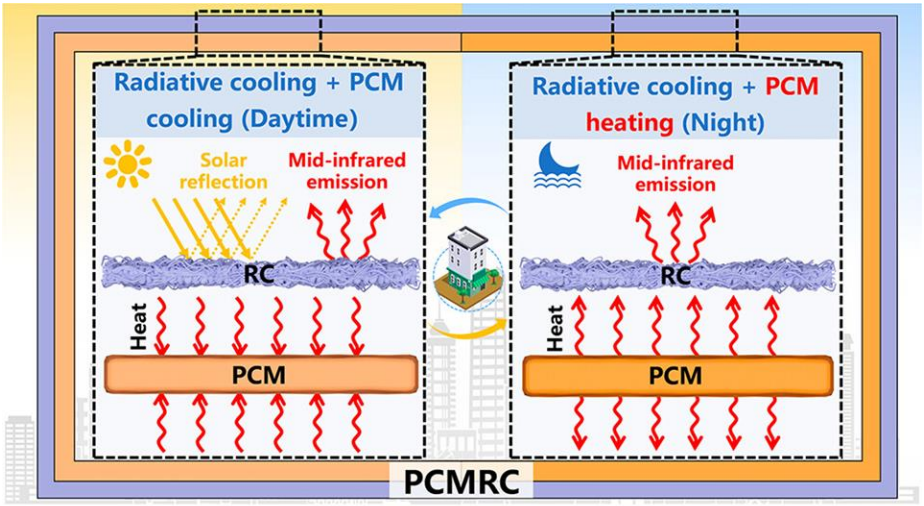

Fig. 1-15 Schematic of the application of the PCM enhanced radiative Cooler in building. Reproduced with permission from ref 64. Copyright 2023, American Chemical Society.

1.4.4 Thermal infrared stealth

Infrared stealth technology is promising in military and industrial fields. The feasibility of infrared stealth technology depends on the difference in infrared radiation energy between the background and the object. Currently, there are two key points to achieve favorable infrared stealth performance: one is to reduce the infrared emissivity of the object's surface, and the other is to reduce the temperature difference between the object and the background. The latter method affects the thermal imaging camera by hiding the infrared radiation through temperature regulation, such as insulation and controlling the heat flux [4, 65]. Nevertheless, thermal insulators are usually thick and

heavy, which is not conducive to heat dissipation, thus cause huge heat build-up. Therefore, PCMs with large latent heat storage capacity have been explored as exploitable infrared emission materials.

PCMs can regulate temperature to hide infrared radiation due to the thermal storage capabilities, providing a viable option for the rational design of infrared stealth materials. Zhou et al. [66] prepared a flexible phase change hydrogel by integrating phase change microspheres into PVA-gel substrate. The phase change hydrogel has the advantages of excellent flexibility and adaptability. Thus, they are conformable to arbitrary targets. Additionally, phase change hydrogels can also be easily coated on ordinary fabrics, as phase change wearable devices, to realize the infrared stealth on the body.

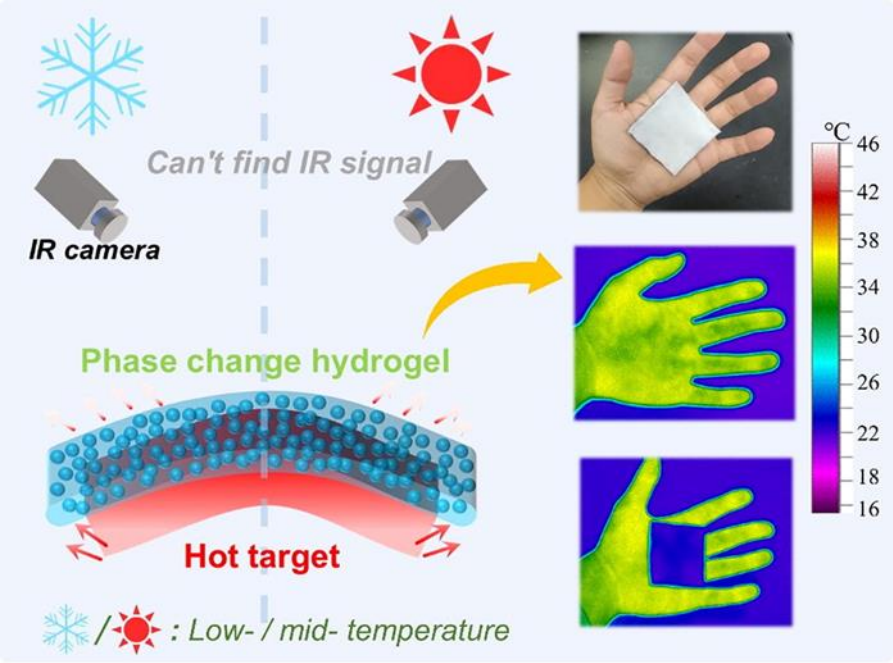

Fig. 1-16 Schematic illustration of the infrared stealth function of phase change hydrogel. Reproduced with permission from ref 66. Copyright 2022, American Chemical Society.

1.5 Purpose and outline of this research

1.5.1 Research purpose

Thermoregulation has pivotal implications for human health and

thermophysiological comfort. Traditional central space heating and cooling systems cause huge electricity consumption, and they fail to satisfy each individual's requirements of thermophysiological comfort that might different from person to person. The emerging advanced textiles designed for personal thermal management (PTM) have shown great promise in energy saving manner, and maintaining personalized thermal comfort.

Our research is aimed to develop the fibrous membrane- based thermoregulating textile with reversible temperature adjustability to improve the wearers' thermal comfort in an all-weather, energy saving, and on-demand manner.

To meet the above requirements, we designed the fibrous membranes based on the following disciplines:

(1) The reversible temperature adjustability can be realized based on the laten heat of phase change materials (PCMs). The phase change membranes could absorb the extra heat energy, playing a cooling effect at high temperature. Conversely, they could release the stored heat energy, playing a warming effect when temperature decreased to a certain level.

(2) Affording positive heating functions through input the extra energy (solar energy and electric energy) based on the light-thermal energy conversion and electric-thermal energy conversion.

(3) Ensuring the necessary wearing comfort, including the flexibility, deformability, tailorability, air and moisture permeability and wearing durability.

1.5.2 Research outline

Phase change materials (PCMs) based on latent heat storage, capable of storing and releasing excess energy, has been regarded as a potential candidate in thermal management. We integrated two typical organic PCMs (PEG and PW) into the fibrous membranes through electrospinning technology to develop the temperature responsive, and bi-directional thermal regulating textiles.

In chapter 2, we presented a green strategy to construct eco-friendly fibrous membranes with responsive reversal thermal regulation properties via electrospinning

and surface crosslinking. Biocompatible and biodegradable polymer PVA and PEG were employed as supporting matrix and functional component, respectively, and toxic organic solvent were excepted from the electrospinning process. Furthermore, high conductive CNTs were introduced into the composite fibers to enhance thermal conductivity. The phase change membranes showed the effective thermal regulation capability, verified the great potential in thermal management field.

In chapter 3, since the single-mode thermal regulation based on PCMs fail to cope with the multi-functional demand for longtime and large temperature range management, multi-mode and more precise thermal regulation textiles are in demand. We proposed an approach for all-day individual thermal management through integrating the reversible phase change property, sustainable solar-heating, and complementary Joule heating into one wearable thermoregulatory textile. Specifically, we designed a hierarchical core-sheath structured fibers which are composed of the core PW, supportive elastic shell polyurethane (PU) and external solar-responsive multilayers of CNTs, PDA, and PEDOT:PSS, where PEDOT:PSS also serves as a conductive layer. The hierarchical core-sheath structure assembled various functional materials into individual fibers, therefore the multiple thermal regulation routes were integrated into one membrane-based textile. The tri-mode thermoregulatory fibrous membrane presented promising potential for application in wearable personal thermal management.

The porous structure is one of the key points for air/moisture permeability. **In chapter 4**, to better maintain the porous structure of the pristine phase change membranes, we applied the in situ polymerization and in situ electroless deposition strategies to introduce the functional materials on the surface of core-shell fibers. In summary, a breathable and thermoregulating fibrous membrane integrated with tri-mode thermal regulating routs was prepared through constructing the hierarchical core-sheath structure of fibers. In addition, the air/moisture permeability and the electromechanical stability was validated. What's more, the fabrication process was simplified compared to the study in chapter 3.

Reference

(1) Yang, J.; Zhou, Y.; Yang, L.; Feng, C.; Bai, L.; Yang, M.; Yang, W. Exploring Next-Generation Functional Organic Phase Change Composites. *Adv Funct Materials* **2022**, *32* (28), 2200792.

(2) Liu, H.; Sun, K.; Shi, X.; Yang, H.; Dong, H.; Kou, Y.; Das, P.; Wu, Z.-S.; Shi, Q. Two-Dimensional Materials and Their Derivatives for High Performance Phase Change Materials: Emerging Trends and Challenges. *Energy Storage Materials* **2021**, *42*, 845–870.

(3) Yuan, K.; Shi, J.; Aftab, W.; Qin, M.; Usman, A.; Zhou, F.; Lv, Y.; Gao, S.; Zou, R. Engineering the Thermal Conductivity of Functional Phase-Change Materials for Heat Energy Conversion, Storage, and Utilization. *Adv. Funct. Mater.* **2020**, *30* (8), 1904228.

(4) Mao, J.; Iocozzia, J.; Huang, J.; Meng, K.; Lai, Y.; Lin, Z. Graphene Aerogels for Efficient Energy Storage and Conversion. *Energy Environ. Sci.* **2018**, *11* (4), 772–799.

(5) Wu, M. Q.; Wu, S.; Cai, Y. F.; Wang, R. Z.; Li, T. X. Form-Stable Phase Change Composites: Preparation, Performance, and Applications for Thermal Energy Conversion, Storage and Management. *Energy Storage Materials* **2021**, *42*, 380–417.

(6) Song, M.; Wang, L.; Shao, F.; Xie, H.; Xu, H.; Yu, W. Thermally Induced Flexible Phase Change Hydrogels for Solar Thermal Storage and Human Thermal Management. *Chemical Engineering Journal* **2023**, *464*, 142682.

(7) Luo, Y.; Yu, W.; Qiao, J.; Zhao, X.; Wu, H.; Sheng, X.; Chen, Y.; Lin, P. Self-Healing Inorganic Hydrated Salt Gels for Personal Thermal Management in the Static and Dynamic Modes. *Chemical Engineering Journal* **2022**, *440*, 135632.

(8) Xi, S.; Wang, L.; Xie, H.; Yu, W. Superhydrophilic Modified Elastomeric RGO Aerogel Based Hydrated Salt Phase Change Materials for Effective Solar Thermal Conversion and Storage. *ACS Nano* **2022**, *16* (3), 3843–3851.

(9) Lu, Y.; Xiao, X.; Fu, J.; Huan, C.; Qi, S.; Zhan, Y.; Zhu, Y.; Xu, G. Novel Smart Textile with Phase Change Materials Encapsulated Core-Sheath Structure Fabricated by Coaxial Electrospinning. *Chemical Engineering Journal* **2019**, *355*, 532–539.

(10) Umair, M. M.; Zhang, Y.; Zhang, S.; Jin, X.; Tang, B. A Novel Flexible Phase Change Composite with Electro-Driven Shape Memory, Energy Conversion/Storage and Motion Sensing Properties. *J. Mater. Chem. A* **2019**, *7* (46), 26385–26392.

(11) Wu, M.; Li, T.; Wang, P.; Wu, S.; Wang, R.; Lin, J. Dual-Encapsulated Highly Conductive and Liquid-Free Phase Change Composites Enabled by Polyurethane/Graphite Nanoplatelets Hybrid Networks for Efficient Energy Storage and Thermal Management. *Small* **2022**, *18* (9), 2105647.

(12) Cheng, P.; Gao, H.; Chen, X.; Chen, Y.; Han, M.; Xing, L.; Liu, P.; Wang, G. Flexible Monolithic Phase Change Material Based on Carbon Nanotubes/Chitosan/Poly(Vinyl Alcohol). *Chemical Engineering Journal* **2020**, *397*, 125330.

(13) Urbain, F.; Smirnov, V.; Becker, J.-P.; Lambertz, A.; Yang, F.; Ziegler, J.; Kaiser, B.; Jaegermann, W.; Rau, U.; Finger, F. Multijunction Si Photocathodes with Tunable Photovoltages from 2.0 V to 2.8 V for Light Induced Water Splitting. *Energy Environ. Sci.* **2016**, *9* (1), 145–154.

(14) Sun, K.; Dong, H.; Kou, Y.; Yang, H.; Liu, H.; Li, Y.; Shi, Q. Flexible Graphene Aerogel-Based Phase Change Film for Solar-Thermal Energy Conversion and Storage in Personal Thermal

Management Applications. *Chemical Engineering Journal* **2021**, *419*, 129637.
(15) Jin, X.; Yang, Z.; Huang, C.; Yang, J.; Wang, Y. PEDOT:PSS/MXene/PEG Composites with Remarkable Thermal Management Performance and Excellent HF-Band & X-Band Electromagnetic Interference Shielding Efficiency for Electronic Packaging. *Chemical Engineering Journal* **2022**, *448*, 137599.
(16) Liu, H., Fu, R., Su, X., Wu, B., Wang H., Xu Y., Liu X. MXene confined in shape-stabilized phase change material combining enhanced electromagnetic interference shielding and thermal management capability, *Composites Science and Technology* **2021**,108835.
(17) Shi, J.; Qin, M.; Aftab, W.; Zou, R. Flexible Phase Change Materials for Thermal Energy Storage. *Energy Storage Materials* **2021**, *41*, 321–342.
(18) Wu, S.; Li, T.; Wu, M.; Xu, J.; Chao, J.; Hu, Y.; Yan, T.; Li, Q.-Y.; Wang, R. Dual-Functional Aligned and Interconnected Graphite Nanoplatelet Networks for Accelerating Solar Thermal Energy Harvesting and Storage within Phase Change Materials. *ACS Appl. Mater. Interfaces* **2021**, *13* (16), 19200–19210.
(19) Liu, P.; An, F.; Lu, X.; Li, X.; Min, P.; Shu, C.; Li, W.; Yu, Z.-Z. Highly Thermally Conductive Phase Change Composites with Excellent Solar-Thermal Conversion Efficiency and Satisfactory Shape Stability on the Basis of High-Quality Graphene-Based Aerogels. *Composites Science and Technology* **2021**, *201*, 108492.
(20) Shao, Y.; Hu, W.; Gao, M.; Xiao, Y.; Huang, T.; Zhang, N.; Yang, J.; Qi, X.; Wang, Y. Flexible MXene-Coated Melamine Foam Based Phase Change Material Composites for Integrated Solar-Thermal Energy Conversion/Storage, Shape Memory and Thermal Therapy Functions. *Composites Part A: Applied Science and Manufacturing* **2021**, *143*, 106291.
(21) Umair, M. M.; Zhang, Y.; Zhang, S.; Jin, X.; Tang, B. A Novel Flexible Phase Change Composite with Electro-Driven Shape Memory, Energy Conversion/Storage and Motion Sensing Properties. *J. Mater. Chem. A* **2019**, *7* (46), 26385–26392.
(22) Chen, L.; Lv, J.; Ding, L.; Yang, G.; Mao, Z.; Wang, B.; Feng, X.; Zapotoczny, S.; Sui, X. A Shape-Stable Phase Change Composite Prepared from Cellulose Nanofiber/Polypyrrole/Polyethylene Glycol for Electric-Thermal Energy Conversion and Storage. *Chemical Engineering Journal* **2020**, *400*, 125950.
(23) Chen, X.; Gao, H.; Hai, G.; Jia, D.; Xing, L.; Chen, S.; Cheng, P.; Han, M.; Dong, W.; Wang, G. Carbon Nanotube Bundles Assembled Flexible Hierarchical Framework Based Phase Change Material Composites for Thermal Energy Harvesting and Thermotherapy. *Energy Storage Materials* **2020**, *26*, 129–137.
(24) Yang, Y.; Lyu, J.; Chen, J.; Liao, J.; Zhang, X. Flame-Retardant Host–Guest Films for Efficient Thermal Management of Cryogenic Devices. *Adv Funct Materials* **2021**, *31* (41), 2102232.
(25) Li, G.; Hong, G.; Dong, D.; Song, W.; Zhang, X. Multiresponsive Graphene-Aerogel-Directed Phase-Change Smart Fibers. *Adv. Mater.* **2018**, *30* (30), 1801754.
(26) Bao, Y.; Lyu, J.; Liu, Z.; Ding, Y.; Zhang, X. Bending Stiffness-Directed Fabricating of Kevlar Aerogel-Confined Organic Phase-Change Fibers. *ACS Nano* **2021**, *15* (9), 15180–15190.
(27) Wu, J.; Hu, R.; Zeng, S.; Xi, W.; Huang, S.; Deng, J.; Tao, G. Flexible and Robust Biomaterial Microstructured Colored Textiles for Personal Thermoregulation. *ACS Appl. Mater. Interfaces* **2020**, *12* (16), 19015–19022.
(28) Wu, M. Q.; Wu, S.; Cai, Y. F.; Wang, R. Z.; Li, T. X. Form-Stable Phase Change Composites: Preparation, Performance, and Applications for Thermal Energy Conversion, Storage and

Management. *Energy Storage Materials* **2021**, *42*, 380–417.
(29) Umair, M. M.; Zhang, Y.; Iqbal, K.; Zhang, S.; Tang, B. Novel Strategies and Supporting Materials Applied to Shape-Stabilize Organic Phase Change Materials for Thermal Energy Storage–A Review. *Applied Energy* **2019**, *235*, 846–873.
(30) Yuan, S.; Yan, R.; Ren, B.; Du, Z.; Cheng, X.; Du, X.; Wang, H. Robust, Double-Layered Phase-Changing Microcapsules with Superior Solar-Thermal Conversion Capability and Extremely High Energy Storage Density for Efficient Solar Energy Storage. *Renewable Energy* **2021**, *180*, 725–733.
(31) Cheng, L.; Kong, L.; Zhang, X.; Kong, X. Form-Stable Phase Change Nanocapsules with Photo and Electric Dual Responses for Multipurpose Applications in Energy Storage and Conversion. *Solar Energy Materials and Solar Cells* **2022**, *235*, 111461.
(32) Zhou, Y.-C.; Yang, J.; Bai, L.; Bao, R.-Y.; Yang, M.-B.; Yang, W. Super-Flexible Phase Change Materials with a Dual-Supporting Effect for Solar Thermoelectric Conversion in the Ocean Environment. *J. Mater. Chem. A* **2023**, *11* (1), 341–351.
(33) Zhang, Z.; Zhang, Z.; Chang, T.; Wang, J.; Wang, X.; Zhou, G. Phase Change Material Microcapsules with Melamine Resin Shell via Cellulose Nanocrystal Stabilized Pickering Emulsion In-Situ Polymerization. *Chemical Engineering Journal* **2022**, *428*, 131164.
(34) Kang, L.; Ren, L.; Niu, H.; Lv, R.; Guo, H.; Bai, S. Paraffin@SiO2 Microcapsules-Based Phase Change Composites with Enhanced Thermal Conductivity for Passive Battery Cooling. *Composites Science and Technology* **2022**, *230*, 109756.
(35) Xiong, J.; Sun, Z.; Yu, J.; Liu, H.; Wang, X. Thermal Self-Regulatory Smart Biosensor Based on Horseradish Peroxidase-Immobilized Phase-Change Microcapsules for Enhancing Detection of Hazardous Substances. *Chemical Engineering Journal* **2022**, *430*, 132982.
(36) Kong, L.; Wang, Z.; Kong, X.; Wang, L.; Ji, Z.; Wang, X.; Zhang, X. Large-Scale Fabrication of Form-Stable Phase Change Nanotube Composite for Photothermal/Electrothermal Energy Conversion and Storage. *ACS Appl. Mater. Interfaces* **2021**, *13* (25), 29965–29974.
(37) Wang, Y.; Liu, J.; Zhao, Y.; Qin, Y.; Zhu, Z.; Yu, Z.; He, H. Temperature-Triggered Fire Warning PEG@wood Powder/Carbon Nanotube/Calcium Alginate Composite Aerogel and the Application for Firefighting Clothing. *Composites Part B: Engineering* **2022**, *247*, 110348.
(38) Rathore, P.; Schiffman, J. D. Beyond the Single-Nozzle: Coaxial Electrospinning Enables Innovative Nanofiber Chemistries, Geometries, and Applications. *ACS Appl. Mater. Interfaces* **2021**, *13* (1), 48–66.
(39) Zhang, Y.; Li, T.; Zhang, S.; Jiang, L.; Xia, J.; Xie, J.; Chen, K.; Bao, L.; Lei, J.; Wang, J. Room-Temperature, Energy Storage Textile with Multicore-Sheath Structure Obtained via in-Situ Coaxial Electrospinning. *Chemical Engineering Journal* **2022**, *436*, 135226.
(40) Liu, Z.; Hu, Q.; Guo, S.; Yu, L.; Hu, X. Thermoregulating Separators Based on Phase-Change Materials for Safe Lithium-Ion Batteries. *Adv. Mater.* **2021**, *33* (15), 2008088.
(41) Li, X.; Li, Q.; Hu, J.; Li, R.; Lin, J.; Liu, Y. Core-Sheath Phase Change Fibers via Coaxial Wet Spinning for Solar Energy Active Storage. *Composites Part B: Engineering* **2022**, *247*, 110346.
(42) Wang, R.; He, Y.; Xiao, Y.; Sun, D.; Yang, J.; Qi, X.; Wang, Y. Weavable Phase Change Fibers with Wide Thermal Management Temperature Range, Reversible Thermochromic and Triple Shape Memory Functions towards Human Thermal Management. *European Polymer Journal* **2023**, *187*, 111890.
(43) Ning, C.; Dong, K.; Gao, W.; Sheng, F.; Cheng, R.; Jiang, Y.; Yi, J.; Ye, C.; Peng, X.; Wang, Z.

L. Dual-Mode Thermal-Regulating and Self-Powered Pressure Sensing Hybrid Smart Fibers. *Chemical Engineering Journal* **2021**, *420*, 129650.

(44) Hu, D.; Han, L.; Zhou, W.; Li, P.; Huang, Y.; Yang, Z.; Jia, X. Flexible Phase Change Composite Based on Loading Paraffin into Cross-Linked CNT/SBS Network for Thermal Management and Thermal Storage. *Chemical Engineering Journal* **2022**, *437*, 135056.

(45) Li, Y.; Chen, J.; Cai, P.; Wen, Z. An Electrochemically Neutralized Energy-Assisted Low-Cost Acid-Alkaline Electrolyzer for Energy-Saving Electrolysis Hydrogen Generation. *J. Mater. Chem. A* **2018**, *6* (12), 4948–4954.

(46) Kou, Y.; Sun, K.; Luo, J.; Zhou, F.; Huang, H.; Wu, Z.-S.; Shi, Q. An Intrinsically Flexible Phase Change Film for Wearable Thermal Managements. *Energy Storage Materials* **2021**, *34*, 508–514.

(47) Sun, K.; Kou, Y.; Dong, H.; Ye, S.; Zhao, D.; Liu, J.; Shi, Q. The Design of Phase Change Materials with Carbon Aerogel Composites for Multi-Responsive Thermal Energy Capture and Storage. *J. Mater. Chem. A* **2021**, *9* (2), 1213–1220.

(48) Tang, Z.; Gao, H.; Chen, X.; Zhang, Y.; Li, A.; Wang, G. Advanced Multifunctional Composite Phase Change Materials Based on Photo-Responsive Materials. *Nano Energy* **2021**, *80*, 105454.

(49) Wang, G.; Tang, Z.; Gao, Y.; Liu, P.; Li, Y.; Li, A.; Chen, X. Phase Change Thermal Storage Materials for Interdisciplinary Applications. *Chem. Rev.* **2023**, acs.chemrev.2c00572.

(50) Chen, X.; Tang, Z.; Gao, H.; Chen, S.; Wang, G. Phase Change Materials for Electro-Thermal Conversion and Storage: From Fundamental Understanding to Engineering Design. *iScience* **2020**, *23* (6), 101208.

(51) Hu, X.; Zhu, C.; Quan, B.; Sheng, M.; Wu, H.; Lu, X.; Qu, J. Engineering Robust Multifunctional Composites with Enhanced Electromagnetic Interference Shielding and All-Weather Thermal Management Capability via Simple Layer-by-Layer Assembly. *Chemical Engineering Journal* **2022**, *446*, 137423.

(52) Gong, S.; Sheng, X.; Li, X.; Sheng, M.; Wu, H.; Lu, X.; Qu, J. A Multifunctional Flexible Composite Film with Excellent Multi-Source Driven Thermal Management, Electromagnetic Interference Shielding, and Fire Safety Performance, Inspired by a "Brick–Mortar" Sandwich Structure. *Adv Funct Materials* **2022**, *32* (26), 2200570.

(53) Zhang, Y.; Wu, K.; Fu, Q. A Structured Phase Change Material with Controllable Thermoconductive Highways Enables Unparalleled Electricity via Solar-Thermal-Electric Conversion. *Adv Funct Materials* **2022**, *32* (6), 2109255.

(54) Zhou, Y.-C.; Yang, J.; Bai, L.; Bao, R.-Y.; Yang, M.-B.; Yang, W. Super-Flexible Phase Change Materials with a Dual-Supporting Effect for Solar Thermoelectric Conversion in the Ocean Environment. *J. Mater. Chem. A* **2023**, *11* (1), 341–351.

(55) Meng, Y.; Zhang, L.; Peng, M.; Shen, D.; Zhu, C.; Qian, S.; Liu, J.; Cao, Y.; Yan, C.; Zhou, J.; Qian, T. Developing Thermoregulatory Hydrogel Electrolyte to Overcome Thermal Runaway in Zinc-Ion Batteries. *Adv Funct Materials* **2022**, *32* (46), 2206653.

(56) Luo, J.; Zou, D.; Wang, Y.; Wang, S.; Huang, L. Battery Thermal Management Systems (BTMs) Based on Phase Change Material (PCM): A Comprehensive Review. *Chemical Engineering Journal* **2022**, *430*, 132741.

(57) Lin, Y.; Kang, Q.; Liu, Y.; Zhu, Y.; Jiang, P.; Mai, Y.-W.; Huang, X. Flexible, Highly Thermally Conductive and Electrically Insulating Phase Change Materials for Advanced Thermal Management of 5G Base Stations and Thermoelectric Generators. *Nano-Micro Lett.* **2023**, *15*

(1), 31.
(58) Guo, C.; He, L.; Yao, Y.; Lin, W.; Zhang, Y.; Zhang, Q.; Wu, K.; Fu, Q. Bifunctional Liquid Metals Allow Electrical Insulating Phase Change Materials to Dual-Mode Thermal Manage the Li-Ion Batteries. *Nano-Micro Lett.* **2022**, *14* (1), 202.
(59) Hu, R.; Liu, Y.; Shin, S.; Huang, S.; Ren, X.; Shu, W.; Cheng, J.; Tao, G.; Xu, W.; Chen, R.; Luo, X. Emerging Materials and Strategies for Personal Thermal Management. *Adv. Energy Mater.* **2020**, *10* (17), 1903921.
(60) Tabor, J.; Chatterjee, K.; Ghosh, T. K. Smart Textile-Based Personal Thermal Comfort Systems: Current Status and Potential Solutions. *Adv. Mater. Technol.* **2020**, *5* (5), 1901155.
(61) Li, X.; Sheng, X.; Fang, Y.; Hu, X.; Gong, S.; Sheng, M.; Lu, X.; Qu, J. Wearable Janus-Type Film with Integrated All-Season Active/Passive Thermal Management, Thermal Camouflage, and Ultra-High Electromagnetic Shielding Efficiency Tunable by Origami Process. *Adv Funct Materials* **2023**, *33* (18), 2212776.
(62) Ma, Z.; Zhao, D.; She, C.; Yang, Y.; Yang, R. Personal Thermal Management Techniques for Thermal Comfort and Building Energy Saving. *Materials Today Physics* **2021**, *20*, 100465.
(63) Li, X.; Sun, B.; Sui, C.; Nandi, A.; Fang, H.; Peng, Y.; Tan, G.; Hsu, P.-C. Integration of Daytime Radiative Cooling and Solar Heating for Year-Round Energy Saving in Buildings. *Nat Commun* **2020**, *11* (1), 6101.
(64) Yang, M.; Zhong, H.; Li, T.; Wu, B.; Wang, Z.; Sun, D. Phase Change Material Enhanced Radiative Cooler for Temperature-Adaptive Thermal Regulation. *ACS Nano* **2023**, *17* (2), 1693–1700.
(65) Li, B.-X.; Luo, Z.; Yang, W.-G.; Sun, H.; Ding, Y.; Yu, Z.-Z.; Yang, D. Adaptive and Adjustable MXene/Reduced Graphene Oxide Hybrid Aerogel Composites Integrated with Phase-Change Material and Thermochromic Coating for Synchronous Visible/Infrared Camouflages. *ACS Nano* **2023**, *17* (7), 6875–6885.
(66) Zhou, Y.-C.; Yang, J.; Bai, L.; Bao, R.-Y.; Yang, M.-B.; Yang, W. Flexible Phase Change Hydrogels for Mid-/Low-Temperature Infrared Stealth. *Chemical Engineering Journal* **2022**, *446*, 137463.

Chapter 2

Ultra-flexible, breathable and form-stable phase change fibrous membranes by green electrospinning for personal thermal management

Chapter 2: Ultra-flexible, breathable and form-stable phase change fibrous membranes by green electrospinning for personal thermal management

2.1 Introduction

Thermal comfort is one of the most essential needs for living. In long history of mankind, clothing has always been playing a vital role in maintaining constant temperature of human beings. With the development of social civilization, extensive emphasis has been placed on the artistic and esthetic effect of clothing, while thermal comfort performance is the primary goal to satisfy the requirements of daily life and labor productivity. Under most circumstance, indoor thermal regulation depends heavily on building heating, ventilation, and air conditioning (HVAC) systems at expense of numerous energy consumption accounting for 40% of that of total building, which contribute to about 30% of greenhouse gas emission.[1,2] Therefore, on the face of energy crises and global warming, it is urged to implement thermal regulation by more efficient energy cost strategies.

In decades, many efforts have been devoted to personal thermal management (PTM) textile benefiting from its local temperature controllability in the microclimate next to the body skin instead of the entire indoor space.[3–7] Smart thermal regulating textiles have attracted great attention and have been recognized as fascinating and promising candidates from the perspective of energy saving, responsive thermal regulation and unrestricted application place including indoor and outdoor condition.[8–10]

Thermal energy storage (TES) technology has been extensively explored in advanced PTM textile.[11] Among various TES strategies, phase change material (PCM) is a competitive option in virtue of its high latent heat storage density, stimuli-responsive and reversible thermal regulating capability.[12,13] PCMs are capable of storing and releasing latent energy during phase transition at almost constant temperature. Combining PCMs with clothing can render temporary cooling or heating effect in microclimate to enhance target thermal comfort.[14–16] In order to solve the leakage issue

of PCMs, form-stable PCMs (FSPCMs) have been developed by physical blending or chemical modifying for the advantages of versatile fabrication, desirable dimensions and cost-effectiveness.[17] FSPCMs are mainly composed of functional component and supporting material. However, the universal PCMs such as fatty acid, paraffin and polyethylene glycol (PEG) have intrinsic rigid characteristic, which restrict their application in wearable thermal management scenario. There are mainly three strategies to fabricate flexible PCMs, (i) impregnating PCMs into 3D porous supporting scaffolds by capillary action,[18–26] (ii) encapsulation by micro-shells,[27–30] (iii) constructing molecular structure-based flexible PCMs, the flexibilities come from the intrinsic elasticity of the cross-linked polymeric skeleton.[31–33]

A high thermal management efficiency required that the PCMs can be conformed to the curved surface of human skin.[34] It is well known that electrospinning is a versatile technique for fabricating ultrafine fibers which have high adaptability to the curvature change of the skin.[35] Therefore, phase change fibers (PCFs) by embedding PCMs in ultrafine polymer framework behaves multi-properties of superior flexibility, breathability, shape-stability, tailorability and phase change ability. However, majority of reported electrospinning nanofibers were based on organic precursor solution, where poisonous solvents evaporate directly into the atmosphere during the electrospinning process.[16,36] Furthermore, the excessive residual solvents in electrospun membranes would be serious threats to human health during the long-time service. On the other hand, these electrospinning polymers only dissolvable in toxic organic solvents are also poorly degradable without recycle treatment, causing second environment pollution. Therefore, developing PCFs based on non-toxic solvent with biodegradable material is highly desirable and overwhelming.[37,38]

Herein, PEG was selected as a functional component due to its high thermal enthalpy, adjustable phase change temperature, biocompatibility, cost-effectiveness and ease of chemical modification. Poly (vinyl alcohol) (PVA) is a kind of semicrystalline polymer, which was employed as electrospinning template polymer to construct a flexible framework, benefiting from its excellent spinnability, biodegradability, nontoxicity and water-solubility. The sacrificial H-bond provides a certain interaction for the insertion

of PEG. Since most of the biodegradable material have weak mechanical properties，[39] and the universal low thermal conductivity of PCMs, [15] a reinforcing additive carbon nanotubes (CNTs) with high thermal conductivity had been introduced into the matrices to promote tensile strength and heat transfer rate. In addition, the intrinsically hydrophilicity of waterborne polymers will suffer water-absorbing, swelling and disintegrating when contact with water. The practical strategy previously reported is chemical crosslinking, which can improve water resistance effectively, such as coating crosslinking and in situ crosslinking. However, the coating crosslinking would inevitably block pores of fibrous membranes, and in situ crosslinking is prone to extensively constrain the movement of PEG chains. In contrast, glutaraldehyde (GA) vapor crosslinking is a mild and biocompatible modification technique, which has been widely used to crosslink hydroxyl-containing polymers, the reactive vapor can penetrate to the porous membrane bulk for effective but not excessive crosslinking. Hence, glutaraldehyde (GA) vapor surface-crosslinking was utilized as a facile way to realize moderate confinement of PEG and maintain the porous structure, and finally achieved the tradeoff between form-stability and thermal performance of phase change membranes. In this work, PEG/PVA/CNTs composite membranes were prepared using uniaxial green electrospinning technology combined with surface crosslinking treatment. This novel concept of eco-friendly electrospinning exhibited marvelous potentiality to fabricate two-dimensional flexible phase change material for thermal regulation.

2.2 Experimental section

2.2.1 Materials

Poly (vinyl alcohol) (PVA, n=3500, partially hydrolyzed), poly (ethylene glycol) (PEG, Mn=1000), glutaraldehyde (GA, 25% w/v), Hydrochloric acid solution (HCl) and ammonium hydroxide ($NH_3 \cdot H_2O$) were obtained from FUJIFILM Wake Pure Chemical Co., Ltd., Japan. Carboxylic carbon nanotubes (CNTs) were purchased from Nanjing Xinfeng Nano Material Technology Co., Ltd., China, and their length and

diameter were 10-20 μm and 10-30 nm, respectively. Distilled water was prepared by our laboratory. All these materials were used without any further treatments.

2.2.2 Preparation of solutions for electrospinning

PVA power were dissolved into absolute distilled water and stirred at 90 °C for 6 h to obtain 10 wt% aqueous solution. PVA/PEG solutions were obtained by adding PEG at different PVA/PEG mass ratios of 100/0, 70/30, 60/40, 50/50, 45/55, 40/60. Moreover, the PVA/PEG/CNTs spinning solutions were prepared with fixed PVA/PEG mass ratio of 45/55, and the concentration of CNTs kept a gradient rise (0, 0.5, 1, and 1.5 wt%) with respect to the PVA content.

2.2.3 Fabrication of fibrous membranes by electrospinning

Green fibrous membranes were constructed utilizing electrospinning machine assembled by our lab. The prepared solutions were poured into a plastic syringe with 21G steel needles, which were pumped out at a constant velocity of 1 mL/h. The applied voltage was 12~15kV, and the distance between the needle tip and a grounded rotator was 15 cm. During spinning process, the temperature and relative humidity (RH) were controlled at 25 ± 3 °C and 30 ± 5 %, respectively. The obtained fibrous membranes with various PVA/PEG mass ratio were denoted as PCFy, where y present the mass ratio of PEG, and PVA/PEG/CNTs membranes were referred to as C_xPCFy, where x is the content of CNTs.

2.2.4 Surface crosslinking treatment

A certain amount of GA aqueous solution was poured into a desiccant tank with a supporting mesh sieve, prepared nanofibrous membranes were placed on the upper portion in the sealed vessel at room temperature for 24 h. Due to the volatility of glutaraldehyde, acetal reaction performed in saturated vapor of GA. Therefore, hydrophilic groups of PVA and PEG reduced, and three-dimensional polymer network is constructed in intra-fibers and inter-fibers. Composite phase change nanofibrous membranes treated by crosslinking were defined as CC_xPCFy.

2.2.5 Characterization

The surface morphology and structure features were determined using a scanning electron microscopy (SEM, JSM-6010LA, JEOL, Japan). Fiber diameters were

investigated by the software Image J, and at least 50 fibers were analyzed. The porous structure including pore size distribution, maximum pore diameter (D_{max}), and mean pore diameter (D_{mean}) of nanofibrous membranes was determined via capillary flow porometer (CFP-1200AI, PMI, America). Porosity was examined by the liquid displacement method with hexane as testing liquid and was calculated as follows: [38]

$$\text{Porosity} = [(V_1 - V_3)/ (V_2 - V_3)] \times 100\% \quad (1)$$

Where V_1 is the initial volume of hexane, V_2 is the total volume of hexane after immersing the corresponding membrane, and V_3 is the volume of residual hexane after removal of the membrane.

The chemical structures of the composite fibers were examined using a Fourier-transform infrared spectrophotometer (FTIR-6600, Jasco, Japan) over the wavenumber range of 400-4000 cm^{-1}. The crystalline properties of prepared membranes were verified using an X-ray diffraction (XRD, MiniFlex300, Rigaku, Japan). The breaking tensile strength and elongation of nanofibrous membranes were characterized with a tensile tester (MCT-2150, A&D, Japan) at a speed of 10 mm/min. Thermal conductivity was evaluated using a thermal contact tester (KES-F7, Kato Tech, Japan). The temperature evolution was recorded by a thermocouple (KE331L, CHINO, Japan) and an infrared thermal imaging camera (Testo 875-2i, German). The thermal properties were further investigated by differential scanning calorimetry (DSCvesta, Rigaku, Japan) in nitrogen flow (50mL/min). The samples were heated or cooled between -10 to 70 °C at a heating/cooling rate of 10 °C /min.

2.3 Results and discussion

2.3.1 Strategy of preparing ecofriendly phase change fibrous membranes

The fabricating processes are schematically presented in Fig. 2-1. We designed the flexible thermal regulating fibrous membranes based on the following principles: (i) the electrospinning process should be green and ecofriendly without toxic solvent. (ii) the fibrous membranes should possess interconnected porous structure for allowance of air transmission. (iii) the obtained phase change nanofibers should have suitable phase

change temperature and good stability in phase transition. In this work, the first criterion was achieved by the water solubility and biodegradability of PVA and PEG. Besides, the interconnected channels were constructed by electrospinning technology, and final flexible membranes were obtained. Furthermore, PEG1000 has an appropriate phase change temperature and high energy density. Most importantly, hydrogen bonding and chemical crosslinking endow the prepared phase change membranes with stable chemical structure to avoid leakage issue.

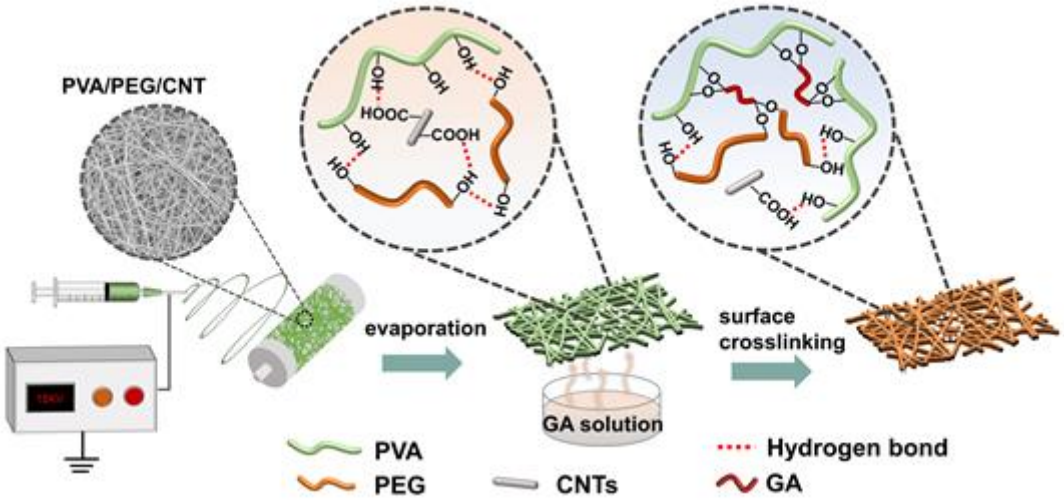

Fig. 2-1. A schematic illustration of the preparation procedure of eco-friendly phase change nanofibrous membranes

2.3.2 Morphology and structure characterizations

Fig. 2-2 (a-f) showed the representative SEM images of PVA/PEG nanofibrous membranes, presenting porous structure with fibers oriented randomly, that could serve as interconnected pathways for air to transmit. The nanofibers in pristine PVA membranes displayed smooth and uniform fiber surface at a diameter of 0.41 μm. With the increasing content of PEG, the diameter of nanofiber obviously increased to 1.23 μm (PCF55), ascribed to the enhanced concentration of spinning solution resulting from the addition of PEG. On the other hand, the membranes presented adhesion structures at the intersecting nanofibers with increasing the content of PEG, due to the incomplete evaporation of solvent, because the strong hydrogen bonding between PVA/PEG and solvent (water) suppressed the volatilization of water . [38] As Fig. 2-2 (f), when the mass ratio of PEG reached to 60 wt%, the membrane exhibited inferior morphology with

severe adhesion and large diameter deviation. Given the consideration of high thermal storage capacity, more PEG content should be contained, the maximum mass ratio of PEG was supposed as 55 wt% for optimal proportion. Subsequently, with the introduction of CNTs, the slightly reduced diameters of nanofibers were observed in Fig. 2-3 (a-c), ascribed to the enhanced conductivity of electrospinning solutions, which boosted the stretching effect of jet stream, leading to the formation of thin fibers. [40] Simultaneously, extensive CNTs also resulted higher viscosity of the spinning solution, causing the fiber diameter to increase again. Additionally, the morphologies of the CC_1PCF55 barely changed after the surface chemical crosslinking process, except for a slight increase in their average diameters (Fig. 2-4 (a, b)). As shown in Fig. 2-4 (c), C_1PCF55 membranes possessed a fluffy structure with a thickness of 40.6 μm, after crosslinking or grafting reaction with glutaraldehyde, CC_1PCF55 membranes displayed a compact structure with a thickness of 25.2 μm. Because the original loosely and randomly stacked fibers possessed a fluffy structure, then the crosslinking behavior produced lots of adhesive bonds connecting the adjacent fibers into a tight and dense structure, which caused a lower thickness of the resultant membrane.

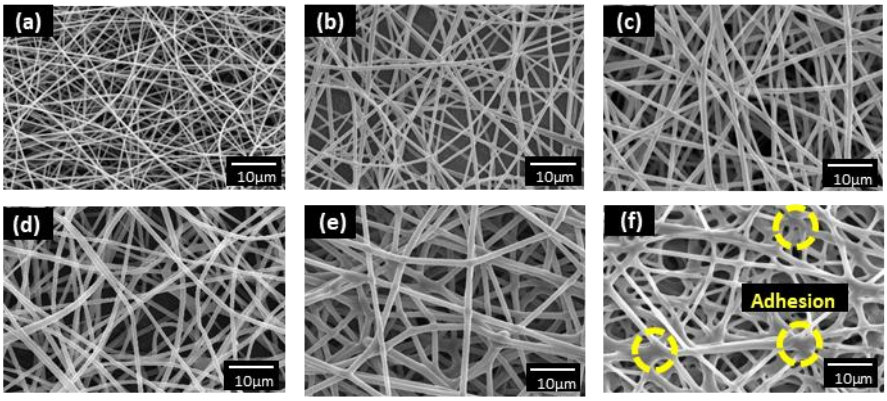

Fig. 2-2. SEM images of (a) PVA, (b) PCF30, (c) PCF40, (d) PCF50, (e) PCF55, (f) PCF60.

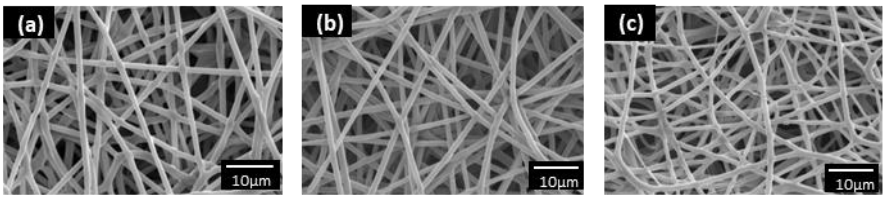

Fig.2-3. SEM images of (a) $C_{0.5}$PCF55, (h) C_1PCF55, (i) $C_{1.5}PCF55$.

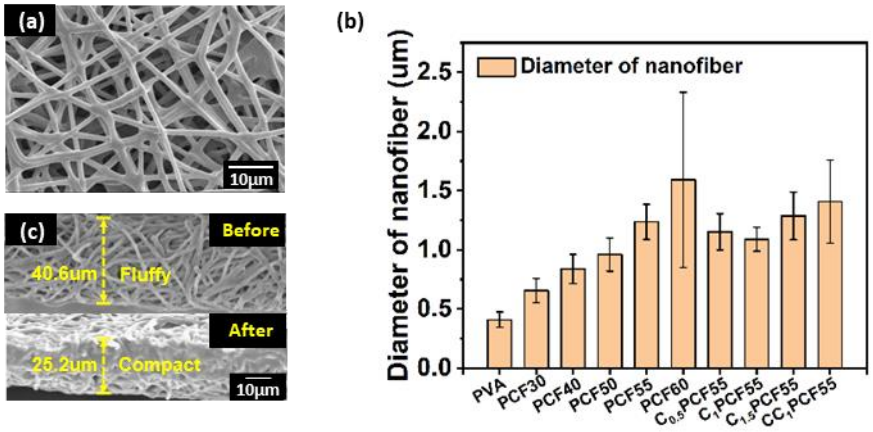

Fig.2-4. (a) SEM image of CC_1PCF55 fibrous membrane, (b) Fiber diameter of prepared fibrous membranes. (c) Cross-sectional SEM images of C_1PCF55 before and after surface crosslinking treatment.

2.3.3 Mechanical properties

Mechanical performance is a very critical property in practical application, because it is inevitable to be stretched for the fibrous membranes in service. The prepared CC_1PCF55 membrane could be folded, curled and stretched from 25 mm to 92 mm without any breakage at room temperature, highlighting excellent flexibility and strength (Fig. 2-5 (a-f)). The flexibility of most reported composite flexible PCMs would drop sharply in crystalline state. [18,20] As shown in Fig. 2-5 (g), benefiting from the admirable high aspect ratio of the ultrafine fibers, the prepared fibrous membranes showed the favorable bending and twisting deformation at 5 °C, which is below the crystallization temperature of PEG (20.2 °C), as well as the ambient temperature of 41°C which is above the melting point of PEG (39.8 °C). The remarkable foldability and flexibility in a wide temperature range capacitate them unique compatibility with the curved human body surface, which is promising in smart wearable textiles for individual thermal regulation.

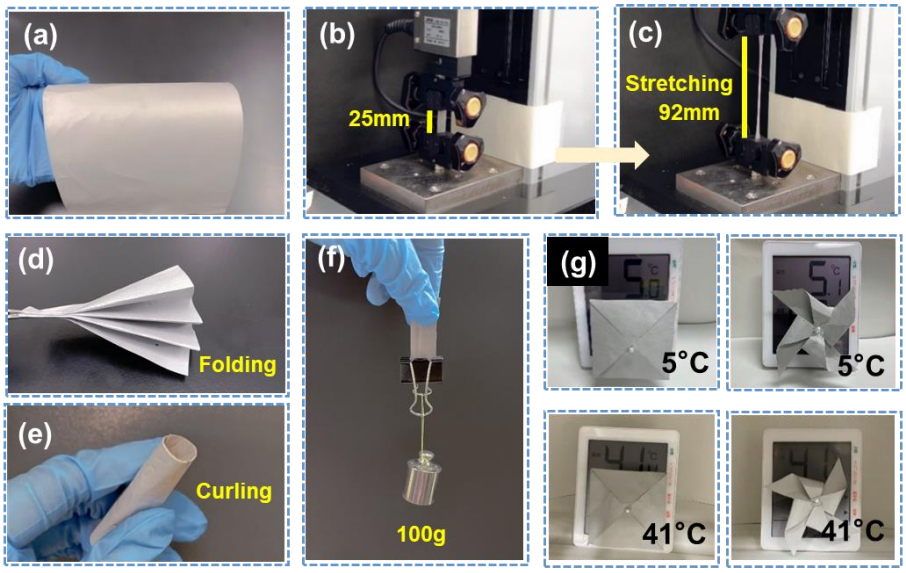

Fig.2-5. (a-f) Optical images showing the flexibility of the CC_1PCF55 membranes: it can be stretched, folded, curled without damage. (g) The reversible deformation and softness of CC_1PCF55 membranes at 5 °C and 41 °C.

Fig. 2-6 showed the tensile stress-strain curves of the obtained membranes, and it could be observed that the tensile property was affected dramatically by the components and structure of nanofibers. The ultimate strength and strain of the pure PVA membrane was measured as 3.72 MPa and 354%, respectively. While that for PCF55 was measured to be 2.48 MPa and 430%, respectively. It is obvious that the integration of PEG has negative effect on tensile strength of resultant composite membranes, which could be ascribed to the reduced entanglement between polymer molecular chains, due to the considerable short molecular chains of PEG compared to PVA. CNTs have been widely applied as one of the optimal reinforcing nanofillers, due to its low density, high strength, superior thermal conductivity, and thermal stability. Then the effect of CNTs content on mechanical properties of composite membranes has been investigated. As the proportion of CNTs increased to 1wt%, the breaking strength improved to 3.34 MPa with a high elongation of 346%, indicating that the strength loss due to the addition of PEG was compensated. Nevertheless, for the $C_{1.5}PCF55$ membranes, the agglomeration of excessive CNTs resulted in a slight decline in tensile strength as well as breaking elongation. [41] Therefore, C_1PCF55 membrane presented the best equilibrium between

heat storage capability and mechanical performance and it was selected for further crosslinking treatment. CC_1PCF55 membrane exhibited improved breaking strength compared to C_1PCF55 membrane. Because fibers in untreated membranes (C_1PCF55) arranged randomly and overlapped with each other, which are prone to slide at lower tensile strength. [38] Benefiting from the numerous bonding joints among adjacent fibers, the tensile strength of CC_1PCF55 membranes significantly increased to 3.45 MPa, and the elongation slightly decreased to 262 %, which still maintained favorable mechanical properties.

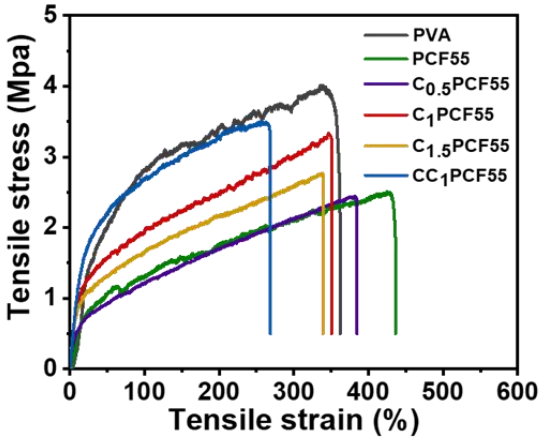

Fig.2-6. Tensile stress–strain curves of the corresponding membranes.

2.3.4 Breathable performance

Air permeability is a crucial property for wearing comfort of PTM textile, The unique open nano-micro channels of fibrous membranes by electrospinning technology allowed air to penetrate effectively. Therefore, we evaluated the porous structure of phase change membranes and investigated the impacts of crosslinking treatment on porous morphology. After surface crosslinking, the porous structure exhibited a left shift of pore size distribution and a slightly reduction of porosity, indicating that the porous structure was well reserved (Fig.2-7 (a, b)). In addition, to evaluate the air permeability of CC_1PCF55 membrane, a glass bottle containing HCl was covered by the composite membrane, then another uncovered glass bottle with $NH_3 \cdot H_2O$ was moved close to it. A large amount of white smoke emerged instantly, confirming the excellent breathable properties of the phase change membranes after crosslinking

treatment (Fig.2-7 (c)).

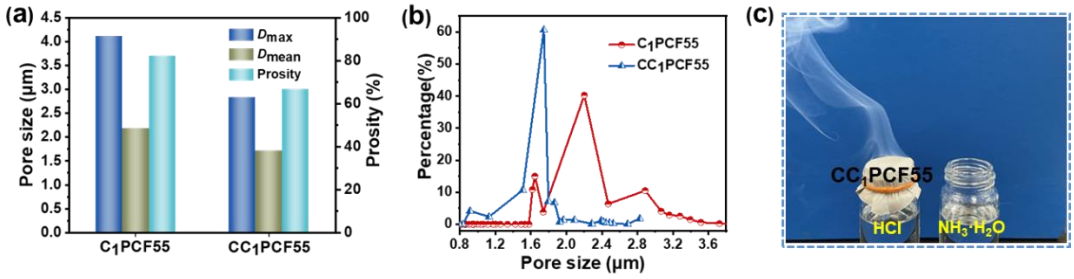

Fig.2-7. (a, b) The porosity and pore size distribution of the corresponding membranes. (c) Breathability confirmation.

2.3.5 Water resistance properties

In general, glutaraldehyde vapor was introduced as a crosslinking agent to enhance the mechanical properties of membranes, the active aldehyde groups at both ends of glutaraldehyde can react with the hydroxyl groups from PEG and PVA under moderate conditions. Crosslinking post treatment can also prevent membranes from swelling and deformation when contact with water. [38,39,42] As shown in Fig. 2-8 (a), the color of the composite membrane changed from grey to black when exposed to water due to the existence of CNTs, and after water immersion for 6 h, the membrane remained the previous morphology, confirming the transform from water-solubility to hydro stability. FT-IR measurements (Fig. 2-8 (b)) indeed confirmed the acetal reaction occurred. The characteristic absorption peak at 3408 cm^{-1} is assigned to the stretching vibration of -OH groups. The peaks observed at 948 and 2878 cm^{-1} are ascribed to the typical stretching vibrations of $-CH_2$ groups, and the peak at 1458 cm^{-1} correspond to the bending vibration of $-CH_2$ groups. Meanwhile, the peaks at about 1250 and 1103 cm^{-1} are attributed to the C-O stretching vibration. It can be seen that the absorption peak of -OH (3408 cm^{-1}) became weaker and the band of C-O-C (around 1103 cm^{-1}) became stronger after vapor crosslinking, demonstrating that the acetal crosslinking reaction was successfully conducted.

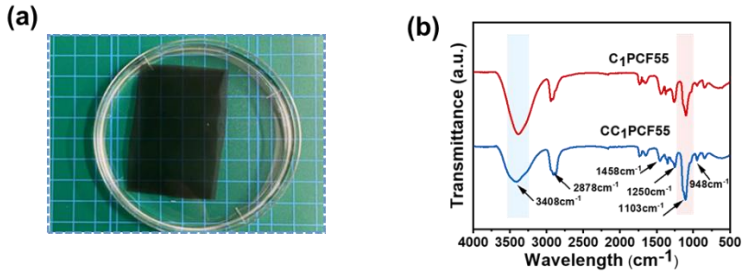

Fig.2-8. (a) Optical images of CC_1PCF55 membranes immersed in water for 6 h. (b) FT-IR spectrum of C1PCF55 and CC1PCF55 membranes.

2.3.6 Thermal behavior and properties

2.3.6.1 Thermal conductivity

The thermal conductivity is one of the crucial properties of PCMs, because high thermal conductivity facilitates energy conversion in phase transition. As Fig. 2-9 presented, the thermal conductivity of $C_{1.5}PCF55$ was increased by 40.4% compared to that of PCF55, it indicated that thermal conductivity of composite membranes can be improved by integration of a small amount of CNTs. The enhanced thermal conductivity is attributed to the heat transfer "bridges" conducted with CNTs, which provide thermal conduction channels for composite phase change membranes. [43-45] On the other hand, the intrinsic fluffy and porous structure of the fibrous membranes may be a vital factor that restrict the improvement of thermal conductivity of the prepared phase change composite membranes. After crosslinking, the thermal conductivity of CC_1PCF55 increased to 0.06492 W/m·K, higher than the untreated one (C_1PCF55). Because the crosslinking treatment connected the adjacent fibers and constructed more heat transfer networks. Besides, the denser structure after crosslinking contained less still air which is poor conductor for heat transmission.

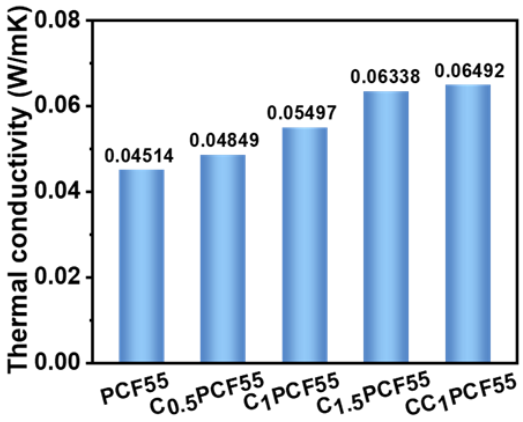

Fig.2-9. Thermal conductivity of corresponding membranes.

2.3.6.2 Phase transition performance and thermal stability

The crystalline behavior was further investigated by the XRD technique, Fig. 2-10 (a) showed the XRD patterns of PEG, C_1PCF55, CC_1PCF55. Two strong and sharp diffraction peaks of pristine PEG around 19.2° and 23.4° are corresponding to the lattice planes of (120) and (132), [32] respectively, indicating the good crystalline properties resulted from linear and symmetric polyether chain, where inter-molecular bonds are prone to be formed and broken during the reversible phase transition. The XRD pattern of the C_1PCF55, CC_1PCF55 exhibits two diffraction peaks at the same location with pure PEG, confirming that PEG worked as a functional component after integrated into fibrous membranes. However, the weaker diffraction peak intensity indicates reduced crystallization of composite nanofiber owing to the restriction of hydrogen bonding and surface covalent crosslinking interaction, which is potential to restrict the PEG segment from changing into liquid and exhibit a macroscopic solid-solid transition phenomenon. It can also be illustrated in Fig. 2-10 (b), The phase change behavior of PEG is bound in the framework of PVA. Due to the steric hindrance effect, the free movement of PEG was restricted, which decreased the phase change enthalpy of samples. On the other hand, sacrificing a part of phase change enthalpy ensured the shape stability in phase change transition process.

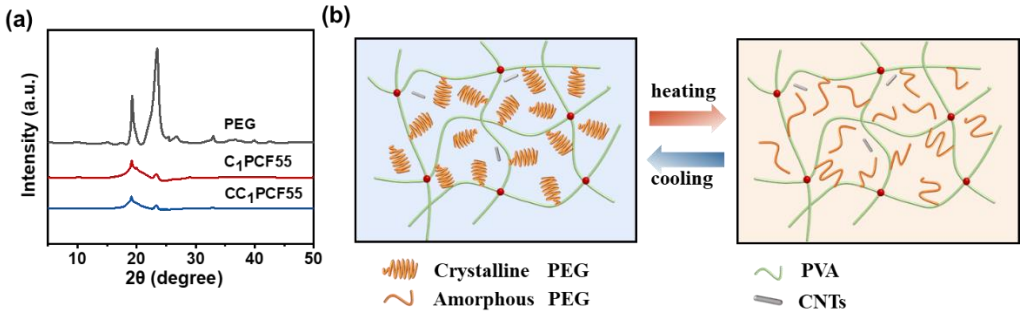

Fig.2-10. (a) XRD patterns of PEG, C_1PCF55, CC_1PCF55. (b) The schematic of reversible phase change mechanism of prepared membranes.

The shape stability was evaluated by placing pure PEG and CC_1PCF55 membrane on a hot plate at 50 °C and the variation of samples was monitored in the process of leaking test (Fig. 2-11). After being heated, the white PEG gradually transfers to transparency, and subsequently, melted and flowed after 15 minutes. While CC_1PCF55 can maintain its original shape without any leakage trace found during the entire heating process. The form-stable ability is attributed to the hydrogen bonds and covalent strength between PEG and polymer framework, which provides abundant physical or chemical effect to prevent the fluidity. [31] It is understandable that the PEG chains are cross-linked in PVA/CNTs matrix and constructed a three-dimensional and cross-linked network by the acetal joints. Therefore, the facile prepared fibrous membranes are potential to be employed in thermal management, not only in personal textile thermal management, but also in electric device thermal controlling system, such as buffering the temperature rise of battery or working as the thermal protective media for another flexible electron device.

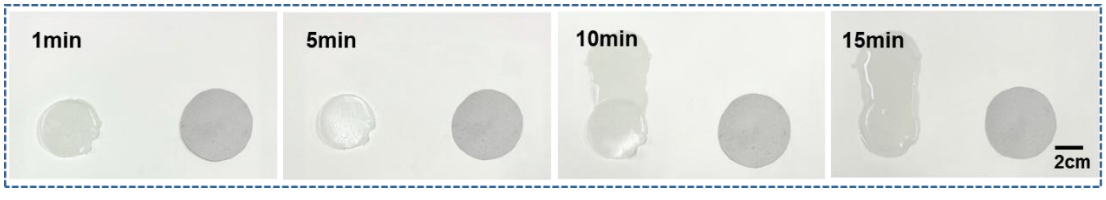

Fig.2-11. Shape stability of PEG and CC_1PCF55 on a hot plate at 50 °C.

2.3.6.3 Phase change temperature and thermal storage capacity

Phase transition behavior is of crucial importance in the perspective of the actual thermal management application. Phase change temperature and thermal energy storage capacity of the membranes integrated with different content of CNTs was investigated by DSC test. As shown in Fig. 2-12 (a, b), PEG and all composite membranes exhibited the same characteristic curve with two endothermic/exothermic peaks in the heating and cooling period, ascribed to the reversible phase transition. The exothermic peak of PEG is attributed to the homogeneously nucleate crystallization, indicating the liquid-solid phase transition. The endothermic peak of PEG is corresponded to the phase change from ordered crystalline phase to disordered amorphous state, representing the solid-liquid transition. The melting/freezing temperatures (T_m/T_c) and melting/freezing latent heat (ΔH_m/ΔH_c) were measured to be 39.8/20.2 °C and 136.1/133.3 J/g for pure PEG, respectively. Melting/freezing latent heat represent the released/absorbed energy in heating/cooling process, which could intuitively reflect the bidirectional thermal regulation capabilities.

The DSC curve of composite membranes demonstrated their admirable thermal enthalpy and appropriate melting/freezing points around the range of the human comfortable temperature, which endowed the fibrous membranes with energy storing/releasing performance for active and reversible thermoregulation. However, melting/freezing latent heat of all the resulted phase change membranes are lower than pure PEG, because only PEG in composite fibers is responsible for phase transition in the temperature range. The introduction of PVA and CNTs reduced the mass proportion of PEG, and the content of PEG was limited by its weak spinnability, while PVA served as a template polymer.

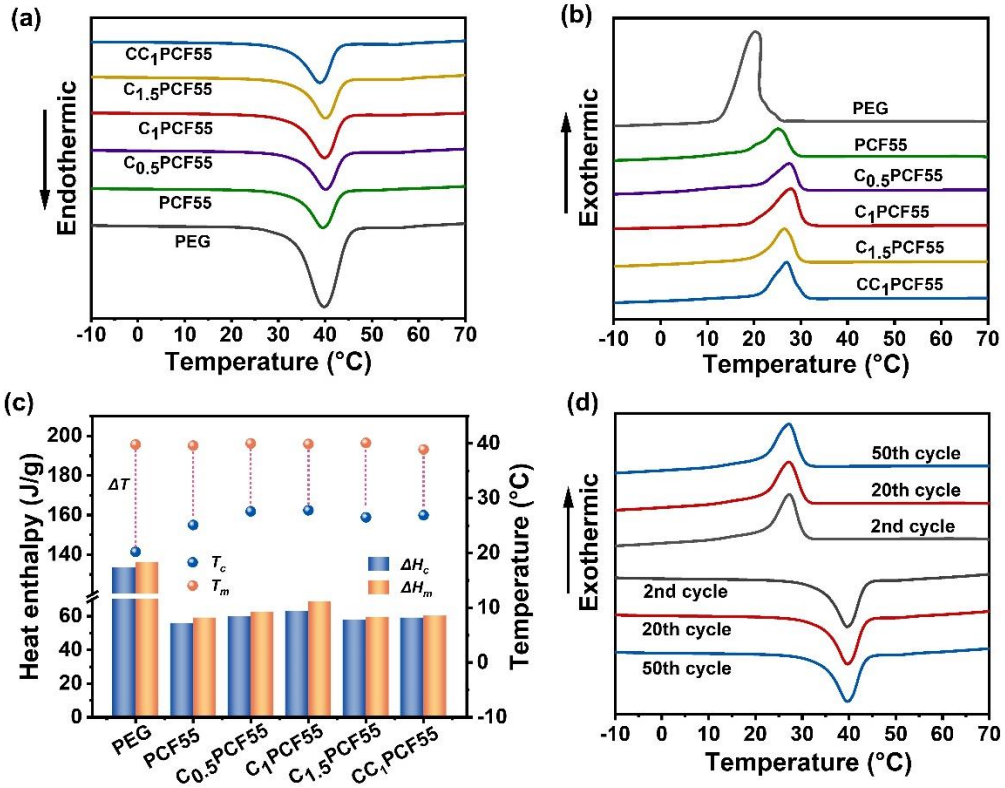

Fig. 2-12. Phase change behaviors of prepared composite membranes. DSC curves of PEG and corresponding phase change membranes in (a) heating process and (b) cooling process. (c) Melting/freezing temperatures (T_m/T_c) and melting/freezing latent heat of PEG and composite membranes. (d) DSC heating and cooling curves of CC_1PCF55 membrane with cycling of 2, 20, 50 times.

As shown in Fig. 2-12 (c), the melting/freezing enthalpies of composite membranes were improved gradually as the CNTs content increased to 1 wt%, that because CNTs served as a heterogeneous nucleation agent which facilitated the phase transition of PEG. [38] Besides, the melting/freezing enthalpies presented a slight decline as the CNTs content reached to 1.5 wt%, because too much CNTs might hinder the movement of PEG and restricted them from growing up as larger crystals. [43] Furthermore, supercooling degree is a significant parameter that should be considered in practical applications. Supercooling extent (ΔT) was calculated from the difference between the melting and crystallization temperatures ($\Delta T = T_m - T_c$). [26] The composite membranes displayed a less supercooling degree, resulting from the up shift of cooling temperature

compared to pure PEG. The potential reasons may be summarized as follows: 1) PVA skeleton and CNTs filler afford rich sites for the heterogenous nucleation of PEG. 2) CNTs constructed thermal conductive bridges to facilitate heat transfer. These factors resulted in a decreased nucleation barrier that PEG was required to overcome to form stable nucleus, therefore crystallization temperature shifted to a higher temperature, generating a reduced supercooling extent.

The actual melting/freezing enthalpies of C_1PCF55 and CC_1PCF55 are 68.7 J/g, 63.2 J/g and 60.1 J/g, 59.1 J/g, which were slightly below their theoretical enthalpy (74.9 J/g, 73.3 J/g) calculated from the weight ratio of PEG (55 wt%) in electrospinning solution. The reduction of thermal enthalpy may be ascribed to the insufficient time for PEG to form highly ordered and well aligned crystalline architecture in solvent evaporation of electrospinning. [40] Apart from this, the free movement of the PEG segment is sterically confined within the PVA network owing to the hydrogen bond between polar groups of PVA and PEG, as well as the covalent crosslinking by acetal junctions, resulting in the depressed crystallization degree of PEG ultimately.

Tab. 2-1. Melting enthalpy and temperature of previous phase change fibers

PCFs	Solvents	T_m (°C)	ΔH_m (J/g)	Reference
PMMA@PW	Toluene/DMF	47.0	58.2	[46]
PS/CP/CS	DMF	24.7	53.7	[47]
PAN/PEG1500/CNTs	DCM/TFA	46.2	44.0	[48]
PET/PTA/CNTs	TFA/DCM	30.4	47.0	[41]
PA6/PEG1000/ TiO_2	Formic acid	36.6	51.1	[49]
PVDF/PVB@ octadecane	Acetone/DMAc	29.0	62.7	[50]
PU@PEG6000	DMF/THF	53.9	60.4	[51]
PHBV/PEG10000	DMF	57.6	62.8	[52]
PVP/PEG/Al_2O_3	Ethanol	47.4	54.3	[53]
Silk/n-octadecane	Water	23.0	40.7	[54]
PVA/PEG1000/CNTs	Water	38.9	60.1	This work

ΔH_m: melting enthalpy, PMMA: polymethyl methacrylate, PW: paraffin wax, PS: polystyrene, CP: capric-palmitic acid, CS: capric-stearic acid, PAN: polyacrylonitrile, PET: polyethylene terephthalate, PTA: poly(tetradecyl acrylate), TFA: trifluoroacetic acid, DCM: dichloromethane, PA6: polyamide 6, PVDF: poly(vinylidene fluoride), PVB: poly(vinyl butyral), PU: polyurethane, PHBV: poly(3-hydroxybutyrate-co-3-hydroxy valerate), PVP: polyvinyl pyrrolidone.

For comprehensively understanding of the advantage of PVA/PEG/CNT nanofibrous membranes prepared in this work, the solvents of precursor solution, melting temperature and thermal energy storage properties by electrospinning in previous reports were compared, as presented in Table 2-1. Obviously, most majority of previously literatures utilized organic solution electrospinning to fabricate continuous nanofibers, such as DMF, DMAc and acetone. Only a few groups have contributed effort to develop green nanofibrous phase change membranes. Moreover, the latent heat in this work is comparable with the one based on organic electrospinning solution, but the distilled water is much cheaper than organic solvent. It should also be noted that the phase change temperature range of CC_1PCF55 (26.9 °C to 38.9 °C) approach the daily surrounding temperature and threshold temperature for human comfort. In the virtue of the appropriate phase change temperature, considerable thermal energy storage density and sustainable characteristic, the composite membranes in our work are irreplaceable in low temperature thermal management field, especially in personal thermal management.

2.3.6.4 Cycle test

To investigate the stability of the phase change membranes, heating/cooling cycles of CC_1PCF55 were conducted in a thermostatic oven between 20 °C and 50 °C. The phase change performance of the CC_1PCF55 was investigated by DSC after 2, 20, 50 cycles. It is observed in Fig. 2-12 (d), the phase change temperature of CC_1PCF55 kept almost unchanged in heating and cooling process after 50 cycles. The original melting phase change enthalpy is 60.1 J/g, which is changed to 58.2 J/g after 50 cycles, just about 3.2% lower than the initial value. And the crystallization enthalpy slightly changed from 59.1 J/g to 58.0 J/g. These results demonstrated that the composite

membranes had a good thermal cycle performance assigned to the crosslinking polymer skeleton, which confirmed its potential in the application of personal thermal management.

2.3.6.5 Thermal regulation behavior

The high phase change enthalpy and appropriate phase change temperature impart electrospun composite fibrous membranes with admirable thermal regulation properties. An IR camera and a thermocouple were employed to record the temperature evaluation of CC_1PCF55 as well as the pure PVA membrane as a control. PVA and CC_1PCF55 were exposed in a simulated exterior environment at the temperature of 20 °C and 50 °C. Fig. 2-13 (a, b) described the infrared thermal images of samples in heating and cooling process. PVA membranes showed a rapid color change from blue to red under the heating process and opposite color evolution under cooling process. While the phase change membranes displayed a slower color variation indicating a delayed thermal response at the same heating and cooling stages. Fig. 2-13 (c, d) showed surface temperature curve. It is found that the temperature curve of PVA showed a distinct sharp increasing and a decline trend before thermal equilibrium. While temperature evolution of CC_1PCF55 undergo three stages. In the first stage, temperature rise rapidly. Then an obvious “platform” appears near the melting point indicating a large amount of latent heat absorbed. Subsequently, the temperatures rise rapidly again, revealing that the phase transition have completed. Similarly, a temperature “platform” appeared near the crystalizing zone during the cooling stage, indicating the release of latent heat. These results confirmed the effective thermal regulation capability of the phase change membranes and verified their great potential in thermal management field, such as temperature controlling of textiles, batteries, buildings, and so on.

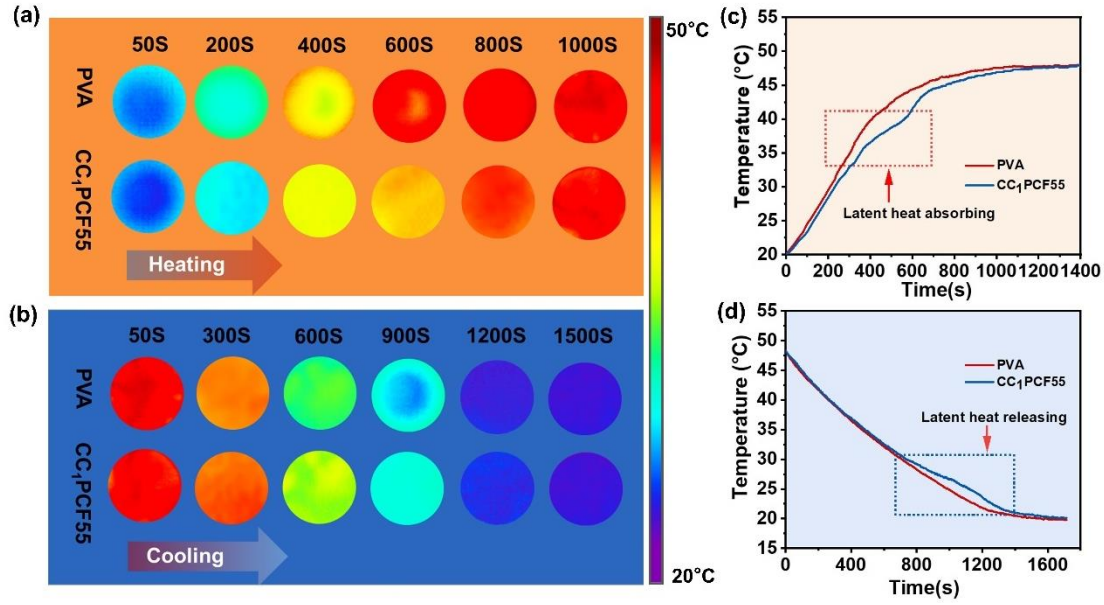

Fig. 2-13. Representative thermal images of PVA and CC_1PCF55 membrane recorded by IR camera in (a) heating and (b) cooling process. Temperature evolution plots of corresponding membranes in (c) heating and (d) cooling process.

2.4 Conclusion

In summary, we presented a green strategy to construct an eco-friendly and degradable micro-nanofibrous membranes with responsive reversal thermal regulation properties via electrospinning and surface crosslinking. Biocompatible and biodegradable polymer PVA and PEG were employed as supporting matrix and functional component, respectively, and toxic organic solvent were excepted from electrospinning process, therefore, the issue of poisonous solvent residue or recovery challenges were also avoided. Subsequently, glutaraldehyde vapor was grafted or crosslinked on the surface of ultrafine fibers to block hydrophilic groups. The mass ratio of PEG can reach to 55 wt% and realized an optimal melting/freezing enthalpy of 60.1/59.1 J/g, which is comparable to these of toxic solvent-based electrospun membranes. Furthermore, high conductive CNTs were integrated into composite fibers to enhance thermal conductivity by 40.4% than the blank one. Besides, the phase change fibrous membranes possessed excellent tensile elongation of 262%, overcoming the intrinsic brittleness of traditional PCMs, and exhibited remarkable shape

tailorability and foldability. Considering the favorable flexibility, breathability and reasonable phase change enthalpy, the resultant phase change fibrous membranes exhibit great potential for further application such as personal thermal management textile and thermal-regulated electric system.

Reference

(1) Farooq, A. S.; Zhang, P. Fundamentals, Materials and strategies for personal thermal management by next-Generation textiles. *Compos. part A-appl s.* **2021**, *142*, 106249, DOI: 10.1016/j.compositesa.2020.10624

(2) Peng, Y.; Cui, Y. Advanced textiles for personal thermal management and energy. *Joule* **2020**, *4* (4), 724–742, DOI: 10.1016/j.joule.2020.02.011

(3) Zeng, S.; Pian, S.; Su, M.; Wang, Z.; Wu, M.; Liu, X.; Chen, M.; Xiang, Y.; Wu, J.; Zhang, M.; Cen, Q.; Tang, Y.; Zhou, X.; Huang, Z.; Wang, R.; Tunuhe, A.; Sun, X.; Xia, Z.; Tian, M.; Chen, M.; Ma, X.; Yang, L.; Zhou, J.; Zhou, H.; Yang, Q.; Li, X.; Ma, Y.; Tao, G. Hierarchical-morphology meta fabric for scalable passive daytime radiative cooling. *Science* **2021**, 373, 692-696, DOI: 10.1126/science.abi5484

(4) Pakdel, E.; Naebe, M.; Sun, L.; Wang, X. Advanced functional fibrous materials for enhanced thermoregulating performance. *ACS Appl. Mater. Interfaces* **2019**, *11* (14), 13039–13057, DOI: 10.1021/acsami.8b19067

(5) Hu, R.; Liu, Y.; Shin, S.; Huang, S.; Ren, X.; Shu, W.; Cheng, J.; Tao, G.; Xu, W.; Chen, R.; Luo, X. Emerging materials and strategies for personal thermal management. *Adv. Energy Mater.* **2020**, *10*, 1903921, DOI: 10.1002/aenm.201903921

(6) Lan, X.; Wang, Y.; Peng, J.; Si, Y.; Ren, J.; Ding, B.; Li, B. Designing heat transfer pathways for advanced thermoregulatory textiles. *Materials Today Physics* **2021**, *17*, 100342, DOI: 10.1016/j.mtphys.2021.100342

(7) Fang, Y.; Chen, G.; Bick, M.; Chen, J. Smart textiles for personalized thermoregulation. *Chem. Soc. Rev.* **2021**, *50*, 9357–9374, DOI: 10.1039/D1CS00003A

(8) Guo, Z.; Sun, C.; Wang, J.; Cai, Z.; Ge, F. High-performance laminated fabric with enhanced photothermal conversion and joule heating effect for personal thermal management. *ACS Appl. Mater. Interfaces* **2021**, *13*, 8851–8862, DOI: 10.1021/acsami.0c23123

(9) Liu, X.; Jin, X.; Li, L.; Wang, J.; Yang, Y.; Cao, Y.; Wang, W. Air-permeable, multifunctional, dual-energy-driven MXene-decorated polymeric textile-based wearable heaters with exceptional electrothermal and photothermal conversion performance. *J. Mater. Chem. A* **2020**, *8*, 12526–12537, DOI: 10.1039/D0TA03048A

(10) Wu, H.; Zhao, L.; Si, Y.; Zhang, S.; Yu, J.; Ding, B. Ultralight and superelastic fibrous sponges with effective heat preservation and photo-thermal conversion for personal cold protection. *Compos. Commun.* **2021**, *25*, 100766, DOI: 10.1016/j.coco.2021.100766

(11) Yuan, K.; Shi, J.; Aftab, W.; Qin, M.; Usman, A.; Zhou, F.; Lv, Y.; Gao, S.; Zou, R. Engineering the thermal conductivity of functional phase-change materials for heat energy conversion, storage, and utilization. *Adv. Funct. Mater.* **2020**, *30*, 1904228, DOI: 10.1002/adfm.201904228

(12) Prajapati, D. G.; Kandasubramanian, B. A review on polymeric-based phase change material

for thermo-regulating fabric application. *Polymer Reviews* **2020**, *60* (3), 389–419, DOI: 10.1080/15583724.2019.1677709

(13) Tang, Z.; Gao, H.; Chen, X.; Zhang, Y.; Li, A.; Wang, G. Advanced multifunctional composite phase change materials based on photo-responsive materials. *Nano Energy* **2021**, *80*, 105454, DOI: 10.1016/j.nanoen.2020.105454

(14) Sun, K.; Dong, H.; Kou, Y.; Yang, H.; Liu, H.; Li, Y.; Shi, Q. Flexible graphene aerogel-based phase change film for solar-thermal energy conversion and storage in personal thermal management applications. *Chem. Eng. J.* **2021**, *419*, 129637, DOI: 10.1016/j.cej.2021.129637

(15) Zhao, X.; Zou, D.; Wang, S. Flexible Phase Change Materials: Preparation, Properties and Application. *Chem. Eng. J.* **2022**, 431, 134231, DOI: 10.1016/j.cej.2021.134231.

(16) Yu, X.; Li, Y.; Yin, X.; Wang, X.; Han, Y.; Si, Y.; Yu, J.; Ding, B. Corncoblike, superhydrophobic, and phase-changeable nanofibers for intelligent thermoregulating and water-repellent fabrics. *ACS Appl. Mater. Interfaces* **2019**, *11* (42), 39324–39333, DOI: 10.1021/acsami.9b12934

(17) Aftab, W.; Huang, X.; Wu, W.; Liang, Z.; Mahmood, A.; Zou, R. Nanoconfined phase change materials for thermal energy applications. *Energy Environ. Sci.* **2018**, *11* (6), 1392–1424, DOI: 10.1039/C7EE03587J

(18) Huang, X.; Chen, X.; Li, A.; Atinafu, D.; Gao, H.; Dong, W.; Wang, G. Shape-stabilized phase change materials based on porous supports for thermal energy storage applications. *Chem. Eng. J.* **2019**, *356*, 641–661, DOI: 10.1016/j.cej.2018.09.013

(19) Chen, L.; Lv, J.; Ding, L.; Yang, G.; Mao, Z.; Wang, B.; Feng, X.; Zapotoczny, S.; Sui, X. A shape-stable phase change composite prepared from cellulose nanofiber/polypyrrole/polyethylene glycol for electric-thermal energy conversion and storage. *Chem. Eng. J.* **2020**, *400*, 125950, DOI: 10.1016/j.cej.2020.125950

(20) Cheng, P.; Gao, H.; Chen, X.; Chen, Y.; Han, M.; Xing, L.; Liu, P.; Wang, G. Flexible monolithic phase change material based on carbon nanotubes/chitosan/poly(vinyl alcohol). *Chem. Eng. J.* **2020**, *397*, 125330, DOI: 10.1016/j.cej.2020.125330

(21) Xue, F.; Qi, X.; Huang, T.; Tang, C.; Zhang, N.; Wang, Y. Preparation and application of three-dimensional filler network towards organic phase change materials with high performance and multi-functions. *Chem. Eng. J.* **2021**, *419*, 129620, DOI: 10.1016/j.cej.2021.129620

(22) Sun, K.; Kou, Y.; Zhang, Y.; Liu, T.; Shi, Q. Photo-triggered hierarchical porous carbon-based composite phase-change materials with superior thermal energy conversion capacity. *ACS Sustainable Chem. Eng.* **2020**, 8 (8), 3445–3453, DOI: 10.1021/acssuschemeng.9b07659

(23) Y. Cao, D. Fan, S. Lin, F.T.T. Ng, Q. Pan, Branched alkylated polynorbornene and 3D flower-like MoS2 nanospheres reinforced phase change composites with high thermal energy storage capacity and photothermal conversion efficiency, *Renew. Energ.* **2021**,*179*, 687–695, DOI: 10.1016/j.renene.2021.07.028

(24) Wei, D.; Wu, C.; Jiang, G.; Sheng, X.; Xie, Y. Lignin-assisted construction of well-defined 3D graphene aerogel/PEG form-stable phase change composites towards efficient solar thermal energy storage. *Sol. Energy Mater. Sol. Cells* **2021**, *224*, 111013, DOI: 10.1016/j.solmat.2021.111013

(25) Zhao, Y.; Sun, B.; Du, P.; Min, X.; Huang, Z.; Liu, Y.; Wu, X.; Fang, M. Hierarchically channel-guided porous wood-derived shape-stabilized thermal regulated materials with enhanced thermal conductivity for thermal energy storage. *Mater. Res. Express* **2019**, *6* (11), 115515, DOI:

10.1088/2053-1591/ab4700

(26) Zhao, Y.; Min, X.; Huang, Z.; Liu, Y.; Wu, X.; Fang, M. Honeycomb-like structured biological porous carbon encapsulating PEG: A shape-stable phase change material with enhanced thermal conductivity for thermal energy storage. *Energy and Buildings* **2018**, *158*, 1049–1062, DOI: 10.1016/j.enbuild.2017.10.078

(27) Becherini, S.; Mitmoen, M.; Tran, C. D. Biocompatible and smart composites from cellulose, wool, and phase-change materials encapsulated in natural sporopollenin microcapsules. *ACS Sustainable Chem. Eng.* **2020**, 8 (27), 10089–10101, DOI: 10.1021/acssuschemeng.0c02001

(28) Huang, H.; Shi, T.; He, R.; Wang, J.; Chu, P. K.; Yu, X. Phase-changing microcapsules incorporated with black phosphorus for efficient solar energy storage. *Adv. Sci.* **2020**, *7* (23), 2000602, DOI: 10.1002/advs.202000602

(29) Wei, H.; He, F.; Li, Y.; Zhang, Q.; Zhou, Y.; Yan, H.; He, R.; Fan, J.; Yang, W. Bifunctional paraffin@CaCO3:Ce3+ phase change microcapsules for thermal energy storage and photoluminescence. *ACS Sustainable Chem. Eng.* **2019,** 7 (23), 18854–18862, DOI: 10.1021/acssuschemeng.9b03935

(30) Sun, Z.; Sun, K.; Zhang, H.; Liu, H.; Wu, D.; Wang, X. Development of poly(ethylene glycol)/silica phase-change microcapsules with well-defined core-shell structure for reliable and durable heat energy storage. *Sol. Energy Mater. Sol. Cells* **2021**, *225*, 111069, DOI: 10.1016/j.solmat.2021.111069

(31) Shi, J.; Aftab, W.; Liang, Z.; Yuan, K.; Maqbool, M.; Jiang, H.; Xiong, F.; Qin, M.; Gao, S.; Zou, R. Tuning the flexibility and thermal storage capacity of solid–solid phase change materials towards wearable applications. *J. Mater. Chem. A* **2020**, *8* (38), 20133–20140, DOI: 10.1039/C9TA13925G

(32) Kou, Y.; Sun, K.; Luo, J.; Zhou, F.; Huang, H.; Wu, Z.-S.; Shi, Q. An intrinsically flexible phase change film for wearable thermal managements. *Energy Storage Mater.* **2021**, *34*, 508–514, DOI: 10.1016/j.ensm.2020.10.014

(33) Du, X.; Qiu, J.; Deng, S.; Du, Z.; Cheng, X.; Wang, H. $Ti_3C_2T_x$@PDA-integrated polyurethane phase change composites with superior solar-thermal conversion efficiency and Improved Thermal Conductivity. *ACS Sustainable Chem. Eng.* 2020, 8 (14), 5799–5806, DOI: 10.1021/acssuschemeng.0c01582

(34) Shi, J.; Qin, M.; Aftab, W.; Zou, R. Flexible phase change materials for thermal energy storage. *Energy Storage Mater.* **2021**, *41*, 321–342, DOI: 10.1016/j.ensm.2021.05.048

(35) Liu, L.; Xu, W.; Ding, Y.; Agarwal, S.; Greiner, A.; Duan, G. A review of smart electrospun fibers toward textiles. *Compos. Commun.* **2020**, *22*, 100506, DOI: 10.1016/j.coco.2020.100506

(36) Lin, C.; Li, W.; Yan, Y.; Ke, H.; Liu, Z.; Deng, L.; Qiu, Z. Ultrafine electrospun fiber based on ionic liquid/AlN/copolyamide composite as novel form-stable phase change material for thermal energy storage. *Sol. Energy Mater. Sol. Cells* **2021**, *223*, 110953, DOI: 10.1016/j.solmat.2020.110953

(37) Xie, W.; Li, T.; Tiraferri, A.; Drioli, E.; Figoli, A.; Crittenden, J. C.; Liu, B. Toward the next generation of sustainable membranes from green chemistry principles. *ACS Sustainable Chem. Eng.* **2021**, 9 (1), 50–75, DOI: 10.1021/acssuschemeng.0c07119

(38) Zhou, W.; Gong, X.; Li, Y.; Si, Y.; Zhang, S.; Yu, J.; Ding, B. Environmentally friendly waterborne polyurethane nanofibrous membranes by emulsion electrospinning for waterproof and breathable textiles. *Chem. Eng. J.* **2022**, *427*, 130925, DOI: 10.1016/j.cej.2021.130925

(39) Li, Y.; Li, S.; Sun, J. Degradable poly(vinyl alcohol)-based supramolecular plastics with high mechanical strength in a watery environment. *Adv. Mater.* **2021**, *33* (13), 2007371, DOI: 10.1002/adma.202007371

(40) Lin, C.; Li, W.; Yan, Y.; Ke, H.; Liu, Z.; Deng, L.; Qiu, Z. Ultrafine electrospun fiber based on ionic liquid/AlN/copolyamide composite as novel form-stable phase change material for thermal energy storage. *Sol. Energy Mater. Sol. Cells* **2021**, *223*, 110953, DOI: 10.1016/j.solmat.2020.110953

(41) Li, S.; Wang, H.; Mao, H.; Li, J.; Shi, H. Light-to-thermal conversion and thermoregulated capability of coaxial fibers with a combined influence from comb-like polymeric phase change material and carbon nanotube. *ACS Appl. Mater. Interfaces* **2019**, *11* (15), 14150, DOI: 10.1021/acsami.9b02387

(42) Lv, D.; Wang, R.; Tang, G.; Mou, Z.; Lei, J.; Han, J.; De Smedt, S.; Xiong, R.; Huang, C. Ecofriendly electrospun membranes loaded with visible-light-responding nanoparticles for multifunctional usages: highly efficient air filtration, dye scavenging, and bactericidal activity. *ACS Appl. Mater. Interfaces* **2019**, *11* (13), 12880–12889, DOI: 10.1021/acsami.9b01508

(43) Chen, X.; Gao, H.; Hai, G.; Jia, D.; Xing, L.; Chen, S.; Cheng, P.; Han, M.; Dong, W.; Wang, G. Carbon nanotube bundles assembled flexible hierarchical framework based phase change material composites for thermal energy harvesting and thermotherapy. *Energy Storage Mater*. **2020**, *26*, 129–137, DOI: 10.1016/j.ensm.2019.12.029

(44) Min, X.; Fang, M.; Huang, Z.; Liu, Y.; Huang, Y.; Wen, R.; Qian, T.; Wu, X. Enhanced thermal properties of novel shape-stabilized PEG composite phase change materials with radial mesoporous silica sphere for thermal energy storage. *Sci Rep* **2015**, *5* (1), 12964, DOI: 10.1038/srep12964

(45) Cheng, F.; Zhang, X.; Wen, R.; Huang, Z.; Fang, M.; Liu, Y.; Wu, X.; Min, X. Thermal conductivity enhancement of form-stable tetradecanol/expanded perlite composite phase change materials by adding Cu powder and carbon fiber for thermal energy storage. *Applied Thermal Engineering* **2019**, *156*, 653–659, DOI: 10.1016/j.applthermaleng.2019.03.140

(46) Lu, Y.; Xiao, X.; Zhan, Y.; Huan, C.; Qi, S.; Cheng, H.; Xu, G. Core-sheath paraffin-wax-loaded nanofibers by electrospinning for heat Storage. *ACS Appl. Mater. Interfaces* **2018**, *10* (15), 12759–12767, DOI: 10.1021/acsami.8b02057

(47) Ke, H.; Wei, Q. Using co-electrospinning method to regulate phase change temperatures of fatty acid eutectic/polystyrene/fatty acid eutectic form-stable phase change composite nanofibrous membranes for thermal energy storage. *Thermochimica Acta* **2020**, *683*, 178438, DOI：10.1016/j.tca.2019.178438

(48) Esmaeilzadeh, Z.; Rezaei, B.; Mousavi Shoushtari, A.; Mojtahedi, M. R. M. Enhancing the thermal characteristics of shape-stabilized phase change nanocomposite nanofibers by incorporation of multiwalled carbon nanotubes within the nanofibrous structure: research article. *Adv Polym Technol* **2018**, *37* (1), 185–193, DOI: 10.1002/adv.21655

(49) Wang, J.; Xu, J.; He, Y. Novel Smart textile with ultraviolet shielding and thermo-regulation fabricated via electrospinning. *J Energy Storage* **2021**, *42*, 103094, DOI: 10.1016/j.est.2021.103094

(50) Yi, L.; Wang, S.; Wang, L.; Yao, J.; Marek, J.; Zhang, M. A Waterproof and breathable nanofibrous membrane with thermal-regulated property for multifunctional textile Application. *J Appl Polym Sci* **2021**, *138* (19), 50391, DOI: 10.1002/app.50391

(51) Feng, W.; Zhang, Y.; Shao, Y.; Huang, T.; Zhang, N.; Yang, J.; Qi, X.; Wang, Y. Coaxial electrospun membranes with thermal energy storage and shape memory functions for simultaneous

thermal/moisture management in personal cooling textiles. *Eur. Polym J.* **2021**, *145*, 110245, DOI: 10.1016/j.eurpolymj.2020.110245

(52) Abdalkarim, S. Y. H.; Yu, H.; Wang, C.; Chen, Y.; Zou, Z.; Han, L.; Yao, J.; Tam, K. C. Thermo and light-responsive phase change nanofibers with high energy storage efficiency for energy storage and thermally regulated on–off drug release devices. *Chem. Eng. J.* **2019**, *375*, 121979, DOI: 10.1016/j.cej.2019.121979

(53) Zhang, X.; Wu, B.; Chen, G.; Xu, Y.; Shi, T.; Huang, Z.; Liu, Y.; Fang, M.; Wu, X.; Min, X. Preparation and characterization of flexible smart glycol/polyvinylpyrrolidone/nano-Al_2O_3 phase change fibers. *Energy Fuels* **2021**, *35* (1), 877–882, DOI: 10.1021/acs.energyfuels.0c03370

(54) Zhao, L.; Luo, J.; Li, Y.; Wang, H.; Song, G.; Tang, G. Emulsion-electrospinning n -octadecane/silk composite fiber as environmental-friendly form-stable phase change materials. J. Appl. Polym. Sci. **2017**, 134 (47), 45538, DOI: 10.1002/app.45538

Chapter 3

A tri-mode thermoregulatory flexible fibrous membrane designed with hierarchical core-sheath fiber structure for wearable personal thermal management

Chapter 3: A tri-mode thermoregulatory flexible fibrous membrane designed with hierarchical core-sheath fiber structure for wearable personal thermal management

3.1 Introduction

Maintaining the constant temperature of the human body is pivotal for humans' thermal comfort and proper functioning.[1-2] However, current strategies for controlling indoor temperatures, such as air conditioning, ventilation, or fuel heating, consume a considerable amount of energy and contribute to aggravating the greenhouse effect.[3-5] Meanwhile, outdoor space, which is an inevitable part for indispensable physical and production activities, always has lacked an implementable approach for realizing thermal management, due to the tremendous open space and fluctuating ambient temperature.[6] Emerging textiles designed for personal thermal management (PTM) can manage the temperature of a localized region around the human body directly to satisfy the individual thermal requirement, which appears to be sustainable and economical for mitigating energy crises, and their applications could be extended in both indoor and outdoor scenarios.[7]

Some people work in air-conditioned rooms and some work in harsh environments such as cold storage, ice rinks, and hot workshops, so they must make the transition at different temperatures from time to time each day. Such frequent changes from normal temperatures to significantly higher or lower temperatures cause discomfort and it can result in illness.[8] Phase change materials (PCMs) capable of absorbing and releasing heat energy are attractive for maintaining a constant temperature in the PTM field. However, the inherently solid rigidity and liquid leakage of PCMs hinder their applications in the wearable thermal regulation field.[9-12] Numerous form-stable strategies have been committed to improving the packaging efficiency of PCMs, such as the 3D aerogel network,[13-15] the polymer-cross-linked skeleton,[16-18] microencapsulation,[19-21] and others. The aforementioned methods based on capillary absorption in porous structure still remain leakage threats at high temperature, and the

other methods that depend on covalent crosslinking are prone to constrain the movement of molecular chains between amorphous and crystalline phases extensively, leading to deteriorated heat enthalpy of PCM composites. In addition, the synthesis method for phase change microcapsules is complex and costly. In addition to form-stability, flexibility also is required for phase change composites to fit the curved surface of the human body in wearable applications. Coaxial electrospinning has been explored to produce core-sheath structured phase change fibers. In this process the PCMs are encapsulated in the center of the fiber to solve the leakage issue.[22-25] Additionally, the high aspect ratio of the ultrafine fibers endows the prepared composite membranes with favorable flexibility. Most importantly, the large specific surfaces of the fibrous membrane provide a platform for functionalized surface modifications. It is highly desirable to integrate multiple functions into textiles.[26] Since the single-mode thermal regulation based on PCMs hardly can cope with the multi-functional demand for longtime and large temperature range management, multi-mode and more precise thermal regulation textiles are in demand.[6,7,27] Recently, multi-source driven heating has attracted significant attention. Solar energy, as an inexhaustible and clean natural energy resource, has played a vital role in various solar-thermal conversion fields. Combining photo-responsive materials with PCMs has the potential to boost energy storage and facilitate continuous heating behavior based on sunlight.[28-30] Furthermore, electro-driven heating has been demonstrated as a compensatory option for further expanding the application scenarios, especially in cloudy, rainy conditions or indoor space.[7,31-33]

Herein, we proposed an approach for all-day individual thermal management through integrating the reversible phase change property, sustainable solar-heating, and complementary Joule heating into one wearable thermoregulatory textile. Specifically, we designed a hierarchical core-sheath structure composed of PCMs, solar absorbers, and conductive polymers to create a tri-mode thermal management system. The multicore-sheath structure assured the effective encapsulation of paraffin wax (PW), resulting in an admirable thermal storage capability (106.86 J/g). Meanwhile, the membrane-based textile proposes favorable solar heating (70.5 °C, 1 sun) and Joule

heating (73.8 °C, 4.2 V) effects, owing to the synergistic photothermal performance between carbon nanotubes (CNTs), polydopamine (PDA) and poly(3,4-ethylenedioxythiophene): polystyrenesulfonate (PEDOT:PSS) as well as the intrinsic high conductivity of PEDOT:PSS. Thanks to the well-designed multicore-shell structure which enables the cooperation of various functional components, the proposed membrane is imparted with an on-demand multi-mode thermal regulation function which allows it to adapt to the environmental temperature changes.

3.2 Experimental section

3.2.1 Materials

Polyurethane (PU, *M*w = 110000, Sigma-Aldrich, USA), paraffine wax (PW, Yijiu Chem., China), Carboxylic carbon nanotubes (CNTs, XFNANO, China) and PEDOT:PSS (Clevios PH1000) were used as received without further purification. N, N-dimethylformamide (DMF), tetrahydrofuran (THF), dopamine hydrochloride (DA, 98%), tris(hydroxymethyl) aminomethane hydrochloride (Tris, 99%), 4-dodecylbenzenesulfonic acid and ethylene glycol (EG) were purchased from FUJIFILM Wako, Japan.

3.2.2 Preparation of PU@PW membranes

The PU@PW membrane was fabricated by coaxial electrospinning. Briefly, PU was dissolved in DMF/THF (50 wt%/50 wt%) for sheath precursor solution, and the core solution was prepared by dissolve melting PW in kerosene (80 wt%). The sheath and core solutions were injected into a dual-needle with outer and inner needles at 17 and 25 gauge, respectively. The applied voltage was 15 kV, and the distance between the needle and the collector was 15 cm. The relative humidity and temperature were controlled at 40 ± 5 % and 30 ± 3 °C, respectively, during the spinning process. The sheath solution was pumped at a constant rate of 1 mL/h, and the core feed rate was controlled as 0.3, 0.4, 0.5, and 0.6 mL/h. Accordingly, the fabricated PU@PW membranes were denoted as PU@PW1, PU@PW2, PU@PW3, and PU@PW4.

3.2.3 Preparation of the CPU@PW, DPU@PW, and EPU@PW membranes

The PU@PW4 membrane was selected for further treatment. A certain amount of CNTs was dispersed in a water/ethanol blend solution (20/80 V/V) at a concentration of 1 mg/mL, and PU@PW4 was immersed in the CNTs suspension and sonicated for 30 min. The prepared membrane was marked as CPU@PW. Next, CPU@PW was immersed in Tris aqueous solution of DA (2 mg/ mL, pH = 8.5) for 24 h. The prepared membrane after PDA decoration was referred to DPU@PW. Subsequently, DPU@PW was dipped in a PEDOT:PSS solution (prepared by mixing 9.5 g PEDOT:PSS, 0.5 g EG, and 0.1 g 4-dodecylbenzenesulfonic acid) and dried at ambient condition. This process was repeated three times to prepare the final EPU@PW membrane.

3.2.4 Characterization

The surface morphology and structure features were observed using a scanning electron microscopy (SEM, JSM-6010LA, JEOL, Japan) and transmission electron microscopy (TEM, JEM-2010, Japan). The Fourier-transform infrared spectrophotometer (FTIR-6600, Jasco, Japan), X-ray diffraction (XRD, MiniFlex300, Rigaku, Japan) and X-ray photoelectron spectroscopy (AXIS-ULTRA HSA SV, Japan) were employed to characterize the chemical composition of the prepared membranes. The temperature evolution was recorded by a thermocouple (KE331L, CHINO, Japan) and an infrared thermal imaging camera (Testo 875-2i, German). Differential scanning calorimetry (Thermo plus EVO2 DSCvesta, Rigaku, Japan) was carried out to characterize the heat storage capacity at a heating/cooling rate of 10 °C /min under N_2 atmosphere (Flow rate = 50 mL/min). Water contact angle was measured by a contact angle measuring instrument (DM400, Kyowa, Japan). The light absorptivity was measured by an ultraviolet-visible-near infrared spectrophotometer (UV-3600, Shimadzu Ltd., Japan).

3.2.5 Calculations for photothermal energy storage efficiency

The light-to-thermal conversion testing was implemented with a xenon lamp (XES-40S3-TT, Japan) with an AM 1.5 filter as light sources, a thermocouple cooperated with a data collector was carried out to record the temperature variation process of the prepared membranes every 0.1 s. The photothermal conversion and storage efficiency

(η_{PT}) of composite membranes was calculated as the following equation:

$$\eta_{PT} = \frac{m \cdot \Delta H_m}{A \cdot p \cdot t} \quad (1)$$

where m is the mass (g) of the composite membranes, ΔH_m is the phase change enthalpy(J/g) obtained from DSC test, A is the irradiated surface aera (cm^2) of the tested membrane, p is the power (mW/cm^2) of irradiation light, t is the time (s) of light-driven phase change period.

3.2.6 Calculations for electrothermal energy storage efficiency

The electrothermal energy conversion and storage experiment was carried out by a DC power. The electrothermal conversion and storage efficiency (η_{ET}) of composite membranes was evaluated as the following equation:

$$\eta_{ET} = \frac{m \cdot \Delta H_m}{U \cdot I \cdot t} \quad (2)$$

where m is the mass (g) of the composite membranes, ΔH_m is the phase change enthalpy(J/g), U is the applied voltage (V) of the tested membrane, I is the current (A), t is the time (s) of electro-driven phase change period.

3.3 Results and discussion

3.3.1 Fabrication and characterization of tri-mode thermoregulatory nonwoven textile

Fig. 3-1a shows the procedure for producing fibrous membranes with the hierarchical fiber structure. The multicore-shell fiber is composed of the internal core PW, intermediate protective and supportive elastic shell polyurethane (PU) and external solar-responsive multilayers of CNTs, PDA, and PEDOT:PSS, where PEDOT:PSS also serves as a conductive layer. This delicate hierarchical structure is achieved by coaxial electrospinning (Fig.3-1b) and three-step surface modification, including ultrasonication assisted decoration, in-situ polymerization, and dip-coating process. The mechanism for the decoration of the CNTs onto the surface of the PU shell has been explained in previous works.[34] The large amount of heat generated by the ultrasonication make the fiber sheath (PU) melt and viscous, and the uniformly

dissipated CNTs with huge kinetic energy hit and in-situ assemble on the surface of PU. Notably, the hydrogen bonding and the π-π stacking between the CNTs and the PU facilitate the decoration process and contribute for a strong interfacial interaction. The main advantages of the ultrasonication assisted decoration of CNTs on the PU shell can be concluded as: 1) realize a sufficient, uniform loading of CNTs. 2) remain the shape of individual fibers and the porous structure of membranes, and 3) increase surface roughness, beneficial for the adhesion of PDA.[35] PDA has been used extensively in functionalized surface modification due to its "green" feature and adhesive ability for almost every substrate.[36] PDA is formed by the self-polymerization of dopamine monomers and attached to the CNTs firmly, *via* π-π stacking or hydrogen bonding with carboxyl on the surfaces of the CNTs.[37] Subsequently, the fiber surface converts from hydrophobic to hydrophilic, which is beneficial to the next dip-coating process of the PEDOT:PSS. It is worth noting that PDA also is a photothermal therapeutic agent with broadband absorbability.[36] PEDOT:PSS is an extensively explored highly conductive polymer as well as an effective photothermal absorbent.[38] The hydrophilic surface of the fiber wrapped by PDA is ideal for PEDOT:PSS aqueous dispersion intimacy wetting. In addition, both PDA and PEDOT:PSS contain aromatic heterocycles and numerous functional groups, which form various intermolecular interactions, such as π–π stacking, and hydrogen bonds, consequently realizing an interfacial reinforcement.[39, 40] In short, the *in situ* polymerized PDA layer has a quadruple effect that: 1) acts as a protective shell to resist PW from leaking and prevent CNTs from falling off; 2) serves as a light harvesting agent for improving the light-thermal conversion; 3) works as a versatile platform for anchoring the PEDOT:PSS on the fiber surface. 4) conducts hydrophilic modification to improve the wettability of the membrane. In brief, we used a systematic, layer-by-layer strategy to fabricate a multifunctional integrated fibrous membrane with triple thermal regulation routes including reversible phase change heating/cooling (Fig. 3-1c), solar heating (Fig. 3-1d) and Joule heating (Fig. 3-1e). Fig.3-1f illustrates in detail the multi-interfacial interactions (hydrogen bonding and π–π interaction) between each layer. The resultant robust hierarchical core-shell structure enabled the cooperation of the various

functional materials.

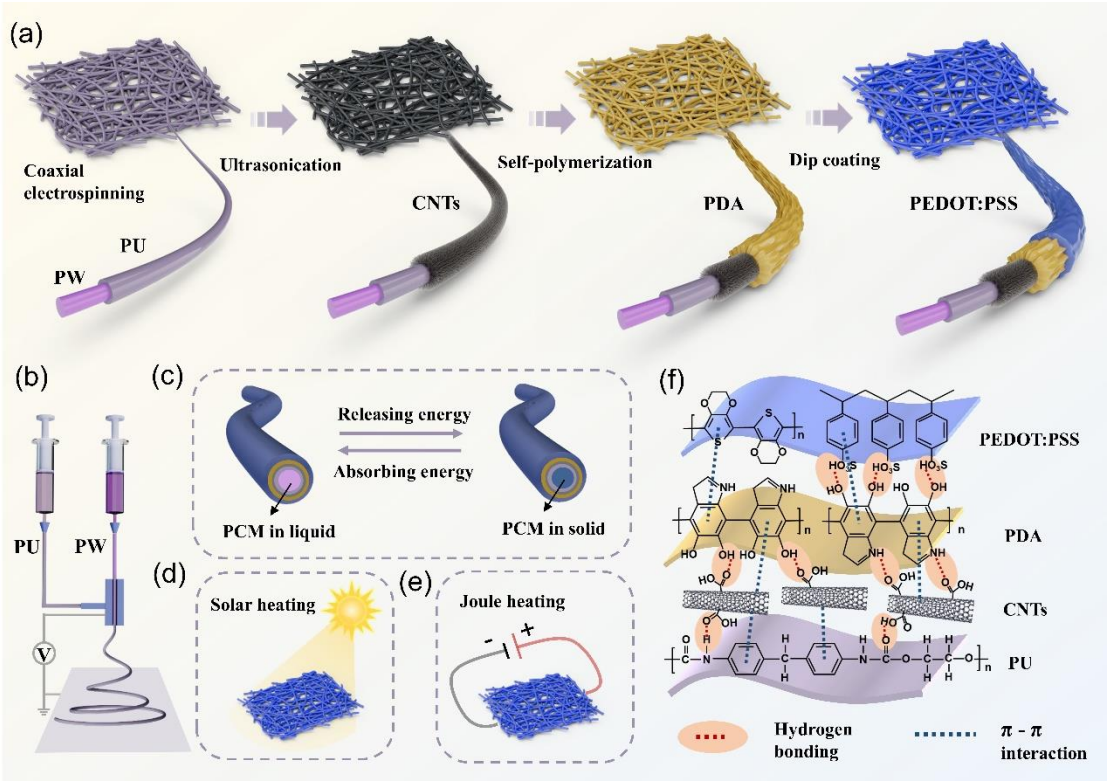

Fig. 3-1. Schematic illustrations of (a) fabrication process of the hierarchical core-sheath constructed fibers, (b) coaxial electrospinning, (c) reversible phase change process of core material, (d) solar heating effect, (e) Joule heating effect, (f) various interfacial interaction.

A series of PU@PW phase change membranes were conducted with coaxial electrospinning technology. Their micro morphology is observed in Fig. 3-2 (a-d). As the core feed rate increased gradually, the fibers demonstrated a larger average diameter and deviation (Fig. 3-2 (i-l)), suggesting a gradual trend toward heterogeneity. When the core feed rate was increased to 0.6 mL/h, the resultant fibers had a slightly "beads-on-a-string" morphology, but the core content can still be encapsulated. As shown in the TEM images of Fig.3-2 (e-h), the PW is completely encapsulated by the elastic PU sheath, forming an ideal core-shell structure. It is predicted that the higher core feed rate could induce a higher encapsulation mass of PW, while the Rayleigh instability restricts the maximum core flow rate. Considering the effective encapsulation of the core content, 0.6 mL/h was set as the maximum core speed in our work.

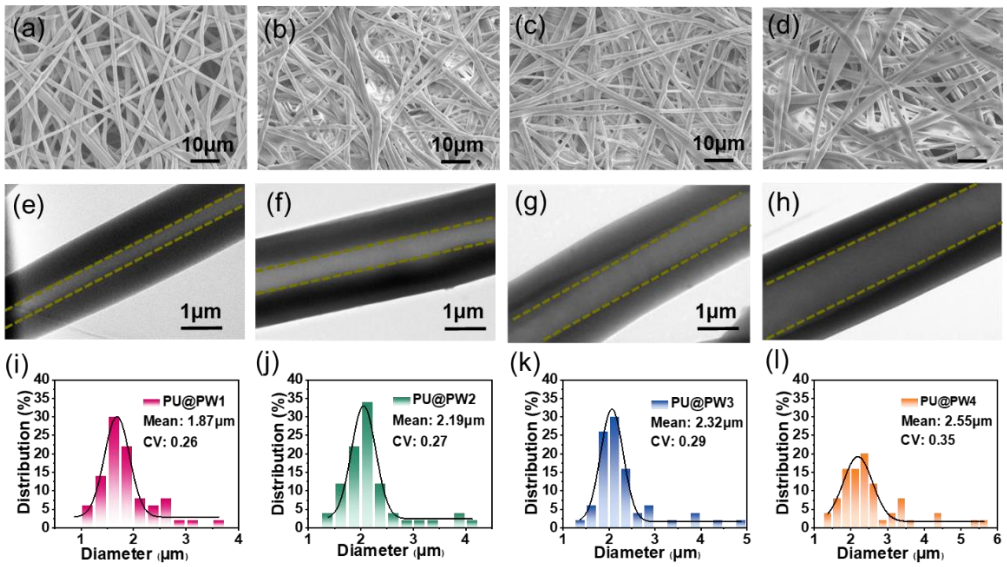

Fig. 3-2. Characterizations and properties of PU@PWs. (a-d) SEM images of PU@PW1, PU@PW2, PU@PW3, and PU@PW4. (e-h) TEM images of PU@PW1, PU@PW2, PU@PW3 and PU@PW4. (i-l) Fiber diameters of membranes

The chemical structures of the PU@PW membranes were characterized by Fourier transform infrared spectroscopy (FTIR) and X-ray diffraction (XRD). As presented in Fig. 3-3a, the characteristic peaks of PU were observed in the FTIR spectra of all PU@PW specimens. The series of absorption peaks at 2960, 2914, 2846, 1468, and 716 cm^{-1} (vibrations of −CH) were reported to be the typical characteristic bands of PW,[41] which also are exhibited in the infrared spectra of PU@PWs. Since no new peaks appeared, it was suggested that the core-shell structure of PU@PWs is only a physical combination. Additionally, the intensities of the characteristic peaks of PW increased gradually from PU@PW1 to PU@PW4, which is corresponding to the larger loading content of PW with an increasing feed speed rate of the core. Meanwhile, since the PU is amorphous, the diffraction peaks in the XRD pattern for PU@PW4 were ascribed to the crystalline PW (Fig. 3-3b). The phase change behavior of PW and PU@PWs were evaluated by differential canning calorimetry (DSC) in Fig.3-3c. Pure PW shows the melting temperature in the range of 20 − 38 °C with a melting enthalpy (ΔH_m) of 203.50 J/g and the crystallization temperature in the range of 12 − 26 °C with a crystallizing enthalpy (ΔH_c) of 203.69 J/g. The DSC curves of PU@PW composites with different core feed speed rates exhibit exothermic and endothermic signals at a temperature

region similar to that of pure PW. The amount of PW and the latent heat of PU@PW membranes are tunable through controlling the core feed speed rate. As shown in Fig.3-3d the melting and crystallizing enthalpy of the PU@PW membranes increased from 83.96 to 120.46 J/g (20 − 35 °C) and from 86.56 to 119.76 J/g (14 − 26 °C) respectively, with the core feed speed rate increasing from 0.3 to 0.6 mL/h. The outstanding heat-storage density and the appropriate phase change temperature are the vital prerequisites for wearable personal thermal regulation.

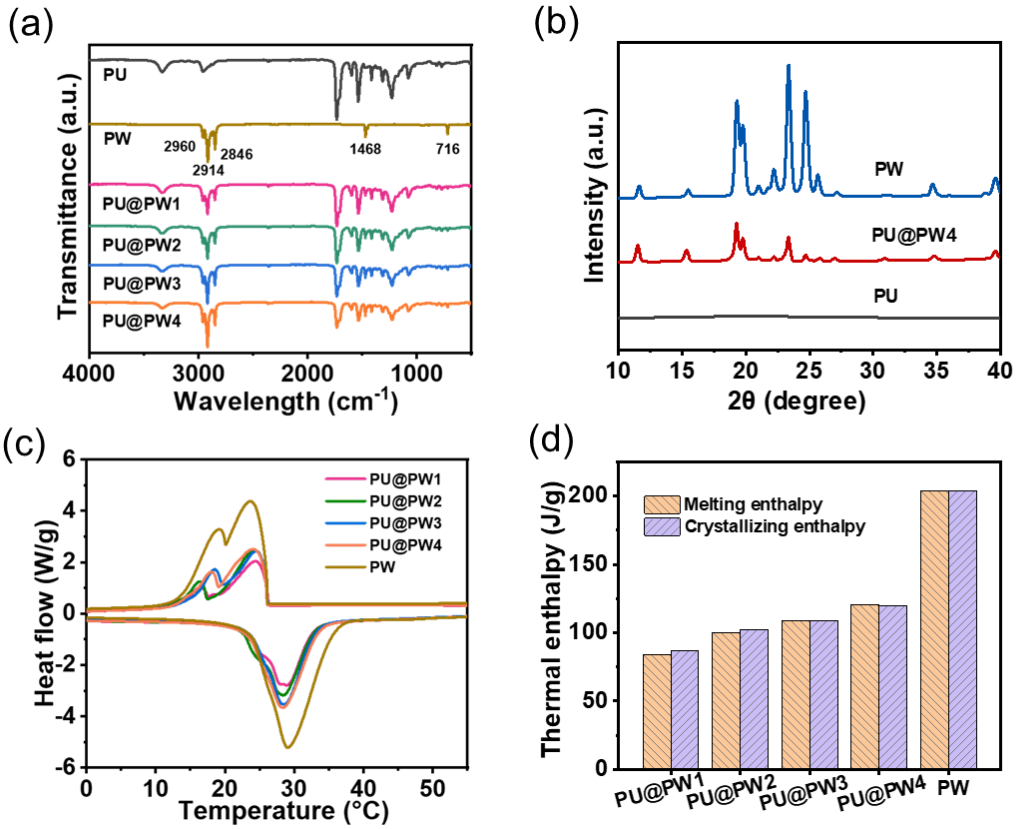

Fig. 3-3. (a) FTIR spectra of PU, PW and PU@PWs. (b) XRD patterns of pure PW, PU@PW4 membrane and PU membrane. (c) DSC curves of pure PW and PU@PWs. (d) Melting and freezing enthalpies of PW and PU@PWs.

Considering the high thermal enthalpy of the PU@PW4 membrane, it was selected as the phase change substrate for further functionalization. Unless stated, PU@PW is referred to PU@PW4 in the following. Fig. 3-4 (a-d) show the digital graphs of the series of decorated phase change membranes. After the introduction of CNTs, the membrane changes from white (PU@PW) to dark grey (CPU@PW). Then, the color

turns dark brown (DPU@PW) through the modification of PDA, and the membrane's color eventually becomes dark (EPU@PW) after the dip-coating of PEDOT:PSS. This apparent color evolution demonstrates a successful orderly surface decoration. The representative SEM images of the PU@PW, CPU@PW, DPU@PW, and EPU@PW membranes are shown in Fig. 3-4 (e_1, e_2 – h_1, h_2). In contrast to the smooth surface of PU@PW, CPU@PW shows a rough surface in the presence of the hair-like CNTs embedded on the surface of the PU shell (Figure 3f_2). Subsequently, PDA nanoparticles are deposited and grown into nanoclusters that wrap around the fiber surface, and they are buried in the outside layer of PEDOT:PSS eventually, forming a slightly crumpled surface (Figures 3g_2, h_2). The EDX elemental mapping images (Fig.3-5) present the homogenous elemental distribution of S on the fiber surface, which further verifies the uniformity of the PEDOT:PSS coating layer. In addition, the membranes were cut to observe their cross-sectional morphologies (Fig.3-6 (a-h)). The cross sections of the fibers at the incision present a hollow cylinder structure, because of the flow of the core fluid. The ordered modifications led to a series of surface evolutions, with the smooth surface of the PU shell being progressively modified by hairy CNTs, PDA nanoclusters, and PEDOT:PSS coatings. The EDS maps confirmed the successful coating treatment of PEDOT:PSS (Fig.3-6 (i-j)).

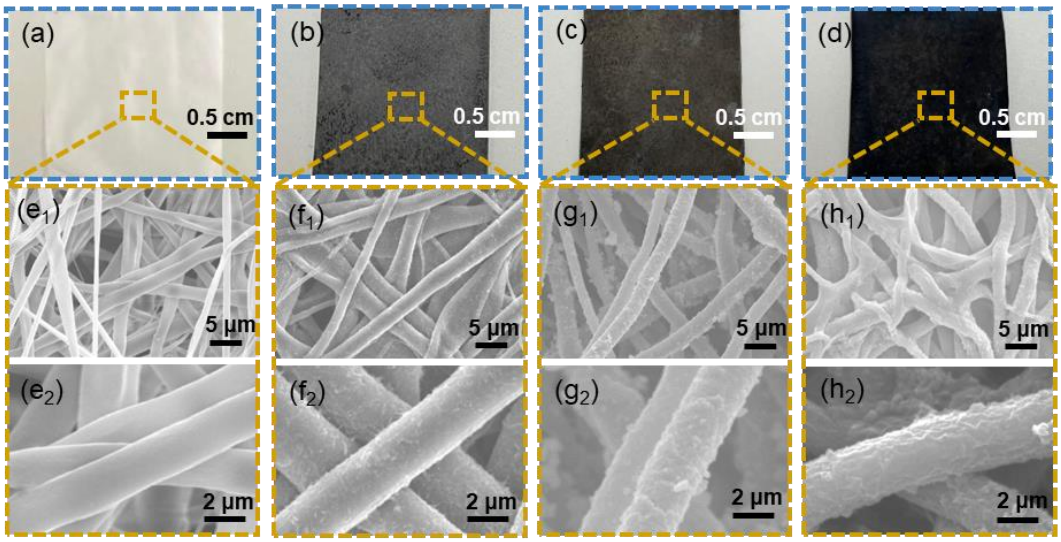

Fig. 3-4. Digital photographs of (a) PU@PW, (b) CPU@PW, (c) DPU@PW, and (d) EPU@PW. SEM images of (e_1) PU@PW, (f_1) CPU@PW, (g_1) DPU@PW, and (h_1) EPU@PW. (e_2-h_2) The

enlarged images show the step-by-step modification of the fiber surface. EDX spectrum

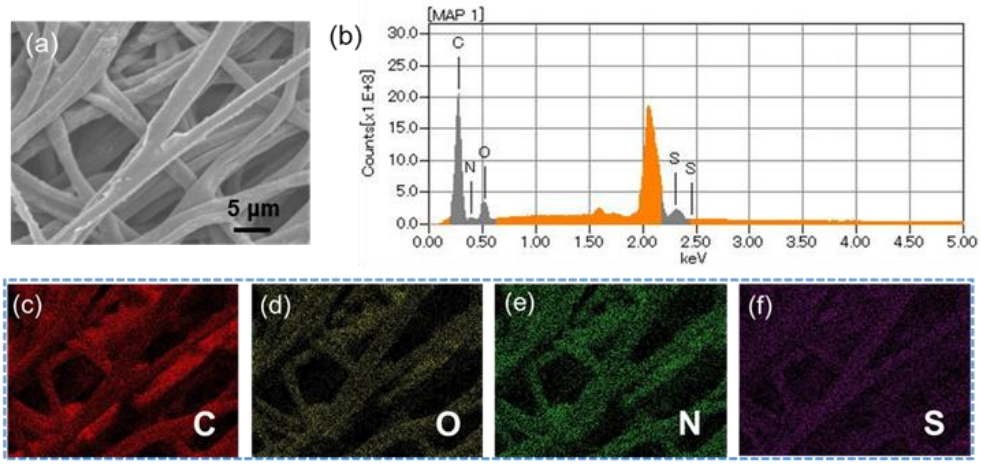

Fig. 3-5. (a) SEM image of EPU@PW. (b) Corresponding EDX spectrum and (c-f) element mapping images.

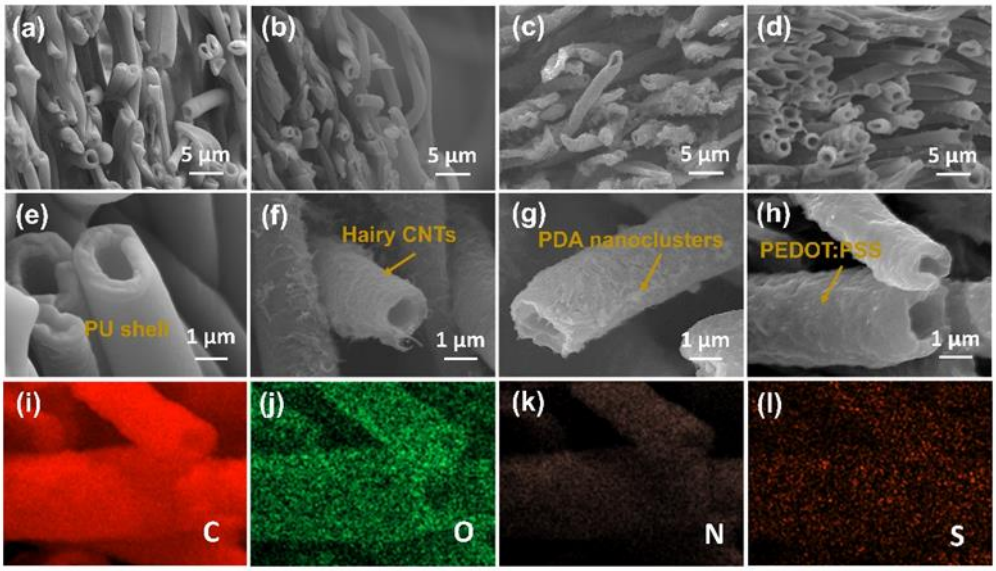

Fig. 3-6. SEM images of the cross-sectional morphologies of (a, e) PU@PW, (b, f) CPU@PW, (c, g) DPU@PW, and (d, h) EPU@PW with low and high magnification, respectively. (i-j) EDS mapping images of EPU@PW.

The digital picture (Fig.3-7a) shows the excellent flexibility and tailorability of EPU@PW membranes, and it reveals a decent mechanical performance for practical application. The typical breaking stress- strain curves of a series of prepared membranes

are displayed in Fig.3-7b. Coaxial spinning is a feasible approach to balance mechanical performance between the core and the sheath components.[42-43] Benefiting from the excellent flexibility and resilience of PU sheath, the PU@PW membrane exhibits a tensile strength of 3.75 MPa with the elongation of 323 %. With the orderly decoration of CNT, PDA, and PEDOT:PSS, the additional adhesive layers promote the tensile strength to 5.07 MPa with a slightly decreased elongation of 264 %. Because the multi-layers can glue nanofibers together to enhance the interconnection within the membrane.

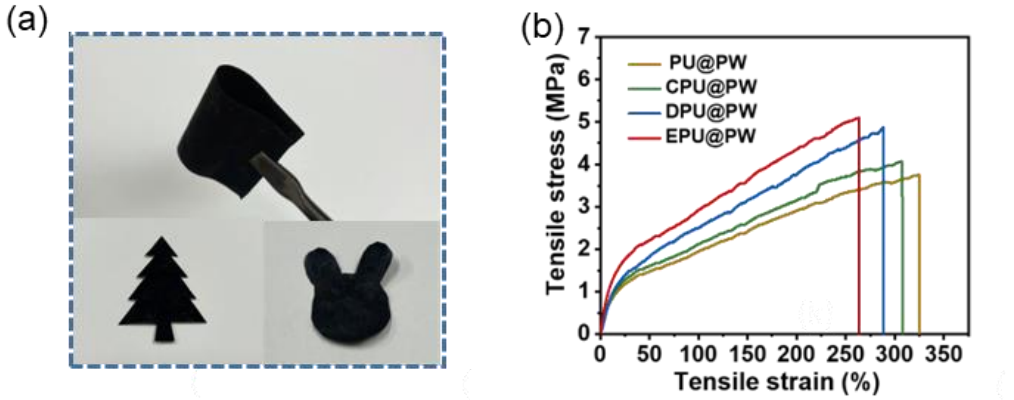

Fig. 3-7. (a) Digital photographs of EPU@PW in the bending state and different shapes. (b) Tensile stress−strain curves of the prepared membranes.

The FTIR spectra of CPU@PW and PU@PW did not exhibit any obvious change except for a blue shift from 3331 cm^{-1} to 3328 cm^{-1}, which is ascribed to the hydrogen bonding between amino-groups and carboxyl groups (Fig. 3-8a). The IR peak around 3328 cm^{-1} became stronger and broader after the decoration of PDA, the similar results have been reported in previous article, explaining this spectral change with an overlap of the stretching vibrations of amino (N−H) and hydroxy (O−H) groups of PDA.[44] Moreover, other peak intensity also exhibits a slight descending trend, suggesting the successful decoration of PDA on the fiber surface. After the dip-coating of PEDOT:PSS, there was almost no change in FTIR spectrum of EPU@PW compared to that of DPU@PW. X-ray photoelectron spectroscopy (XPS) analysis was performed to further probe the surface information on each layer of the integrated fibers. Fig.3-8b shows the survey spectra of PU@PW, CPU@PW, DPU@PW, and EPU@PW. Three characteristic

peaks for C 1s, O 1s, and N 1s are exhibited in the survey spectra of PU@PW, while the peak of N 1s almost disappeared and the peak intensity of O 1s decreased significantly after CNTs decoration, indicating that the CNTs are stacking up on the surface of PU@PW. After self-polymerization of dopamine, the peak of N 1s reappears, and the peak intensity of O 1s is increased on DPU@PW, resulting from the catechol and amine functional groups of the PDA layer. To further confirm the existence of PDA, the high-resolution N 1s spectra of DPU@PW is deconvoluted into three peaks at 397.7, 399.5, and 401.3 eV ascribed to –N=, –NH, and $–NH_2$, respectively (Fig.3-8c). The –N= peak originated from the indole group through structure evolution during the oxidative self-polymerization of dopamine, which confirmed the successful deposition of adherent PDA on the fiber surface, and these results are consistent with the phenomenon reported in the previous literature.[45] The spectrum of EPU@PW shows a new peak around 164 eV, which is ascribed to the characteristic peaks for S 2p. One peak with a binding energy of 166 − 172 eV originates from the sulfur atoms of PSS, and the other peak at 162 − 166 eV corresponds to the sulfur atoms of PEDOT (Fig3-8d), suggesting the attachment of PEDOT:PSS on the fiber surface.[46]

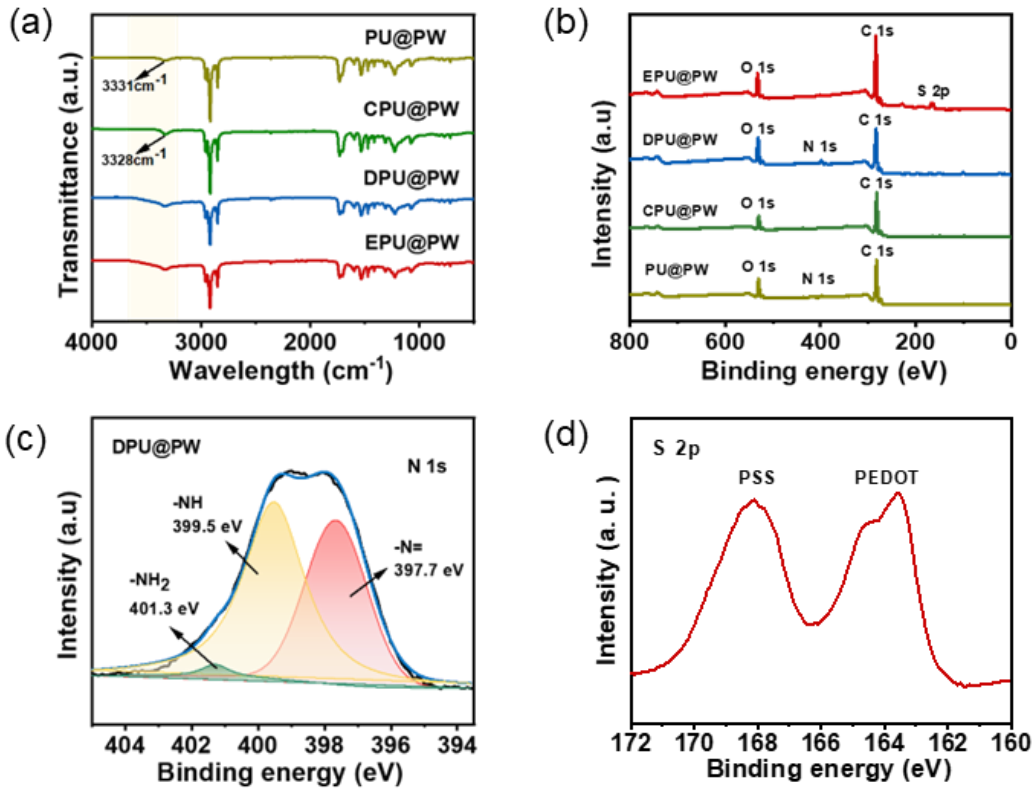

Fig. 3-8. (a) FT-IR spectra of a series of the prepared membranes. (b) Wide XPS spectra. (c) N 1s XPS spectra of DPU@PW. (d) High-resolution XPS S 2p spectrum of EPU@PW membrane.

As mentioned, PDA significantly improved the hydrophilicity of the CPU@PW membrane, which is shown in Fig. 3-9. The PU@PW and CPU@PW membranes present as hydrophobic surfaces, while the PDA modified membrane shows an impressive hydrophilicity; a water droplet can completely wet and be absorbed within 10 s, because of the abundant hydrophilic groups of PDA and the surface roughness constructed by CNTs and PDA. After modification of PEDOT:PSS, the better hydrophilicity originates from the synergistic effect between the two hydrophilic materials, *i.e.* PDA and PEDOT:PSS.

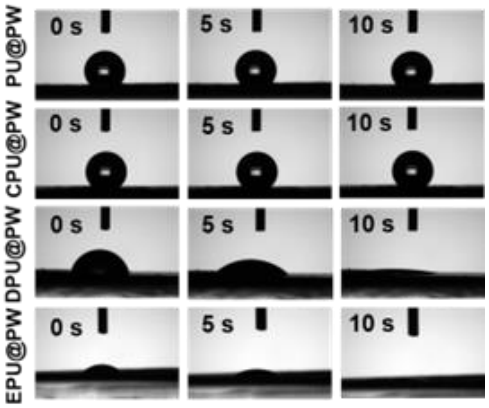

Fig. 3-9. The surface wetting behavior of the composite membranes.

3.3.2 Phase change performance

As is well known, PCMs are capable of absorbing and releasing latent heat in the phase change process, which can act as a reversible thermoregulatory medium to manage the local temperature near the skin. When the external temperature rises above the melting point, the PCMs absorb and store the extra heat to mitigate the transfer of heat to skin. Once the external temperature decreases below the crystallization point, the latent heat stored by PCMs will be released spontaneously to buffer the drastic decrease of temperature. The appropriate responsive temperature, energy storage density, and charging/discharging capability are significant parameters that determine the service performance of phase change composite fibers.

Fig.3-10a exhibits the DSC curves of a series of orderly functionalized composite membranes during the heating and cooling process, and the relevant thermal enthalpies are indicated in Fig.3-10b. Benefiting from the stable phase transition performance of the core-shell fiber PU@PW, the composite membranes of CPU@PW, DPU@PW and EPU@PW also exhibit significant endothermic and exothermic peaks at similar locations with melting enthalpies of 112.44, 109.25, and 106.86 J/g (about 20 − 35 °C), and crystallization enthalpies of 111.35, 108.38, and 104.94 J/g (around 14 − 26 °C), respectively. Their thermal enthalpies show a slight, gradual decrease compared to that of pristine PU@PW, because the introduction of CNTs, PDA and PEDOT:PSS make no contribution for phase change and reduce the mass fraction of PW in membrane.

However, the thermal enthalpy still remains at an ideal level. Fig.3-10c shows that the melting enthalpy of EPU@PW is significantly higher than the recently reported results by electrospinning (in a reasonable temperature range for human life between 22 − 46 °C),[22-24,43-48] which reveals that EPU@PW is a promising candidate for responsive thermoregulatory textile. As seen in Fig.3-10d, the DSC thermograms exhibit a favorable coincidence regarding the locations and intensities of the melting and cooling peaks in 50 cycles, demonstrating the stable reversibility of the phase change behavior.

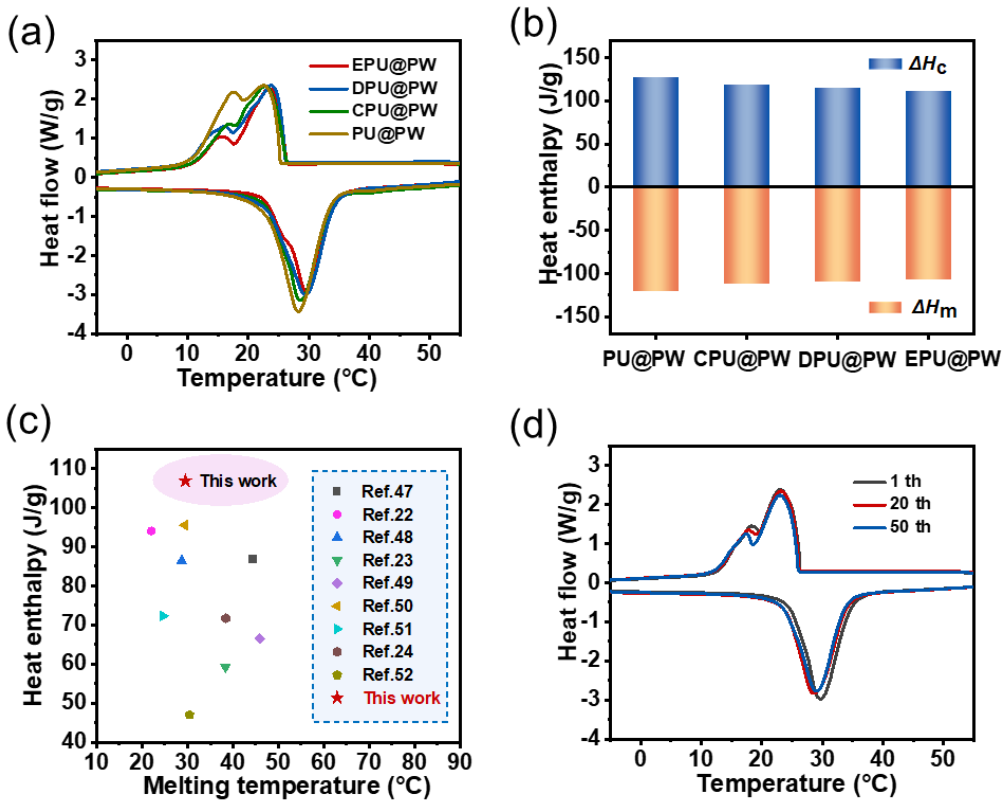

Fig.3-10. (a) DSC curves of a series of the prepared membranes. (b) Melting and freezing enthalpy of the corresponding membranes. (c) A comparison of melting enthalpy from the latest reported phase change membranes by electrospinning. (d) DSC heating and cooling curves of EPU@PW in 50 times.

The temperature self-regulation performance of EPU@PW was investigated through monitoring the temperature evolution using a thermocouple and an infrared camera.

The EPU membrane without the PW core was examined as a control. These samples are placed on a heating plate (temperature increasing from 10 to 60 °C), and then moved quickly to a cold plate (at 5 °C). Compared to EPU@PW, EPU shows a faster color change from violet to orange during the heating process, and it shows a quicker evolution of the opposite color during the cooling process (Fig.3-11 (a, b)). Fig.3-11 (c, d) present the real-time temperature records. There are two obvious temperature hysteresis regions in the heating and cooling processes, which are accompanied with the heat energy storing and releasing owing to the phase change of PW. This phenomenon confirms that the prepared phase change membranes can create a valid heating or cooling effect according to the changing environment.

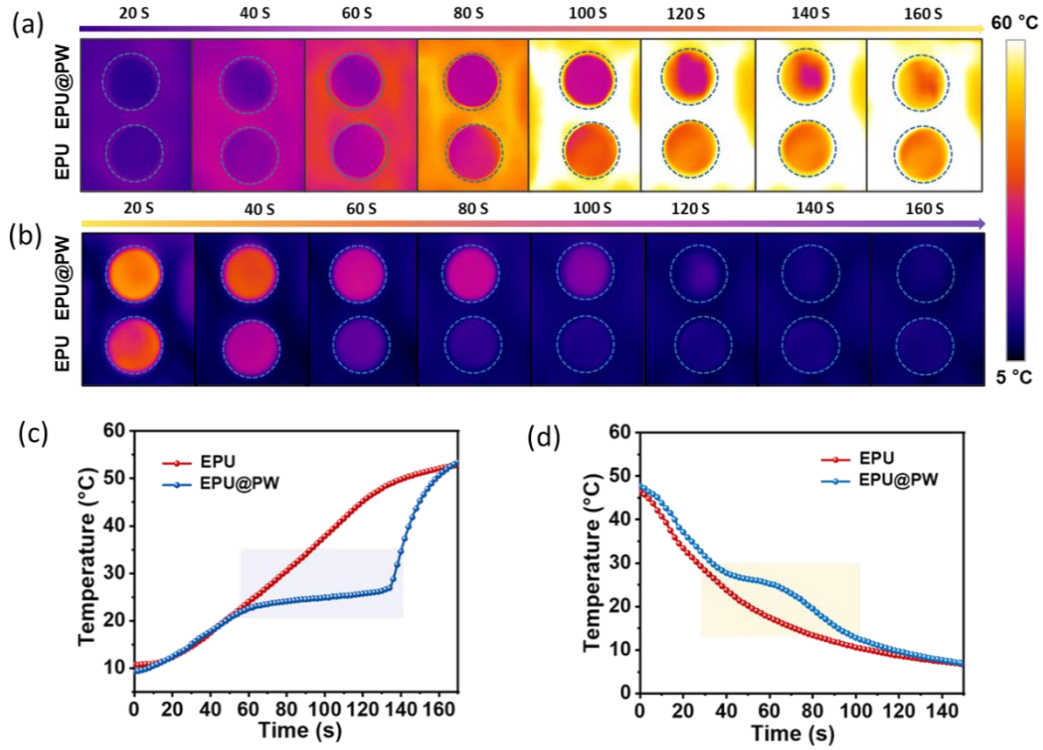

Fig. 3-11. (a, b) Representative IR thermal images in the heating and cooling process, respectively. (c, d) Temperature evolution plots in the heating and cooling process, respectively.

3.3.3 Photothermal conversion performance

The excellent solar-thermal properties of CNTs, PDA and PEDOT:PSS would endow the phase change membrane with an ideal photothermal performance. A scenario is described in Fig.3-12 (a, b), solar energy can be harvested rapidly and stored in PCMs,

continuously transferring heat to the human body. When the person subsequently enters into an indoor place or other conditions without sufficient sun radiation, the energy stored in the PCMs will be released spontaneously and keep the body warm. The above conceives can be demonstrated in the following experiments.

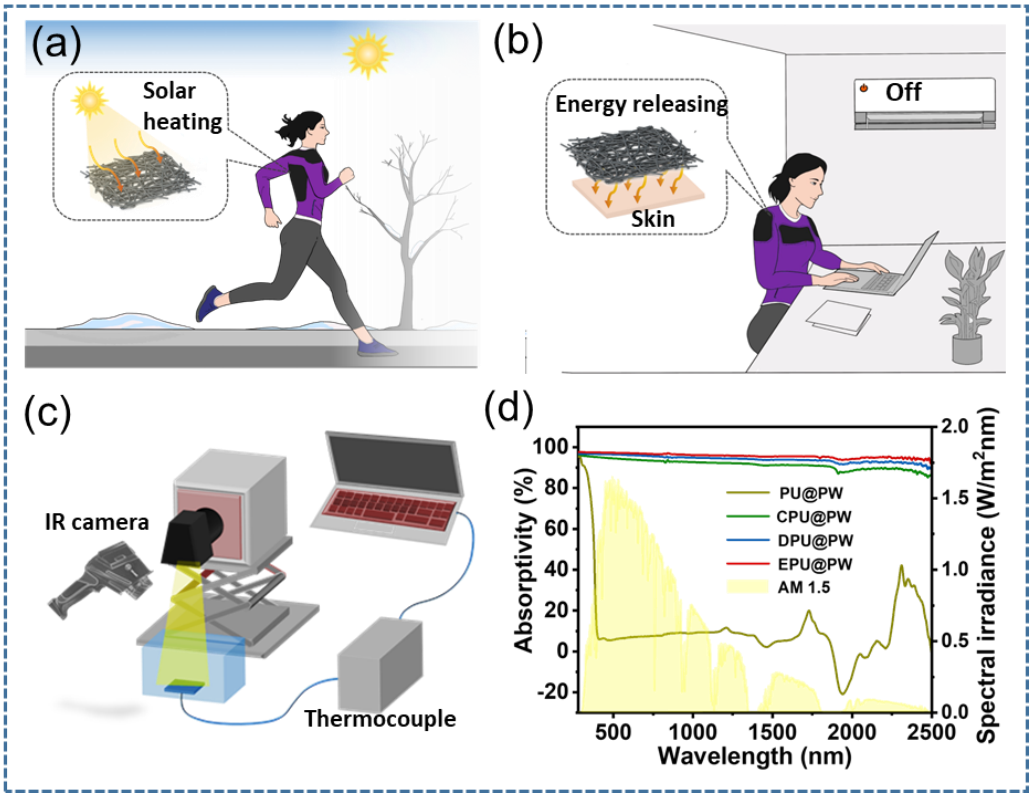

Fig 3-12. Schematic illustration of (a) photothermal conversion and energy storage in the membrane sewed on the clothing under sunlight and (b) the laten energy releasing to keep warm without sunlight. (c) Photothermal conversion testing device. (d) UV–vis–NIR light absorptivity of the obtained membranes, and the yellow shaded area is the AM 1.5G solar spectra.

To investigate the photothermal conversion performance, the evolutions of surface temperatures of the prepared membranes were recorded under a simulated sunlight source (Fig. 3-12c). As shown in Fig. 3-12d, EPU@PW has a steady high light absorbance over the entire solar spectrum (250 to 2500 nm), and the light absorptivity of EPU@PW (95.8%) is higher than that of DPU@PW, and CPU@PW, evidenced the synergistic effect of the three types of solar-thermal agents. Furthermore, the porous cavities of the fibrous membrane and the hierarchical structure of the single fiber

contribute the incident light to being reflected multiple times and captured.[53] Fig. 3-13a shows the temperature-time plot of EPU@PW, DPU@PW, CPU@PW, and PU@PW under a light radiation of 100 mW/cm^2 (1 sun). These membranes exhibit rapidly increasing temperatures at the initial stage until a plateau is reached, indicating the conversion and storage of solar energy through phase transition. After the phase change process is completed, the temperature rises rapidly again until it reaches a saturated temperature. When the simulated light is turned off, the temperatures of these membranes decrease sharply, until the second temperature plateau appears, which represents the heat releasing process and suggests a buffering effect on the decreasing temperature. In contrast, the temperature of PU@PW increases slowly under the same light intensity, and it couldn't reach the melting temperature of PW. The disappearance of the exact phase change platforms indicates that PU@PW failed to store solar energy without the help of the light absorbers. In order to evaluate the photothermal conversion performance, the saturated temperature and photothermal conversion efficiency were calculated and showed in Fig. 3-13b and Tab. 3-1. The saturated temperature of EPU@PW reaches 70.5 °C with a high thermal conversion efficiency of 92.43 %, which is higher than the values presented in most of the previously reported literatures (Table S3). It can be explained as follows: 1) The fibrous membranes possess large specific surface area for light harvesting.[54] 2) The synergistic interaction of hierarchical configurating CNTs, PDA, and PEDOT:PSS also contributes to the high saturation temperature and photothermal conversion efficiency. 3) Because of the longitudinal core-shell fiber structure and interconnect network, solar energy is captured by the outer shell and transferred to the core (PW) directly without redundant heat transfer paths. As shown in Fig. 3-13c, EPU@PW is exposed to different light intensities (50, 75 mW/cm^2), and the saturated temperatures are 60.4 °C (75 mW/cm^2) and 45.7 °C (50 mW/cm^2), respectively. Taking advantage of the synergistic photothermal converters, the membrane can be optical charged and applied heating effect even under a relatively lower intensive radiation. The saturated temperature and photothermal conversion efficiency in 100 mW/cm^2 is higher than that in 75 and 50 mW/cm^2 (Fig. 3-13d), because of the faster photothermal charging rate and the shortened phase change period

which can result in less heat loss (*via* dissipation to the external environment).[55] The repeated solar heating and cooling tests were conducted (100 mW/cm^2) for 10, 20, and 50 cycles to investigate the solar heating stability. Fig. 3-14 shows that all of the cycles exhibited almost identical temperature-time profiles in the heating and cooling processes, confirming the reliability of EPU@PW as a solar heater in wearable photothermal conversion and storage systems.

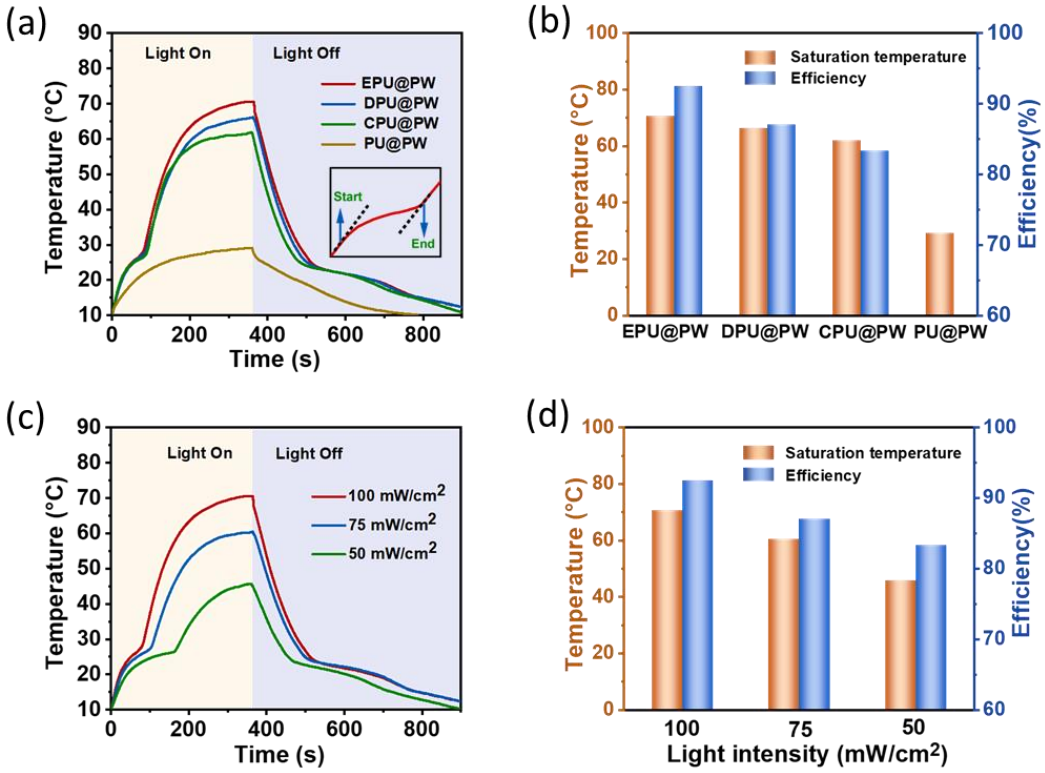

Fig. 3-13. (a) Temperature variation curves of the composite membranes under sunlight radiation of 100 mW/cm^2. (b) Saturated temperature of the corresponding membranes and the calculated photothermal conversion efficiency under radiation of 100 mW/cm^2. (c) Temperature variation curves of EPU@PW under sunlight radiation of 50, 75 and 100 mW/cm^2. (d) Saturated temperature and the calculated photothermal conversion efficiency of EPU@PW under radiation of 50, 75 and 100 mW/cm^2.

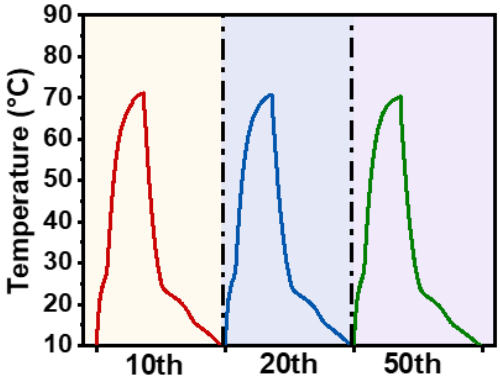

Fig. 3-14. Temperature variation curves of EPU@PW with cycling of 10, 20, 50 times under radiation of 100 mW/cm^2.

Tab. 3-1. Photothermal conversion efficiency

Sample	CPU@PW	DPU@PW	EPU@PW		
p (mW/cm^2)	100	100	100	75	50
A (cm^2)	4.41	4.41	4.41	4.41	4.41
t (s)	85	75	65	94	153
m (g)	0.245	0.246	0.248	0.248	0.248
[a] Input energy (J)	33.49	33.08	28.67	31.09	33.74
[b] Storage energy (J)	27.55	26.88	26.50	26.50	26.50
η_{PT} (%)	73.49	81.26	92.43	85.24	78.54

[a] Input energy= $A \cdot p \cdot t$

[b] Thermal energy storage = $m \cdot \Delta H$

As a proof of concept, both EPU@PW and PU@PW were attached to the arm skin under the light intensity of 100 mW/cm^2, the time-dependent temperature variations were recorded by an IR camera (Fig. 3-15). The temperature of PU@PW maintains the sync slightly changing temperature as the skin. By contrast, the temperature of EPU@PW increases from the initial skin temperature (30.6 °C) to 65.1 °C in 120 s. This result demonstrated the fast localized solar-heating performance of EPU@PW.

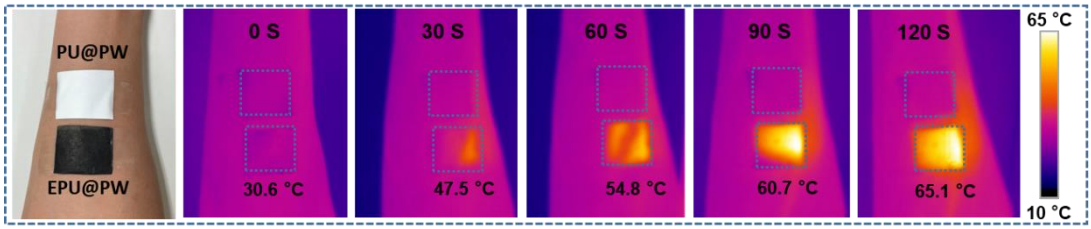

Fig.3-15. A digital photo and IR thermal images of EPU@PW and PU@PW placed on the arm at 100 mW/cm^2 sunlight illumination.

3.3.4 Electrothermal conversion performance

In the case of insufficient sunlight, like a rainy, cloudy day, or at night, or in an indoor space, electro-driven heating is necessary as a supplementary solution. Fig. 3-16a depicts that the membrane attached on one's clothing could be heated through a portable battery at night, and the generated heat would compensate for the heat a person would lose in cold environments. In another scenario (Fig. 3-16b), the membrane could be charged in advance, and the stored energy in PCMs would be released to keep warm in the absence of electricity. Therefore, as a promising candidate to perform as an electric heater, the steady heating temperature, electro-response sensitivity, temperature uniformity, heating adjustability and cyclic stability of EPU@PW were evaluated in detail.

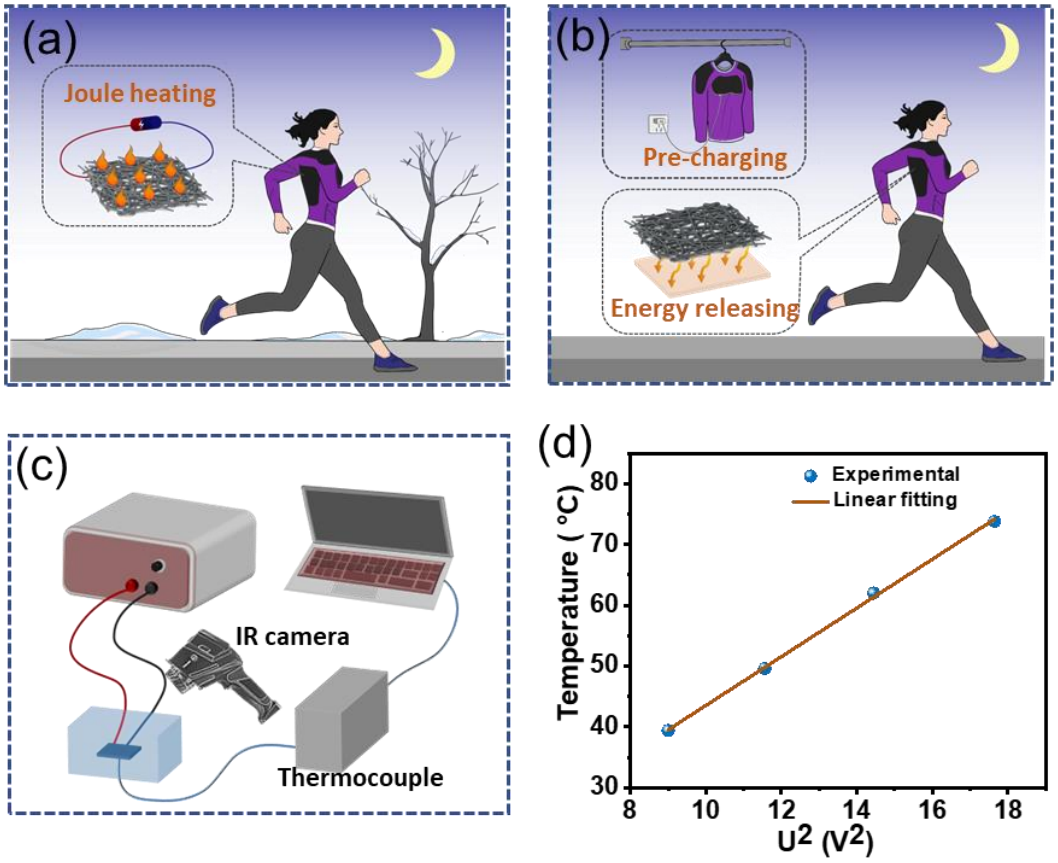

Fig. 3-16. Schematic illustrations of (a) electrothermal conversion and energy storage in the membrane sewed on the clothing under sunlight and (b) the latent energy being released to keep warm without electricity. (c) Electrothermal conversion testing device.

Different constant DC voltages were applied on EPU@PW for the Joule heating test, and the real temperatures were recorded as displayed in Fig. 3-16c. The time-dependent temperature profiles at controlled voltages are plotted in Fig. 3-17a. Two temperature plateaus with reduced slopes also appeared in the heating and cooling process, suggesting the responsive thermal storage and release to maintain a comfortable temperature. In addition, a higher voltage results in a faster electro-thermal response as well as a higher saturated temperature. The saturated temperature can reach 39.4 °C (3 V), 49.6 °C (3.4 V), 62.0 °C (3.8 V), and 73.8 °C (4.2 V), increasing from the room temperature of 10 °C, the driving voltages are far below the safe threshold of 36 V. Fig. 3-16d shows the positive linear relationship between saturated temperatures and the square of the applied voltages, conforming to Joule's law.

Additionally, the electrothermal storage efficiencies at different voltages are calculated and displayed in Fig. 3-17b, Tab. 3-2, which are comparable or superior to those of the previously reported phase change composites (Tab. 3-3). The faster electrothermal responsibility and shorter charging time at a higher voltage cause the reduction of heat loss, so a higher electrothermal conversion efficiency is produced.[56] As shown in Fig. 3-17c, the temperature variation is consistent with the applied alternating voltage, indicating a flexible and sensitive heating behavior. In Fig. 3-17 d, the electro-heating and cooling tests at a constant voltage of 3.4 V were conducted numerous times to valid the electrothermal cycle stability, which exhibited perfect reproducibility in 50 cycles. In addition, EPU@PW was heated at a constant voltage of 3.4 V for a long-term test. EPU@PW maintained a stable temperature around 51.5 °C for more than 1800 s (Fig. 3-17e), validating its stability in long-term service.

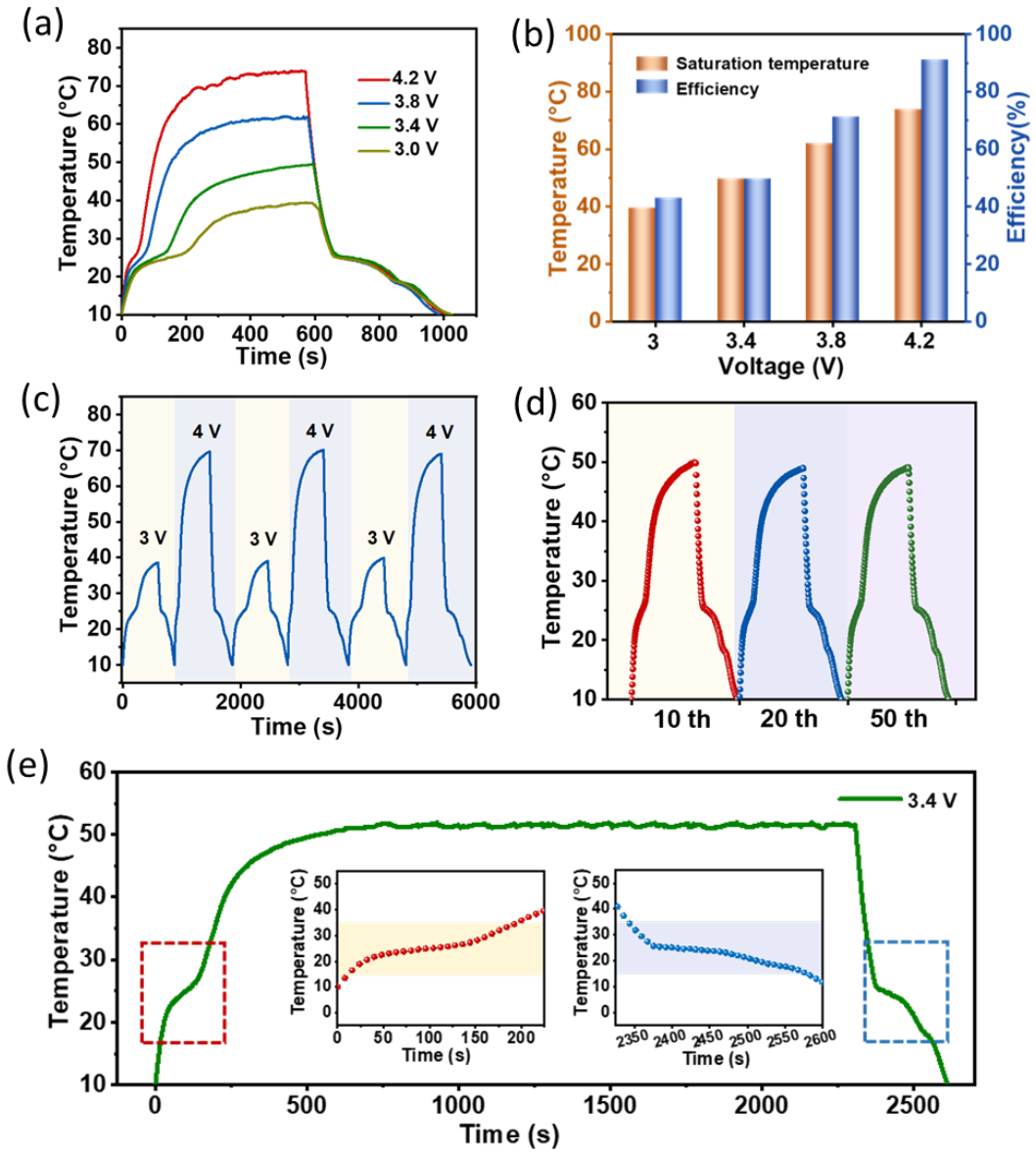

Fig. 3-17. (a) Temperature variation curves of EPU@PW at different voltages. (b) Saturated temperature and the calculated electrothermal conversion efficiency of EPU@PW under corresponding driving voltages. (c) Temperature variation curve at an alternating voltage. (d) Temperature variation curves of EPU@PW with cycling of 2, 20, 50 times at 3.4 V. (e) Long-term heating test at 3.4 V.

Tab. 3-2. Electrothermal conversion efficiency of EPU@PW

U (V)	3	3.4	3.8	4.2
I (mA)	105	120	140	165
t (s)	196	131	70	42

m (g)	0.248	0.248	0.248	0.248
[a] Input energy (J)	61.74	53.45	37.24	29.11
[b] Storage energy (J)	26.50	26.50	26.50	26.50
η_{ET} (%)	42.92	49.58	71.16	91.03

[a] Input energy= $U \cdot I \cdot t$

[b] Thermal energy storage = $m \cdot \Delta H$

Besides, as an ideal Joule heater, EPU@PW exhibits a homogenous temperature distribution at voltages from 3 V to 4.2 V (Fig. 3-18a). Moreover, as seen in Fig. 3-18b, the membrane is wrapped directly around the human finger, generating heating effect by electro-driving. Due to the excellent flexibility, the membrane heater easily can conform to the bent finger with stable heating performance. The prepared membrane also exhibited an interesting sewability (Fig.3-18c). When the cut membrane is stitched by a cotton yarn, the extinguished LED is lighted on again, and it exhibits a good healing ability of conductivity by sewing, which is compatible with the process of manufacturing clothing. These results verified the great potential of EPU@PW for application in thermal therapy and wearable thermal management.

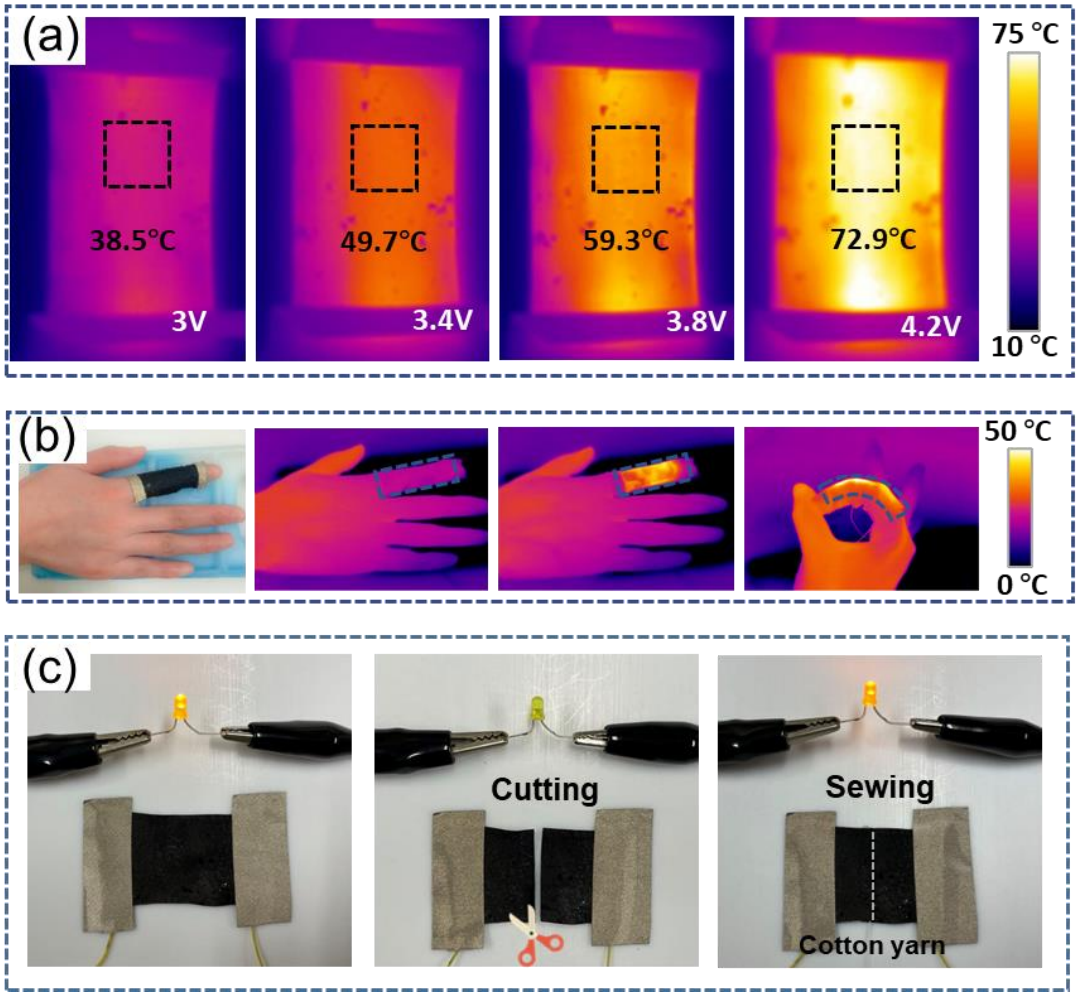

Fig. 3-18. (a) IR thermal photos of EPU@PW at different voltages. (b) The digital and thermal photos of EPU@PW wrapped around a finger for heating. (c) Conductivity healing by sewing.

3.4 Conclusion

In summary, we report a fibrous membrane-based textile with tri-mode thermoregulatory performance that includes reversible temperature-responsive phase change property, solar-heating, and Joule heating effects. The integrated multimodal thermal regulating system is attributed to the cooperation between the intrinsic properties of the employed materials and the delicately designed hierarchical core-sheath fiber structure. The favorable thermal storage capability originated from the effective encapsulation of PW through coaxial electrospinning technology, where the plastic elastomer PU, as a protective and supportive shell, assures decent mechanical properties. The introduction of light absorbers of CNTs, PDA, and PEDOT:PSS through

various surface modifications achieved a synergistic photothermal conversion, reaching a high saturated temperature of 70.5 °C (1 sun). Owing to the low resistance of PEDOT:PSS, the prepared membrane possessed an favorable electrothermal conversion performance with a high saturated temperature of 73.8 °C (4.2 V). The combination of phase change, solar-heating, and Joule heating effect enables the phase change membrane to be charged by either solar energy or electrical energy, and it provides multiple thermal regulation routes, which presents promising potential for application in wearable personal thermal management.

Reference

(1) Hu, R.; Liu, Y.; Shin, S.; Huang, S.; Ren, X.; Shu, W.; Cheng, J.; Tao, G.; Xu, W.; Chen, R.; Luo, X. Emerging Materials and Strategies for Personal Thermal Management. *Adv. Energy Mater.* **2020**, 1903921.

(2) Fang, Y.; Chen, G.; Bick, M.; Chen, J. Smart Textiles for Personalized Thermoregulation. *Chem. Soc. Rev.* **2021**, *50* (17), 9357–9374.

(3) Peng, Y.; Cui, Y. Advanced Textiles for Personal Thermal Management and Energy. *Joule* **2020**, *4* (4), 724–742.

(4) Pakdel, E.; Naebe, M.; Sun, L.; Wang, X. Advanced Functional Fibrous Materials for Enhanced Thermoregulating Performance. *ACS Appl. Mater. Interfaces* **2019**, 11, 13039–13057.

(5) Tabor, J.; Chatterjee, K.; Ghosh, T. K. Smart Textile-Based Personal Thermal Comfort Systems: Current Status and Potential Solutions. *Adv. Mater. Technol.* **2020**, *5*, 1901155.

(6) Luo, H.; Zhu, Y.; Xu, Z.; Hong, Y.; Ghosh, P.; Kaur, S.; Wu, M.; Yang, C.; Qiu, M.; Li, Q. Outdoor Personal Thermal Management with Simultaneous Electricity Generation. *Nano Lett.* **2021**, *21* (9), 3879–3886.

(7) Shi, M.; Shen, M.; Guo, X.; Jin, X.; Cao, Y.; Yang, Y.; Wang, W.; Wang, J. Ti3C2Tx MXene-Decorated Nanoporous Polyethylene Textile for Passive and Active Personal Precision Heating. *ACS Nano* **2021**, 15,11396–11405.

(8) Wang, Y.; Liang, X.; Zhu, H.; Xin, J. H.; Zhang, Q.; Zhu, S. Reversible Water Transportation Diode: Temperature-Adaptive Smart Janus Textile for Moisture/Thermal Management. *Adv. Funct. Mater.* **2020**, 30, 1907851.

(9) Yuan, K.; Shi, J.; Aftab, W.; Qin, M.; Usman, A.; Zhou, F.; Lv, Y.; Gao, S.; Zou, R. Engineering the Thermal Conductivity of Functional Phase-Change Materials for Heat Energy Conversion, Storage, and Utilization. *Adv. Funct. Mater.* **2020**, 30, 1904228.

(10) Shi, J.; Qin, M.; Aftab, W.; Zou, R. Flexible Phase Change Materials for Thermal Energy Storage. *Energy Storage Mater.* **2021**, *41*, 321–342.

(11) Zhao, X. Flexible Phase Change Materials: Preparation, Properties and Application. *Chem. Eng. J.* **2022**, 431,134231.

(12) Wu, J.; Wang, M.; Dong, L.; Zhu, C.; Shi, J.; Morikawa, H. Ultraflexible, Breathable, and Form-Stable Phase Change Fibrous Membranes by Green Electrospinning for Personal Thermal

Management. *ACS Sustainable Chem. Eng.* **2022**, 10 (24), 7873–7882.

(13) Xi, S.; Wang, L.; Xie, H.; Yu, W. Superhydrophilic Modified Elastomeric RGO Aerogel Based Hydrated Salt Phase Change Materials for Effective Solar Thermal Conversion and Storage. *ACS Nano* **2022**, *16* (3), 3843–3851.

(14) Li, Y. Anisotropy-Functionalized Cellulose-Based Phase Change Materials with Reinforced Solar-Thermal Energy Conversion and Storage Capacity. *Chem. Eng. J.* **2021**, 415,129086.

(15) Xue, F. Preparation and Application of Three-Dimensional Filler Network towards Organic Phase Change Materials with High Performance and Multi-Functions. *Chem. Eng. J.* **2021**, 419,129620.

(16) Cui, J.; Li, W.; Wang, Y.; Yu, H.; Feng, X.; Lou, Z.; Shan, W.; Xiong, Y. Ultra-Stable Phase Change Coatings by Self-Cross-Linkable Reactive Poly(Ethylene Glycol) and MWCNTs. *Adv Funct Materials* **2022**, *32* (10), 2108000.

(17) Kou, Y.; Sun, K.; Luo, J.; Zhou, F.; Huang, H.; Wu, Z.-S.; Shi, Q. An Intrinsically Flexible Phase Change Film for Wearable Thermal Managements. *Energy Storage Mater.* **2021**, *34*, 508–514.

(18) Shi, J.; Aftab, W.; Liang, Z.; Yuan, K.; Maqbool, M.; Jiang, H.; Xiong, F.; Qin, M.; Gao, S.; Zou, R. Tuning the Flexibility and Thermal Storage Capacity of Solid–Solid Phase Change Materials towards Wearable Applications. *J. Mater. Chem. A* **2020**, *8* (38), 20133–20140.

(19) Xiong, J.; Sun, Z.; Yu, J.; Liu, H.; Wang, X. Thermal Self-Regulatory Smart Biosensor Based on Horseradish Peroxidase-Immobilized Phase-Change Microcapsules for Enhancing Detection of Hazardous Substances. *Chem. Eng. J.* **2022**, *430*, 132982.

(20) Zhang, Z.; Zhang, Z.; Chang, T.; Wang, J.; Wang, X.; Zhou, G. Phase Change Material Microcapsules with Melamine Resin Shell *via* Cellulose Nanocrystal Stabilized Pickering Emulsion In-Situ Polymerization. *Chem. Eng. J.***2022**, *428*, 131164.

(21) Liu, L.; Shan, X.; Hu, X.; Lv, W.; Wang, J. Superhydrophobic Silica Aerogels and Their Layer-by-Layer Structure for Thermal Management in Harsh Cold and Hot Environments. *ACS Nano* **2021**, *15* (12), 19771 – 19782.

(22) Cao, R.; Xia, Y.; Wang, J.; Jia, X.; Jia, C.; Zhu, S.; Zhang, W.; Gao, X.; Zhang, X. Suppressing Thermal Negative Effect and Maintaining High-Temperature Steady Electrical Performance of Triboelectric Nanogenerators by Employing Phase Change Material. *ACS Appl. Mater. Interfaces* **2021**, 13, 41657–41668.

(23) Lu, Y.; Xiao, X.; Fu, J.; Huan, C.; Qi, S.; Zhan, Y.; Zhu, Y.; Xu, G. Novel Smart Textile with Phase Change Materials Encapsulated Core-Sheath Structure Fabricated by Coaxial Electrospinning. *Chem. Eng. J.* **2019**, *355*, 532–539.

(24) Xu, T.; Zhang, S.; Han, S.; Qin, Y.; Liu, C.; Xi, M.; Yu, X.; Li, N.; Wang, Z. Fast Solar-to-Thermal Conversion/Storage Nanofibers for Thermoregulation, Stain-Resistant, and Breathable Fabrics. *Ind. Eng. Chem. Res.* **2021**, 60, 5869–5878.

(25) Yoon, J.; Yang, H.-S.; Lee, B.-S.; Yu, W.-R. Recent Progress in Coaxial Electrospinning: New Parameters, Various Structures, and Wide Applications. *Adv. Mater.* **2018**, 30, 1704765.

(26) Liu, L.; Chen, W.; Zhang, H.; Wang, Q.; Guan, F.; Yu, Z. Flexible and Multifunctional Silk Textiles with Biomimetic Leaf-Like MXene/Silver Nanowire Nanostructures for Electromagnetic Interference Shielding, Humidity Monitoring, and Self-Derived Hydrophobicity. *Adv. Funct. Mater.* **2019**, 29 (44), 1905197.

(27) Hsu, P.-C.; Liu, C.; Song, A. Y.; Zhang, Z.; Peng, Y.; Xie, J.; Liu, K.; Wu, C.-L.; Catrysse, P. B.; Cai, L.; Zhai, S.; Majumdar, A.; Fan, S.; Cui, Y. A Dual-Mode Textile for Human Body Radiative

Heating and Cooling. *Sci. Adv.* **2017**, *3* (11), e1700895.

(28) Li, Y. One-Step Synthesis of Graphene-Based Composite Phase Change Materials with High Solar-Thermal Conversion Efficiency. *Chem. Eng. J.* **2022**, 429, 132439.

(29) Gong, S.; Sheng, X.; Li, X.; Sheng, M.; Wu, H.; Lu, X.; Qu, J. A Multifunctional Flexible Composite Film with Excellent Multi-Source Driven Thermal Management, Electromagnetic Interference Shielding, and Fire Safety Performance, Inspired by a "Brick–Mortar" Sandwich Structure. *Adv. Funct. Mater.* **2022**, 2200570.

(30) Sun, K.; Dong, H.; Kou, Y.; Yang, H.; Liu, H.; Li, Y.; Shi, Q. Flexible Graphene Aerogel-Based Phase Change Film for Solar-Thermal Energy Conversion and Storage in Personal Thermal Management Applications. *Chem. Eng. J.* **2021**, *419*, 129637.

(31) Guo, Z.; Sun, C.; Wang, J.; Cai, Z.; Ge, F. High-Performance Laminated Fabric with Enhanced Photothermal Conversion and Joule Heating Effect for Personal Thermal Management. *ACS Appl. Mater. Interfaces* **2021**, *13* (7), 8851–8862.

(32) Wang, X.; Lei, Z.; Ma, X.; He, G.; Xu, T.; Tan, J.; Wang, L.; Zhang, X.; Qu, L.; Zhang, X. A Lightweight MXene-Coated Nonwoven Fabric with Excellent Flame Retardancy, EMI Shielding, and Electrothermal/Photothermal Conversion for Wearable Heater. *Chem. Eng. J.* **2022**, *430*, 132605.

(33) Tang, P.; Deng, Z.; Zhang, Y.; Liu, L.; Wang, Z.; Yu, Z.; Zhang, H. Tough, Strong, and Conductive Graphene Fibers by Optimizing Surface Chemistry of Graphene Oxide Precursor. *Adv Funct. Materials* **2022**, 2112156.

(34) Tian, G. Coating of Multi-Wall Carbon Nanotubes (MWCNTs) on Three-Dimensional, Bicomponent Nonwovens as Wearable and High-Performance Piezoresistive Sensors. *Chem. Eng. J.* **2021**, 425,130682.

(35) Zeng, L.; Liu, X.; Chen, X.; Soutis, C. π - π Interaction between Carbon Fibre and Epoxy Resin for Interface Improvement in Composites. *Composites Part B: Engineering* **2021**, *220*, 108983.

(36) Li, Z.; Zhang, X.; Wang, S.; Yang, Y.; Qin, B.; Wang, K.; Xie, T.; Wei, Y.; Ji, Y. Polydopamine Coated Shape Memory Polymer: Enabling Light Triggered Shape Recovery, Light Controlled Shape Reprogramming and Surface Functionalization. *Chem. Sci.* **2016**, *7* (7), 4741–4747.

(37) Wang, Z. A PDA Functionalized CNT/PANI Self-Powered Sensing System for Meat Spoilage Biomarker NH_3 Monitoring. *Sensors and Actuators* **2022**, 356,131292.

(38) Adekoya, G. J.; Sadiku, R. E.; Ray, S. S. Nanocomposites of PEDOT:PSS with Graphene and Its Derivatives for Flexible Electronic Applications: A Review. *Macromol. Mater. Eng.* **2021**, 306, 2000716.

(39) Gan, D.; Huang, Z.; Wang, X.; Jiang, L.; Wang, C.; Zhu, M.; Ren, F.; Fang, L.; Wang, K.; Xie, C.; Lu, X. Graphene Oxide-Templated Conductive and Redox-Active Nanosheets Incorporated Hydrogels for Adhesive Bioelectronics. *Adv. Funct. Mater.* **2020**, 30, 1907678.

(40) Zhang, X. Synergistic Work of Photo-Thermoelectric and Hydroelectric Effects of Hierarchical Structure Photo-Thermoelectric Textile for Solar Energy Harvesting and Solar Steam Generation Simultaneously. *Chem. Eng. J.* **2021**, 426, 131923.

(41) Sun, K.; Kou, Y.; Zhang, Y.; Liu, T.; Shi, Q. Photo-Triggered Hierarchical Porous Carbon-Based Composite Phase-Change Materials with Superior Thermal Energy Conversion Capacity. *ACS Sustainable Chem. Eng.* 2020, 8, 3445−3453.

(42) Liu, L.-X.; Chen, W.; Zhang, H.-B.; Zhang, Y.; Tang, P.; Li, D.; Deng, Z.; Ye, L.; Yu, Z.-Z. Tough and Electrically Conductive Ti_3C_2T MXene–Based Core–Shell Fibers for High–Performance Electromagnetic Interference Shielding and Heating Application. *Chem. Eng. J.* **2022**, 430, 133074.

(43) Liu, L.-X.; Chen, W.; Zhang, H.-B.; Ye, L.; Wang, Z.; Zhang, Y.; Min, P.; Yu, Z.-Z. Super-Tough and Environmentally Stable Aramid. Nanofiber@MXene Coaxial Fibers with Outstanding Electromagnetic Interference Shielding Efficiency. *Nano-Micro Lett*. **2022**, 14 (1), 111.

(44) Chen, S.; Cao, Y.; Feng, J. Polydopamine as an Efficient and Robust Platform to Functionalize Carbon Fiber for High-Performance Polymer Composites. *ACS Appl. Mater. Interfaces* **2014**, 6, 349–356.

(45) Guo, H.; Chen, T.; Yu, L.; Chen, A.; Sun, T.; Wang, J.; Wang, C.; Zhang, J.; Yang, Y. Enhanced Performance of Si/PEDOT: PSS Heterojunction Solar Cells *via* Multi-Walled Carbons Coated with Polydopamine. *Optical Materials* **2021**, *120*, 111375.

(46) Ma, H.; Shao, Y.; Zhang, C.; Lv, Y.; Feng, Y.; Dong, Q.; Shi, Y. Enhancing the Interface Contact of Stacking Perovskite Solar Cells with Hexamethylenediammonium Diiodide-Modified PEDOT:PSS as an Electrode. *ACS Appl. Mater. Interfaces* **2020**, *12* (37), 42321– 42327.

(47) Liu, Z.; Hu, Q.; Guo, S.; Yu, L.; Hu, X. Thermoregulating Separators Based on Phase-Change Materials for Safe Lithium-Ion Batteries. *Adv. Mater.* **2021**, *33* (15), 2008088.

(48) Yu, X.; Li, Y.; Yin, X.; Wang, X.; Han, Y.; Si, Y.; Yu, J.; Ding, B. Corncoblike, Superhydrophobic, and Phase-Changeable Nanofibers for Intelligent Thermoregulating and Water-Repellent Fabrics. *ACS Appl. Mater. Interfaces* **2019**, *11* (42), 39324–39333.

(49) Song, S.; Ai, H.; Zhu, W.; Qiu, F.; Wang, Y.; Zhou, J. Eco-Friendly Electrospun Nanofibrous Membranes with High Thermal Energy Capacity and Improved Thermal Transfer Efficiency. *Renewable Energy* **2020**, *148*, 504–511.

(50) Wang, S.; Yi, L.; Wang, L.; Yao, J.; Militky, J.; Venkataramam, M.; Wiener, J.; Zhang, M. Preparation of Core-Sheath Nanofibers with High Latent Heat by Thermal Cross-Linking and Coaxial Electrospinning. *Polymer* **2021**, *228*, 123958.

(51) Zhu, W.; Wang, Y.; Song, S.; Ai, H.; Qiu, F.; Li, D.; Dong, L. Environmental-Friendly Electrospun Phase Change Fiber with Exceptional Thermal Energy Storage Performance. *Sol. Energy Mater. Sol. Cells* **2021**, *222*, 110939.

(52) Li, S.; Wang, H.; Mao, H.; Li, J.; Shi, H. Light-to-Thermal Conversion and Thermoregulated Capability of Coaxial Fibers with a Combined Influence from Comb-like Polymeric Phase Change Material and Carbon Nanotube. *ACS Appl. Mater. Interfaces* **2019**, *11* (15), 14150–14158.

(53) Zhou, Z.; Song, Q.; Huang, B.; Feng, S.; Lu, C. Facile Fabrication of Densely Packed Ti_3C_2 MXene/Nanocellulose Composite Films for Enhancing Electromagnetic Interference Shielding and Electro-/Photothermal Performance. *ACS Nano* **2021**, 15, 12405−12417.

(54) Peng, Y.; Zhao, W.; Ni, F.; Yu, W.; Liu, X. Forest-like Laser-Induced Graphene Film with Ultrahigh Solar Energy Utilization Efficiency. *ACS Nano* **2021**, *15*, 19490–19502.

(55) Aftab, W.; Mahmood, A.; Guo, W.; Yousaf, M.; Tabassum, H.; Huang, X.; Liang, Z.; Cao, A.; Zou, R. Polyurethane-Based Flexible and Conductive Phase Change Composites for Energy Conversion and Storage. *Energy Storage Materials* **2019**, *20*, 401– 409.

(56) Wu, M.; Li, T.; Wang, P.; Wu, S.; Wang, R.; Lin, J. Dual-Encapsulated Highly Conductive and Liquid-Free Phase Change Composites Enabled by Polyurethane/Graphite Nanoplatelets Hybrid Networks for Efficient Energy Storage and Thermal Management. *Small* **2021**, 2105647.

Tab. 3-3. Summary of photothermal conversion and electrothermal conversion performance of recently reported phase change composite materials

Materials	Photothermal conversion			Electrothermal conversion			Refs
	p (mW/cm^2)	T_{PT} (°C)	η_{PT} (%)	U (V)	T_{ET} (°C)	η_{ET} (%)	
SAT/RGO	100	72.3	86.3	--	--	--	S1
PEG/ carbon cloth @ZIF	100	102	61.1	3	59	55.7	S2
PEG/porous carbon	110	78	89	3.5	--	84.6	S3
PEG/graphene	--	--	--	4.8	--	86.3	S4
PEDOT:PSS/MWCNTs/LA/PU	100	72	82.8	15	52	--	S5
PEG@PU-RGNPs	--	--	--	1.2	--	92.1	S6
PEG-PU-CNT	100	--	80.5	--	--	--	S7
PW/ porous carbon	110	--	91	3.6	--	74	S8
PW@PDVB-12/PPy	100	47	85.2	2.5	54	89.6	S9
PEDOT:PSS@PDA@CNTs@PU@PW	100	70.5	92.4	4.2	73.8	91.0	**This work**

T_{PT}: saturated temperature of photothermal conversion; T_{ET}: saturated temperature of electrothermal conversion

Reference in Tab. 3-3

(S1) Xi, S.; Wang, L.; Xie, H.; Yu, W. Superhydrophilic Modified Elastomeric RGO Aerogel Based Hydrated Salt Phase Change Materials for Effective Solar Thermal Conversion and Storage. *ACS Nano* **2022**, *16* (3), 3843–3851.

(S2) Dong, C.; Li, A.; Wang, C.; Li, J.; Gao, H.; Chen, X.; Wang, Y.; Li, L.; Zheng, Y.; Wang, G. Engineering Attractive Interaction in ZIF-Based Phase Change Materials for Boosting Electro- and Photo- Driven Thermal Energy Storage. *Chem. Eng. J.* **2022**, *430*, 133007.

(S3) Yin, C.; Weng, L.; Fei, Z.-X.; Shi, L.-Y.; Yang, K.-K. Form-Stable Phase Change Composites Based on Porous Carbon Derived from Polyacrylonitrile Hydrogel. *Chem. Eng. J.* **2022**, *431*, 134206.

(S4) Kou, Y.; Sun, K.; Luo, J.; Zhou, F.; Huang, H.; Wu, Z.-S.; Shi, Q. An Intrinsically Flexible Phase Change Film for Wearable Thermal Managements. *Energy Stor. Mater.* **2021**, *34*, 508–514.

(S5) Niu, Z.; Yuan, W. Smart Nanocomposite Nonwoven Wearable Fabrics Embedding Phase Change Materials for Highly Efficient Energy Conversion–Storage and Use as a Stretchable Conductor. *ACS Appl. Mater. Interfaces* **2021**, *13* (3), 4508–4518.

(S6) Wu, M.; Li, T.; Wang, P.; Wu, S.; Wang, R.; Lin, J. Dual-Encapsulated Highly Conductive and Liquid-Free Phase Change Composites Enabled by Polyurethane/Graphite Nanoplatelets Hybrid Networks for Efficient Energy Storage and Thermal Management. *Small* **2022**, *18* (9), 2105647.

(S7) Shi, J.; Aftab, W.; Liang, Z.; Yuan, K.; Maqbool, M.; Jiang, H.; Xiong, F.; Qin, M.; Gao, S.; Zou, R. Tuning the Flexibility and Thermal Storage Capacity of Solid–Solid Phase Change Materials towards Wearable Applications. *J. Mater. Chem. A* **2020**, *8* (38), 20133–20140.

(S8) Maleki, M.; Karimian, H.; Shokouhimehr, M.; Ahmadi, R.; Valanezhad, A.; Beitollahi, A. Development of Graphitic Domains in Carbon Foams for High Efficient Electro/Photo-to-Thermal Energy Conversion Phase Change Composites. *Chem. Eng. J.* **2019**, *362*, 469–481.

(S9) Kong, L.; Wang, Z.; Kong, X.; Wang, L.; Ji, Z.; Wang, X.; Zhang, X. Large-Scale Fabrication of Form-Stable Phase Change Nanotube Composite for Photothermal/Electrothermal Energy Conversion and Storage. *ACS Appl. Mater. Interfaces* **2021**, *13* (25), 29965–29974.

Chapter 4

Highly integrated, breathable, metalized phase change fibrous membranes based on hierarchical coaxial fiber structure for multimodal personal thermal management

Chapter 4: Highly integrated, breathable, metalized phase change fibrous membranes based on hierarchical coaxial fiber structure for multimodal personal thermal management

4.1 Introduction

Thermophysiological comfort is crucial for human health, which means that the body temperature should be maintained within a relatively narrow range for normal functional performance.[1,2] Considering the huge energy consumption of the indoor centralized space cooling/heating technologies, personal thermal management (PTM) strategy based on advanced textiles is urgently desirable for alleviating the global energy crisis, because of its more energy saving manner that emphasizes thermal regulation on the individual level.[3-5] Generally, designing smart textiles for heating purpose are based on two mechanisms: 1) Confining the heat from human body for suppressed heat lose, which contains several passive warming strategies based on insulating textiles with lower thermal conductivity,[6-7] lower-Mid-IR emission and higher-IR reflection,[8-10] but the extent of heating effect is limited. 2) Providing extra heat to human body. Photothermal conversion is appealing in various applications due to the renewable, clean and easy availability feature of solar energy. Photothermal materials such as plasmonic nanoparticles,[11] carbon-based materials,[12-13] and conjugated polymers,[14] are capable to convert solar energy into thermal energy directly, and this unique self-heating feature is promising for personal heating. However, solar heating depends on intensive sunlight seriously, which is uncontrollable and intermittent. Therefore, electro-heating has always been considered as a complementary option in the absence of solar energy, such as rainy, cloudy day, at night.[15-17] Much effort has been made to investigate the textiles cooperated with optical and electric dual-heating functions, which combined the advantages of energy saving and precise controllability of solar heating and Joule heating, respectively.[18-21] Nevertheless, electric heaters must be connected a power source in service, which hinders their

universal application. Therefore, thermal energy storage (TES) technology is necessary to relieve the mismatch between the energy supply and demand.[22-23] Phase change materials (PCMs) based on latent heat storage, capable of storing and releasing excess energy, has been regarded as a potential candidate in thermal management.[24-25] Besides, organic PCMs also character with the high energy density, non-corrosion, and small supercooling.[26-27] Therefore, the synergistic thermal regulation strategy integrated with photothermal/electrothermal conversion and energy storage performance is promising in all-weather, on-demand personal thermal management.[28-30] However, current researches on thermal management mainly focused on the integration with high-performance based on dense impermeable substrates.[28,30-33] Alternatively, the employed porous substrates were usually treated with incompatible processes that induce pores to be filled, resulting in inhibited penetration.[34-36] The limited breathability leads to a major concern for long-term wearing comfort. Therefore, it remains challenging for structural design and compatible functionalization process to achieve the high integration of multimodal thermoregulating routes without compromising structural permeability.

Herein, we fabricated a breathable and synergistic thermoregulating fibrous membrane integrated with photothermal/electrothermal conversion and energy storage/release performance for all-weather, energy-saving and personalized thermal management. Coaxial electrospinning was employed to fabricate composite phase change membranes, where paraffine wax (PW) was encapsulated in the core-sheath structured fibers, and the high aspect ratio of these fibers as well as the porous structure of the prepared membranes endowed them with favorable flexibility and breathability. In particular, the resultant core-sheath phase change fibers were further functionalized by Ag nanoparticles (AgNPs) through polydopamine (PDA) assisted metal deposition technique for complementary photo/electrothermal conversion performance. Specifically, PDA, as an intermediate modified layer, facilitates the uniform deposition of AgNPs and ensures a strong interfacial adhesion through the “bridge” effect between the metal layer and the polymer fiber substrates. Therefore, the metalized phase change fibers with a specific hierarchical coaxial structure, combining the functional

components orderly (AgNPs@PDA@PU@PW), achieved a high integration of the multi-thermoregulating routes. As a result, the all-in-one fibrous membrane exhibited a high heat enthalpy originating from the core PW, a decent photothermal conversion capability owing to the synergistic effect of PDA and AgNPs, and an excellent electrothermal conversion performance due to the metal conductive pathways. What's more, the favorable air permeability, flexibility and washability make the resulting membrane extremely promising for wearable personal thermal management.

4.2 Experimental section

4.2.1 Materials

Polyurethane (PU, Mw = 110,000), was purchased from Sigma-Aldrich Chemical Co, USA. Paraffine wax (PW) was obtained from Shanghai Yijiu Chemical Co., Ltd, China. N, N-dimethylformamide (DMF), tetrahydrofuran (THF), dopamine hydrochloride (DA, 98%), tris(hydroxymethyl) aminomethane hydrochloride (Tris, 99%), glucose ($C_6H_{12}O_6$), silver nitrate ($AgNO_3$), ammonia solution (NH_3 aq, 28%), hydrochloric acid (5 mol/L) and kerosene were purchased from FUJIFILM Wako, Japan. All the chemical materials were used as received.

4.2.2 Preparation of PCF (PU@PW) fibrous membranes

The phase change membranes were prepared by coaxial electrospinning. Briefly, PU solution in DMF/THF mixture (5/5, w/w) with a concentration of 18 wt % was used as the precursor solution for the sheath layer. Core solution was prepared by adding melted PW in kerosene (80 wt %). These solutions were injected into a coaxial needle with the speed of 1.2 mL/h and 0.6 mL/h for outer and inner jet flow, respectively. The applied voltage was 15 kV, and the relative humidity and temperature were controlled at 40 ± 5% and 30 ± 3 °C.

4.2.3 Preparation of DPCF (PDA@PU@PW) and APCF (AgNPs@PDA@PU@PW) fibrous membranes

Prior to the silver electroless deposition, the phase change membrane PCF was

activated by a PDA layer. First, PCF was immersed in the DA solution (pH=8.5) with a concentration of 2 g/L and stirred for 12 h. Then the obtained membrane (denoted as DPCF) was washed by deionized water to remove the excess PDA microspheres. After that the silver electroless plating bath was prepared by dropwise adding aqueous NH_3 (28%) into $AgNO_3$ solution (2 g/L) until the solution became transparent again. DPCF was immersed in the above solution for 30 min, then the reducing agent glucose was added into the mixture with a concentration of 4 g/L. The reaction time was controlled at 20, 40 and 60 min, the resulting membranes were denoted as APCF20, APCF40 and APCF60, respectively.

4.2.4 Characterization

The morphology and elemental composition of the samples were observed by Field-emission scanning electron microscopy (FE-SEM, JSM-IT800SHL, Japan) with energy-dispersive spectrometry (EDS) and transmission electron microscopy (TEM, JEM-2010, Japan). The crystalline and chemical properties were investigated by the Fourier-transform infrared spectrophotometer (FTIR-6600, Jasco, Japan), X-ray diffraction (XRD, MiniFlex300, Rigaku, Japan) and X-ray photoelectron spectroscopy (XPS, AXIS-ULTRA HSA SV, Japan). Thermal energy storage and release properties were characterized by differential scanning calorimetry (Thermo plus EVO2 DSCvesta, Rigaku, Japan) with a heating/cooling rate of 10 °C $\cdot min^{-1}$ under N_2 atmosphere (Flow rate = 50 mL$\cdot min^{-1}$). The optical property was detected by an ultraviolet-visible-near infrared spectrophotometer (UV-3600, Shimadzu Ltd., Japan). Infrared photos were taken with an infrared thermal imaging camera (Testo 875-2i, German). The photothermal conversion and storage performance was studied via simulated solar irradiation (XES-40S3-TT, San-electric, Japan) and the temperatures were documented by a thermal couple (KE331L, CHINO, Japan). The electrothermal conversion and storage performance was investigated by applying certain voltages through a DC power supply (AD-8724D, A&D, Japan). The electromechanical property is evaluated by measuring the relative resistance change ($\Delta R/R_0$, $\Delta R = R\text{-}R_0$, where R_0 is the original

resistance, *R* is the transient resistance under deformation).

4.3 Results and discussion

4.3.1 Fabrication process and characterization

The fabricated process of the synergistic multimodal thermoregulating membranes consisting of hierarchical coaxial constructed fibers is illustrated in Fig. 4-1a. The preparation process consists of two steps, coaxial electrospinning and PDA assisted metal deposition, the former one is used to prepare flexible phase change composites, and the later one is employed for further functionalization. First, coaxial electrospinning is employed to construct 1D core-sheath structure for encapsulation of PCMs. Here, PW is contained in the elastic sheath of PU as it undergoes the phase change transition of melting and freezing. The as-prepared phase change fibrous membrane possessed inherently high surface area, flexibility, as well as breathability, serving as a favorable substrate for further functionalization. Subsequently, the membrane was modified by PDA through the self-polymerization of DA monomers. Finally, AgNPs were grown on the fiber surface through electroless plating. Here, PDA worked as the "linking bridge" between the substrate of phase change fibers and the outer layer of AgNPs, because the abundant catechol moieties and amine groups endowed it with the strong chelating ability to metal ions.[37] As illustrated in Fig. 4-1b, Ag ions were firstly absorbed on the PDA layer, and then in situ reduced into AgNPs, attributed to the mild reducibility of PDA.[38] The resultant AgNPs act as seeds to facilitate the formation of silver coating.[39] Thanks to the collaboration of the core and sheath components, the integrated membrane was endowed with the synergistic photo/electro-thermal energy conversion (solar/Joule heating) and energy storage (phase change behavior) performance (Fig. 4-1c).

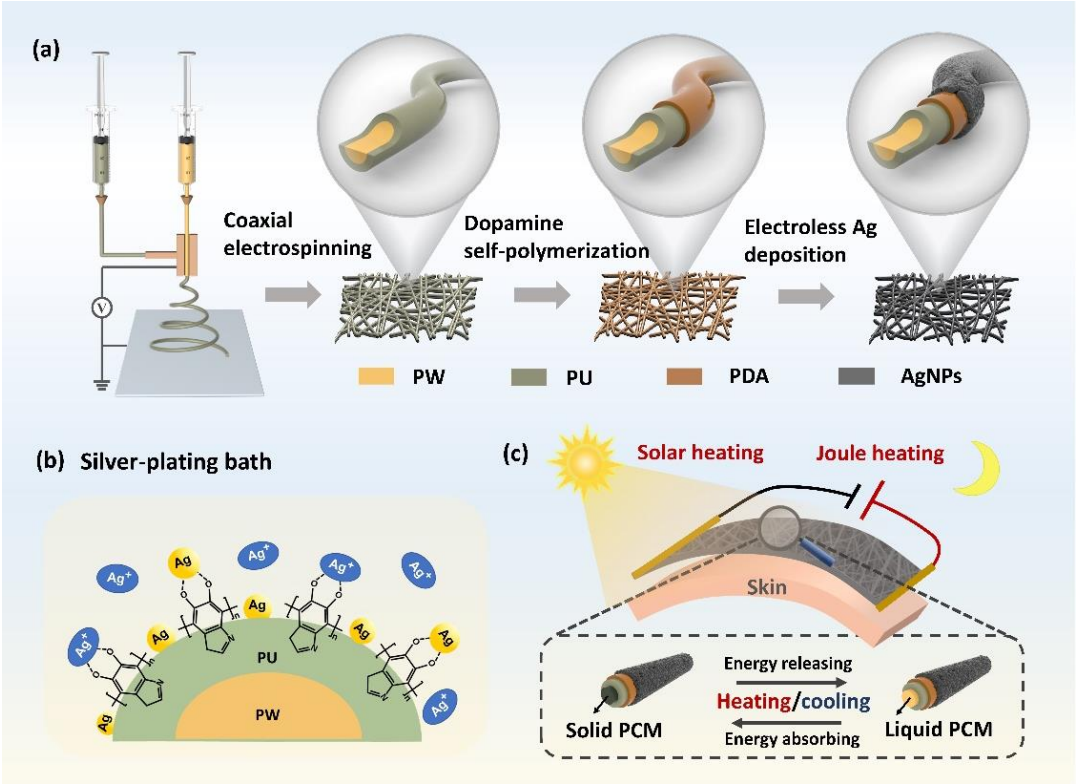

Fig. 4-1. Schematic illustrations of (a) fabrication process of metallized, hierarchical coaxial constructed fibers. (b) Ag seeds uniformly grown on PDA-modified core-sheath fibers by chelation and in situ reduction. (c) Multimodal thermoregulating routes integrated with solar heating, Joule heating and reversible heating/cooling effects by phase change process.

The morphology of the hierarchical coaxial fiber structure is crucial to the integrated thermal regulatory performance. TEM image clearly revealed the coaxially structure of PCF in Fig. 4-2a. To further illustrate the core-sheath structure of the phase change fibers, the cross-sectional morphology was observed by a microscopy (SEM) image (Fig. 4-2b), after removing the melting core (PW). The obvious holes in the core zone of the fibers confirmed the well-defined core-sheath structure (PW@PU) through coaxial electrospinning.

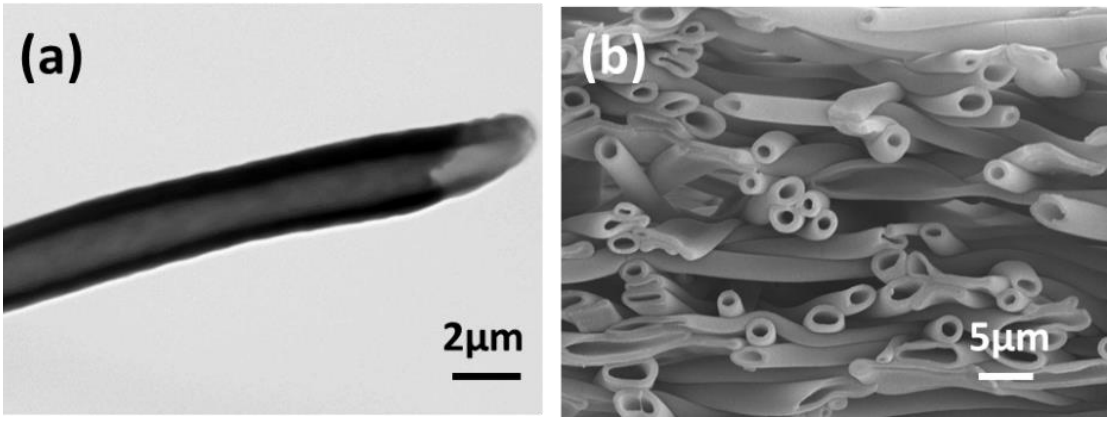

Fig. 4-2. (a) TEM image of PCF. (b) SEM image of the cross-sectional morphology of PCF.

For the insight into the process of PDA-assisted silver deposition, the evolution of the fiber surface is revealed (Fig. 4-3(a, a'-c, c')). Compared to the smooth surface of PCF (Fig. 4-3a, a'), the surface of DPCF turned to be rougher, attributed to the deposition of a thin layer of PDA as well as some PDA nanoclusters (Fig. 4-3b, b'). To demonstrate the successful modification of PDA, x-ray photoelectron spectroscopy (XPS) was used to analyze the surface composition. In comparison with membrane PCF, PDA modified membrane DPCF shows higher peaks of O 1s and N 1s, due to the catechol and quinone groups of the PDA polymer (Fig. 4-4a). Moreover, the N 1s spectrum of PCF contains only one peak at 400.0 eV, which is attributed to –NH species, originating from the PU polymer. Nevertheless, the N1s spectrum of DPCF can be deconvolved into three peaks at 399.2, 400.0, and 401.1 eV, which correspond to –N=, –NH and $–NH_2$, respectively (Fig. 4-4b). The –N= species results from the oxidative product of dopamine (indole derivatives). The presence of a small amount of $–NH_2$ suggests the co-existence of self-assembled dopamine in PDA layer, which is consistent with the previously proposed model of the formation of PDA.[40-41]

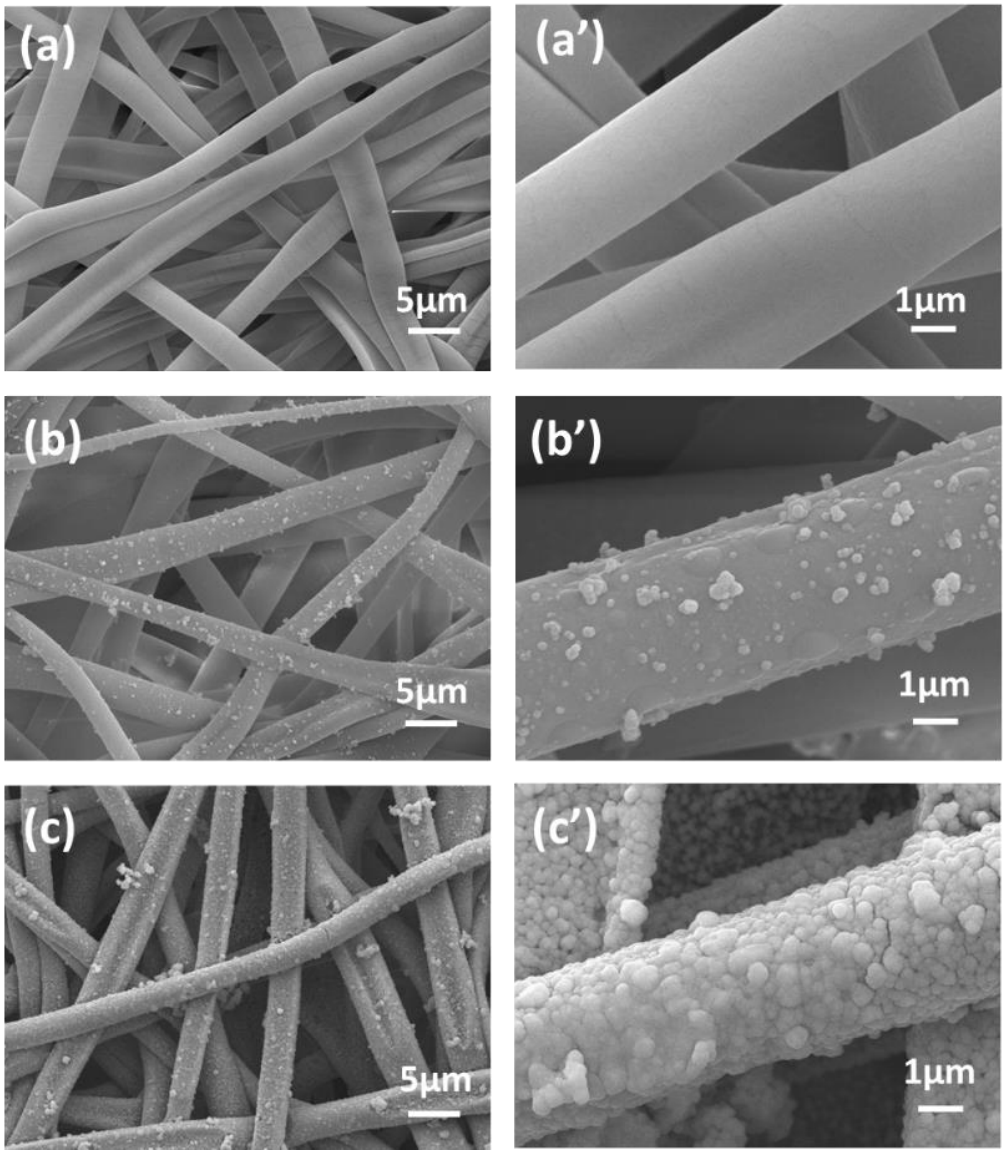

Fig. 4-3. Surface morphology of (a, a') PCF, (b, b') DPCF, (c, c') APCF40.

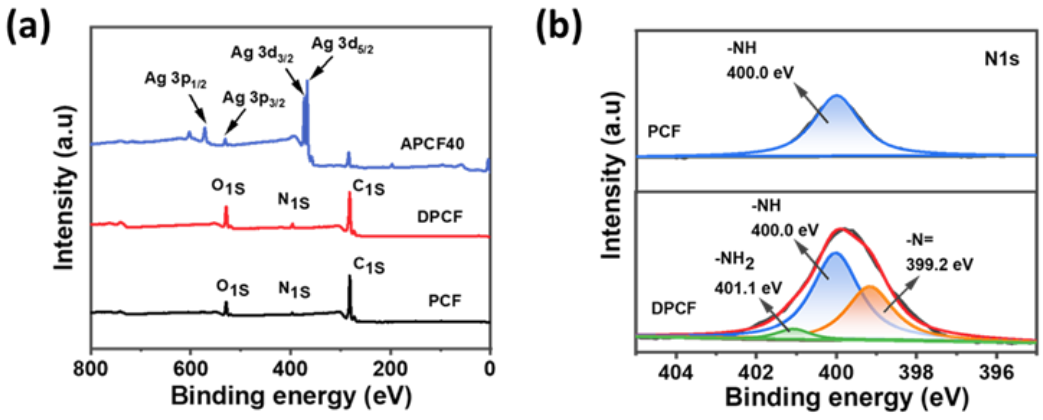

Fig. 4-4. (a) XPS full spectrum. (b) High-resolution XPS spectra of N1s.

As well known, the surface deposition of silver layer via electroless plating involves the sequential processes of nucleation, growth, and coalescence of AgNPs into a continuous layer.[42] As aforementioned, the chelation and reducing nature of PDA toward Ag ions promote the nucleation of AgNPs. The SEM images (Fig. 4-5(a-c)) further demonstrated the influence of PDA on in situ silver deposition. Obviously, there are small isolated nanoparticles uniformly attached on the fiber surface of DPCF after immersion in silver ammonia solution (before adding glucose), and the element mapping of Ag validated the formation of Ag nucleuses from the precursors, which provide growth sites for the subsequent glucose-reduced AgNPs.

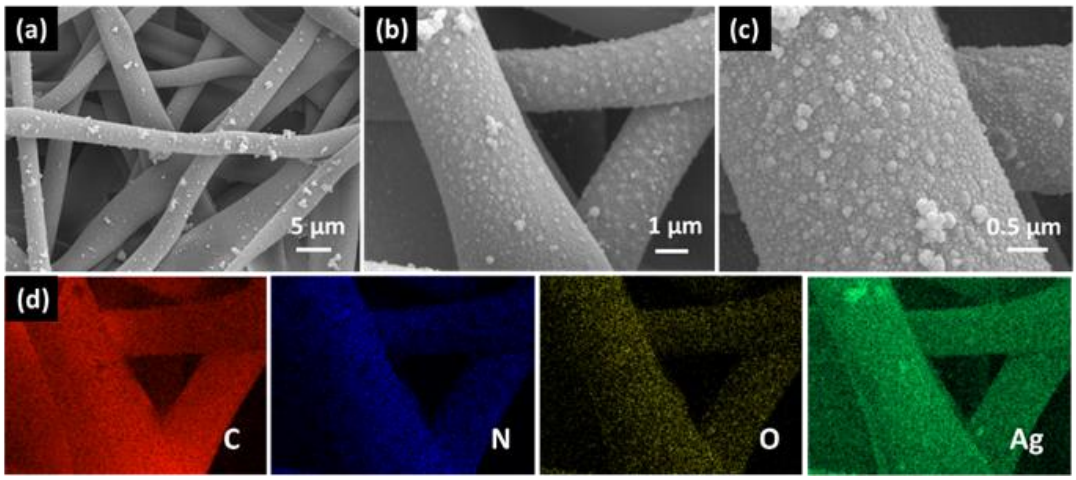

Fig. 4-5. (a-c) SEM images of DPCF with Ag seeds grown on the fiber surface after immersion in silver ammonia solution for 30 min. (d) The corresponding EDS elemental mapping images.

What's more, the denseness of silver layer can be easily controlled via tuning the reduction time with glucose. After reduction for 20 min, the Ag nucleuses grow into small and discrete nanoparticles. The fiber surface was not fully covered, and some small gaps can be observed (Fig. 4-6a, a'). As the reaction time increases, AgNPs grow to be larger and the interconnections occurred between them at the point of about 40 min, forming a uniform and compact silver layer (Fig. 4-6b, b'). The corresponding elemental mapping images demonstrate the homogenous distribution of C, N, O, and Ag elements throughout the membrane APCF40 (Fig. 4-7). For longer reaction time (about 60 min), the extensively grown AgNPs aggregate to be larger nanoclusters along the fiber radial direction, which reduced the homogeneity of the silver layer (Fig. 4-6c,

c'). Thus, the surface evolution process is schematically illustrated in Fig. 4-6(a''-c''). The denseness of silver layer has significant influence on the light absorptivity and the electrical conductivity of the resulting membranes, which are discussed in the following sections.

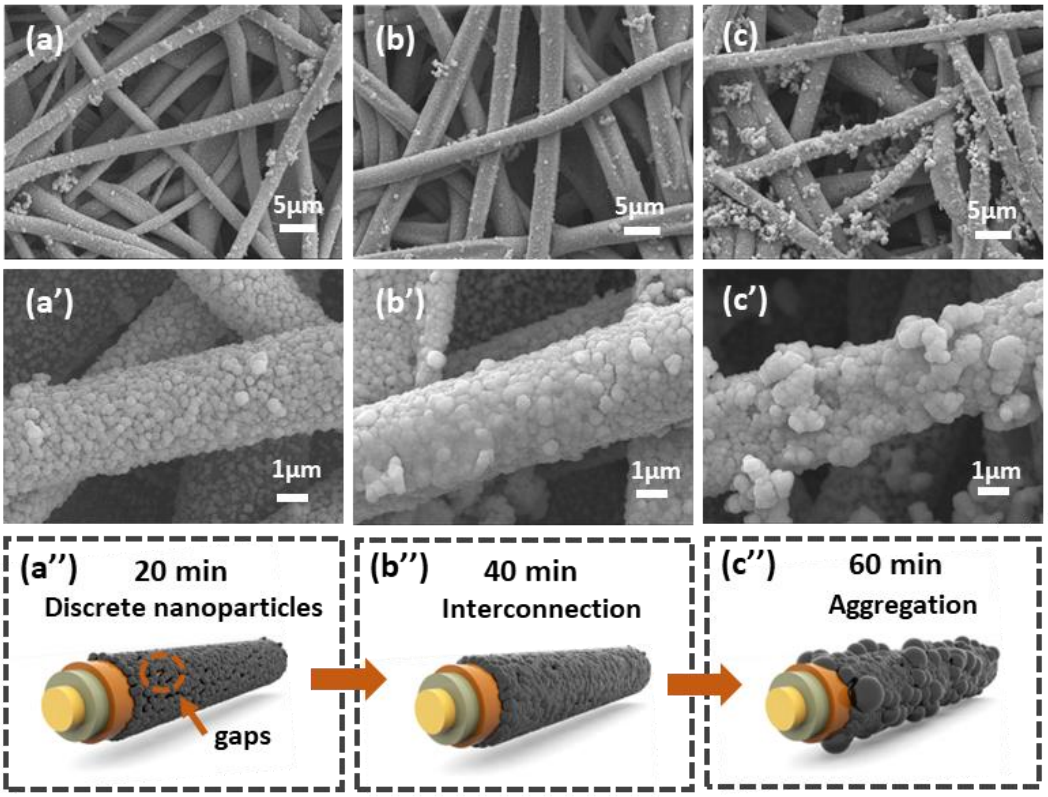

Fig. 4-6. Surface morphology of (a, a') APCF20, (b, b') APCF40, and (c, c') APCF60 with low and high magnification, respectively. (a''–c'') Schematic diagrams of the evolution process of fiber surface.

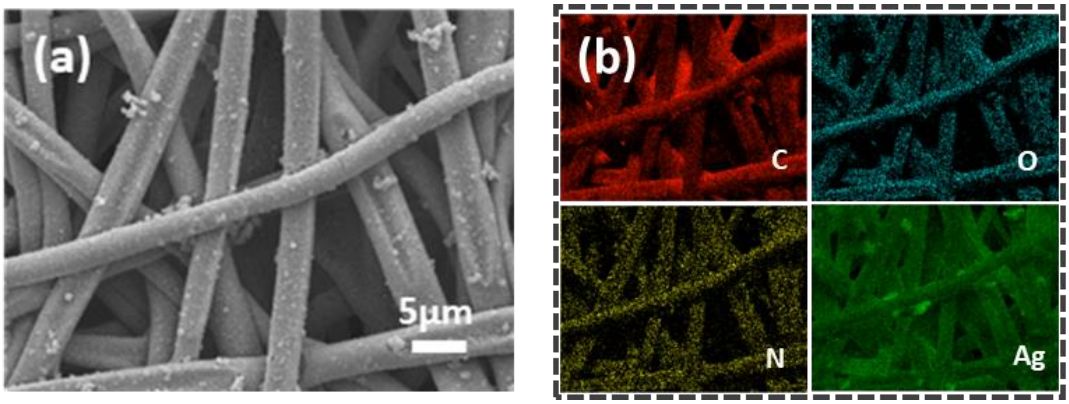

Fig. 4-7. (a) SEM images of APCF40. (b) The corresponding elemental mapping images.

To verify the construction of the hierarchical structure in APCF40 membranes, the enlarged cross-sectional view and EDS mapping of a single metalized fiber is shown in Fig. 4-8, the hollow polymer fiber (after removing the melting PW) is wrapped with AgNPs and forming a hierarchical structure. The effective deposition of AgNPs is further confirmed by XRD and XPS results. In the XRD patterns (Fig. 4-9a), the additional five characteristic peaks in APCF40 are attributed to the (111), (200), (220), (311), and (222) lattice planes of silver, respectively.[43] Besides that, the Ag 3d XPS spectrum of APCF40 was deconvolved into two peaks at 368.2 and 374.2 eV for Ag $3d_{5/2}$ and Ag $3d_{3/2}$, respectively, and the distance between the spin energy values was 6.0 eV, which confirmed the existence of silver in the form of Ag (0) (Fig. 4-9b).[44,45] To further validate the positive effect of the interface modifications of PDA on electroless deposition of AgNPs on fibers, the phase change membrane PCF without PDA modification after immersion in silver ammonia solution was directly reduced by glucose as a control experiment. As shown in Fig. 4-10, fibers are attached by the nonuniform, and discontinuous silver coatings, which consist of the aggregated large particles. This result proves that PDA, severing as an anchoring polymer, plays a critical role for the uniform deposition of AgNPs.

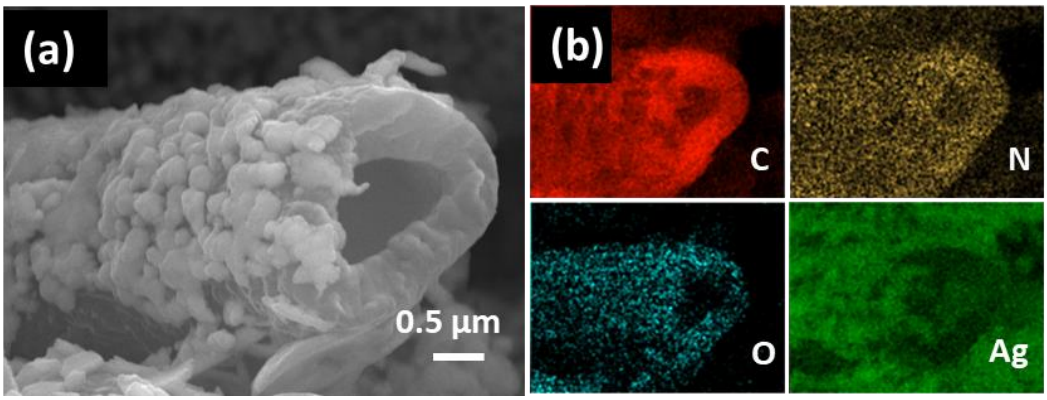

Fig. 4-8. (a-b) SEM image and EDS elemental mapping images of the cross-section of APCF40.

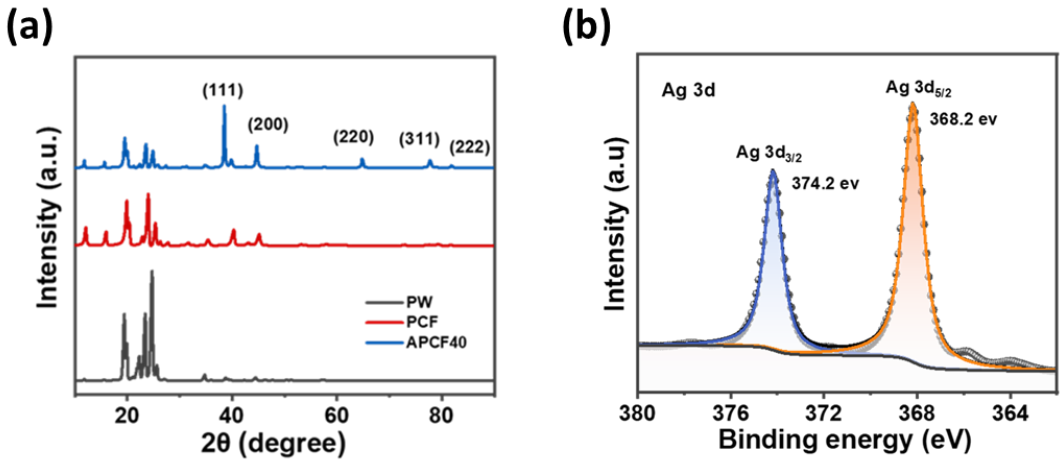

Fig. 4-9. (a) XRD pattern of PW, membrane PCF and APCF. (b) High-resolution XPS spectra of Ag 3d.

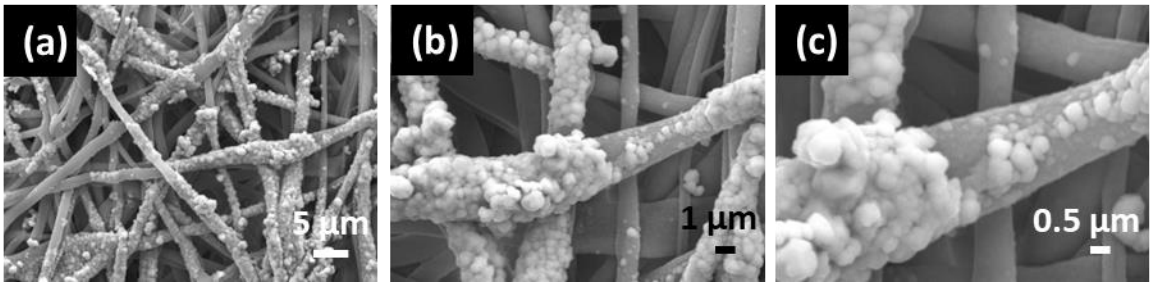

Fig. 4-10. (a-c) SEM images of the metalized phase change membrane treated by electroless silver plating directly without the assistance of PDA after reduction for 40 min, showing a nonuniform silver coating.

4.3.2 Phase change performance

The phase change enthalpies and temperatures are used to determine the efficiency and applicability for thermal energy storage. The DSC curves of PCF, DPCF and APCF40 exhibit distinct endothermic and exothermic peaks from 20 to 35 °C and 26 to 12°C, respectively, similar to that shown by pure PW (Fig. 4-11(a, b)). Compared with pristine PW (203.4 J/g), PCF exhibits a lower value of latent heat (113.6 J/g). There are two reasons accounting for the decreased thermal storage capacity:[46] (1) the support material of PU polymer makes no contribution to the latent heat; (2) the PCM is confined in the narrow space of the fiber core, thus the crystallization and melting behavior of the partial chain segments of PW are restricted. The former reason also accounts for the slight, and gradual decrease in heat enthalpy of DPCF (111.7 J/g) and

APCF40 (101.1 J/g), after sequentially loading PDA and AgNPs (Fig. 4-11c). The FTIR spectra are shown in Fig. S5, the characteristic peaks of PW (2960, 2925 and 2854 cm^{-1}) can be found in the spectra of all composite phase change membranes. The intensities of these peaks weaken slightly after loading PDA and AgNPs, which is in accordance with the decreased value of heat enthalpy from DSC test. In Fig. 4-11d, the intensities and locations of the endothermic and exothermic peaks in DSC curves of APCF40 did not change significantly after 50 thermal cycling, confirming the decent phase change reliability and stability. These results presented that the core PW plays a dominant role for phase change behavior, and the multiple layers of PU, PDA and AgNPs, as protective shells, effectively avoid the leakage of PW. In order to investigate the temperature self-regulation performance, the temperature evolution was recorded using a thermocouple. The metalized phase change membrane APCF40 and a control sample APU containing no PW were placed on a hot (45 °C) plate and a cool (0 °C) plate for simulating heating and cooling process. In Fig.4-11 (e, f), there are two distinct temperature hysteresis regions from 21 to 28°C and from 26 to 17 °C in heating and cooling process, which is consistent with the endothermic and exothermic temperature range of APCF40. It verified that the prepared membrane APCF40 has the practical cooling and warming effects when the contained PW undergo phase change. The reversible cooling/heating behaviors are based on the work mechanism of heat energy storing and releasing through PCMs, which are beneficial for humans to buffer the ambient temperature fluctuation, and keep a comfort temperature for longer time.

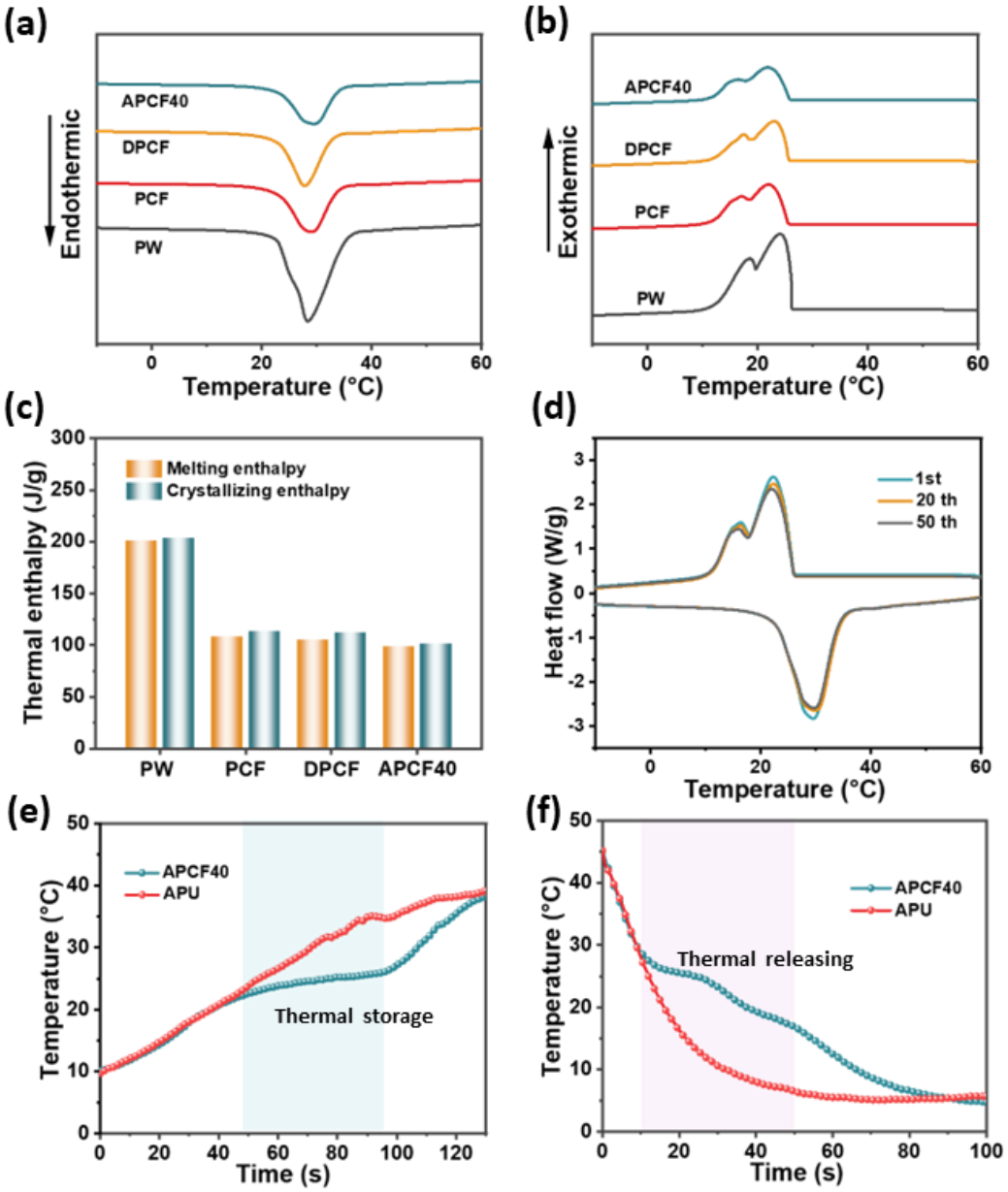

Fig. 4-11. (a, b) DSC curves in heating and cooling process, respectively. (c) The corresponding melting and crystallizing enthalpy. (d) DSC heating and cooling curves of APCF40 in 50 cycles. (e, f) Temperature change curves in heating and cooling processes, respectively.

4.3.3 Photothermal conversion and storage performance

Solar spectrum is mainly composed of ultraviolet light (280–400 nm), visible light (400–760 nm), and near infrared radiation (NIR) light (760–2500 nm), which constitute around 3, 44, and 53% of solar energy, respectively.[47] One of the key strategies of high photothermal conversion efficiency is to broaden the absorption band.[48] PDA is a

representative black melanin pigment and has been widely employed as a photothermal agent. However, its high absorption only appears in UV and visible regions, without covering the entire solar spectrum.[49] As the Fig. 4-12a shows, DPCF improved solar absorption in visible region, but it exhibits much lower absorptivity in NIR region. As well known, noble metallic nanostructures have the attractive localized surface plasmon resonance (LSPR) effect, rendering them excellent photothermal conversion ability. With the assembly of AgNPs, APCF20, 40 and 60 exhibit relatively high absorptivity in whole solar spectrum. There are two components attributed to the achieved high broadband absorption: 1) The random and wide size distributions of AgNPs (Fig. 4-12b) could generate a series of plasmon resonances at different optical frequencies, which enable a hybridized LSPR effect located in a wide optical frequency. 2) The plasmon near-field coupling effect could be excited from the ultranarrow gaps (less than 10 nm) between adjacent metallic nanoparticles or clusters. [50,51] By further increasing the deposition time, the extensive growth of AgNPs led to the interconnections between each other, causing the gradual disappearance of the nanoscale gaps, which leads to the reduced coupling effect. Therefore, with the increasing deposition time, the membrane showed a lower absorptivity in solar spectrum. In addition, except for the synergistic photothermal conversion effect of PDA and AgNPs, the porous structure of membrane also can promote light capturing through internal multireflection, scattering, and absorption of incident light,[12] thus the APCF membranes were endowed with the admirable photothermal conversion performance. On the other hand, PW can store and release the resulting thermal energy, which realizes a synergistic thermal management behavior.

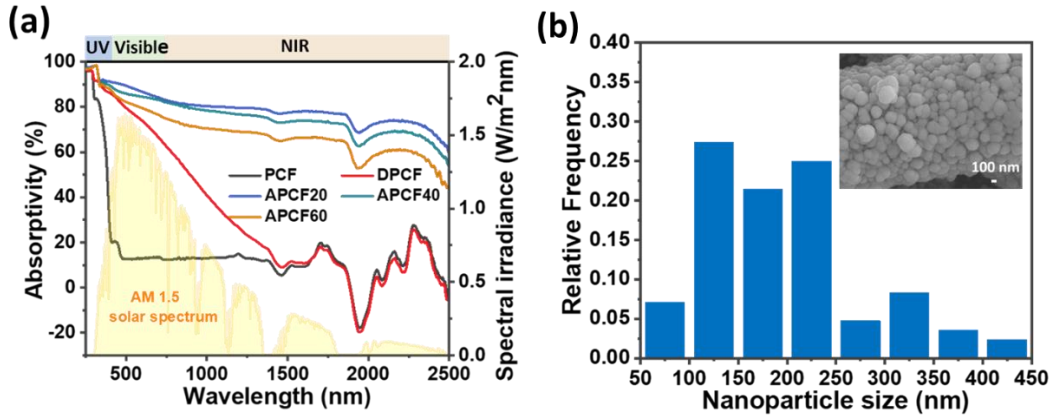

Fig. 4-12. (a) UV-vis-NIR absorption spectra. (b) The size distribution of AgNPs and the embedded figure is the SEM image of AgNPs on fiber surface.

To demonstrate the photothermal conversion and thermal energy storage performance of APCFs, the temperature change was recorded under a simulated solar light source. As shown in Fig.4-13, during the starting phase, APCFs showed a sharp temperature rising, until it reached the melting point of PW, PW changed from solid to liquid state, accompanied by the heat storage, and the temperature remained almost constant during this process. After phase change was completed, the temperature continued to rise, until it reached equilibrium state. When the light was turned off, temperature decreased sharply, until another temperature plateau appeared in cooling process, indicating that the stored heat was released.

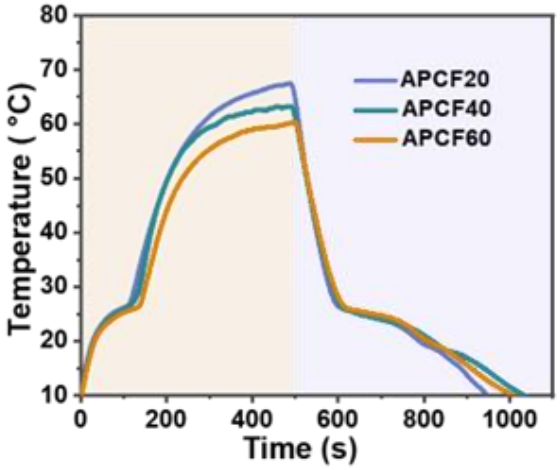

Fig. 4-13. Temperature evolution of APCF20, 40 and 60 under light irradiation of 100 mW/cm^2.

It was interesting to note the applicability of the synergistic photothermal conversion and energy storage behavior under the day-night alternation in the natural world (Fig. 4-14). In the daytime, light energy could be harvested and converted into heat energy through LSPR effect of AgNPs (outer layer), followed by transferred and stored in PW (core layer). While at night or in cold environment, the stored thermal energy can be released to buffer the temperature decrease. The seamless coaxial configuration facilitates the interfacial heat transfer between the multiple layers in individual fibers, which ensures the uniform heat absorbing and releasing processes through the membrane. This synergistic behavior of photothermal conversion and storage is highly desirable for the sustainability of thermal management systems.

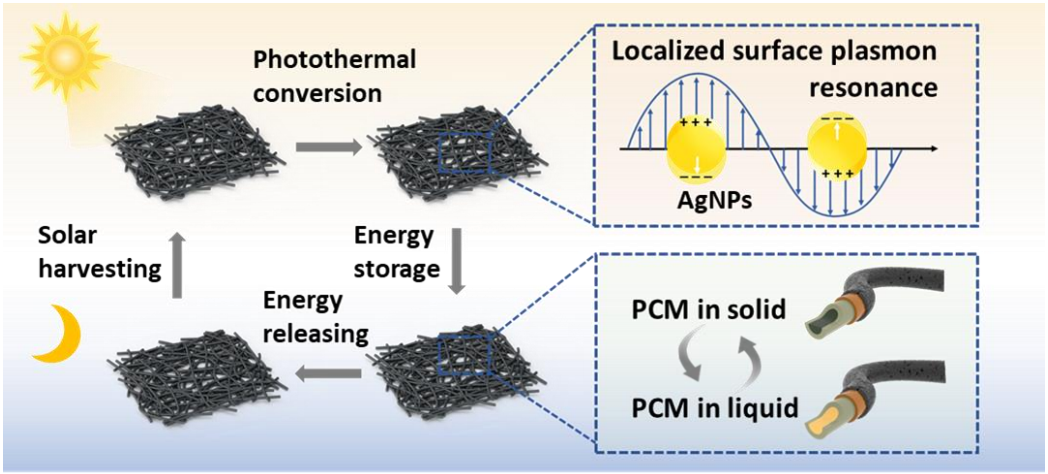

Fig. 4-14. Schematic illustration of photothermal conversion and energy storage.

It is noteworthy that the increasing reduction time slightly decreased the light absorptivity of the resulting membrane, but lead to a better electrical conductivity (Fig. 4-15), suggesting that the solar light absorptivity and electrical conductivity is adjustable for achieving alterable trade-off between solar heating and Joule heating toward different application scenarios. Here, we selected APCF40 for further research, because it exhibited both decent light absorptivity and electrical conductivity.

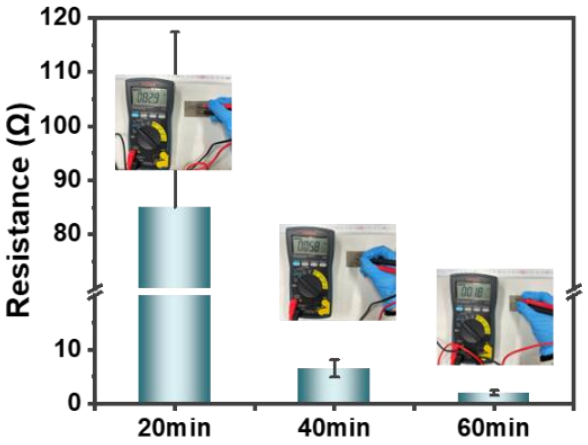

Fig. 4-15. The electrical resistance of APCF20, APCF40 and APCF60.

The steady-state saturation temperature of APCF40 can reach to 63.2, 54.3, 47.1 and 41.9 °C at different light intensities of 100, 75, 50 and 25 mW/cm^2, respectively (Fig. 4-16a). The platform areas near 25°C in both temperature rising and falling processes suggest a stable capability to maintain the temperature in a comfortable range. Fig. 4-16b shows the temperature variation under repeated on-off light irradiation cycles, the temperature plot presents good reproducibility in heating/cooling cycles, which highlights its good reliability in long-term service. The infrared imaging pictures are shown in Fig. 4-16c, APCF40, APU (without PCMs) and PCF (without solar-heating agents) were exposed to the light radiation of 100 mW/cm^2, simultaneously. APCF40 and APU exhibited much higher saturation temperatures than that of PCF, demonstrating the favorable solar-heating effect. Besides, APCF40 showed a slower rise of temperature than that of APU in heating period, because the PW in APCF40 is capable of storing thermal energy and alleviating the temperature rise. Once the light was turned off, the temperatures of all samples decreased instantly. APCF40 and PCF displayed a higher temperature than that of APU at last, owing to the release of the latent thermal energy through the solidification of PW in APCF40 and PCF, which buffered the temperature decrease effectively. These results proved the importance of the cooperation between core and sheath materials, where AgNPs and PDA determined the photothermal conversion effect, and the resulting heat energy is then transferred to the core PW and stored. The collaboration between each layers enabled the sustainable and synergistic thermal regulating capability, which presents significant potential in

terms of automatic, energy-saving and wearable thermal management.

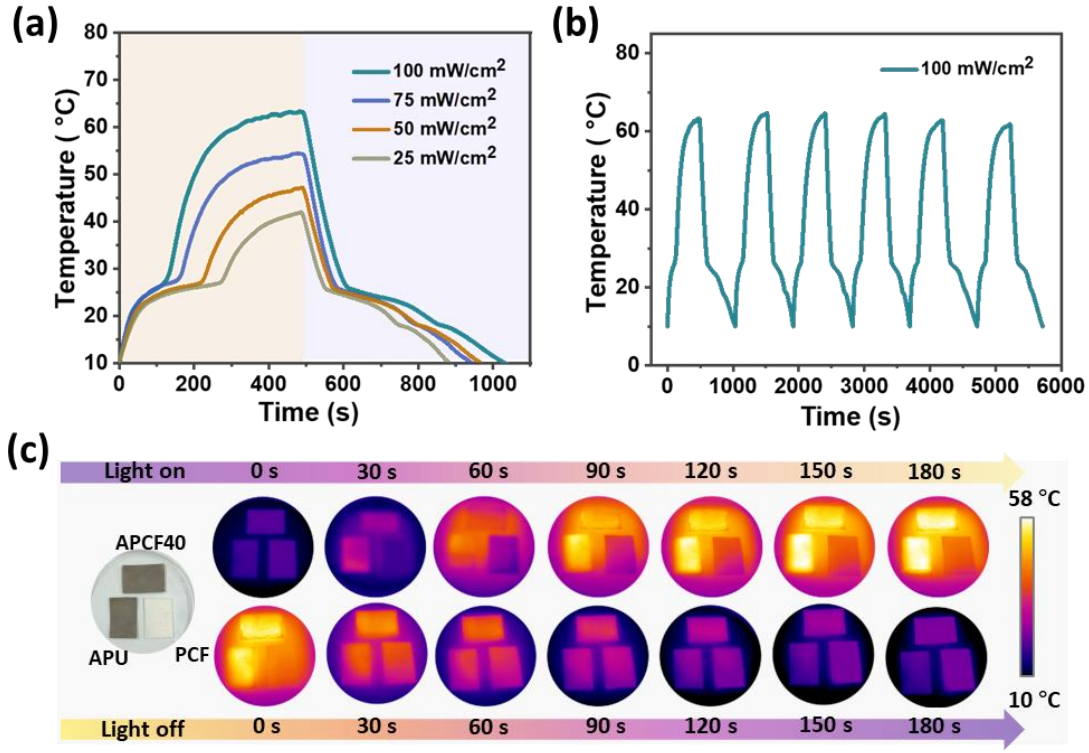

Fig. 4-16. (a) Temperature evolution of APCF40. (b) Temperature profiles of APCF40 in repeated heating/cooling cycles. (c) The real-time infrared images of APCF40, APU, and PCF exposed to the light irradiation of 100 mW/cm^2.

4.3.4 Electrothermal conversion and storage performance

Wearable electrical heaters show great potential for emerging applications in thermotherapy and warmth retention. The low electrical resistivity is one of the keys to high efficiency of electrothermal conversion.[52] The nearly linear voltage–current curve of APCF40 conforms to Ohm's law (Fig. 4-17a), indicating its low and stable resistance. The Joule heating performance was systematically investigated under constant driving voltages from 2 to 3.5 V, the low driving voltages are safe for use and can be provided by a portable power source. The linear relationship between the saturation temperatures and the square of driving voltages is in consistence with Joule's Law (Fig. 4-17b), which demonstrates an admirable heating controllability by adjusting the input voltages.

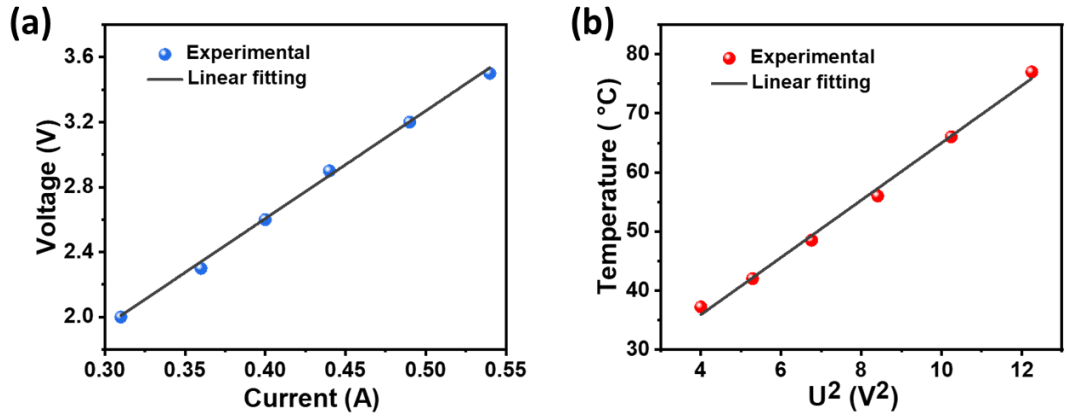

Fig. 4-17. (a) Voltage-current curve of APCF40 at different driving voltages. (b) Experimental data and linear fitting of saturation temperature versus U^2.

As shown in Fig.4-18a, the saturation temperatures increased from 37.2 to 76.8 °C under the increasing voltages from 2.0 to 3.5 V by gradient. Meanwhile, the temperature plateaus of APCF40 temperature-time plots, corresponding to the phase change of PW, can also be observed in each heating and cooling processes. This synergistic electrothermal conversion and storage performance resulted from the cooperation between the phase change core PW and the highly conductive sheath of AgNPs. Besides, a higher input voltage generated a higher heating rate and shortened the energy storing duration. What's more, APCF40 exhibited a flexible and precise response to the changing applied voltages. As Fig. 4-18b shown, APCF40 was loaded and unloaded by two different voltages (2.0 and 3.2V) at interval, the temperature revealed a regular rising and falling in turn. Meanwhile, the membrane was subjected to 3 consecutive cycles of electrical on/off at different input voltages (2.3, 2.9, and 3.5 V), revealing a consistent temperature variation with the applied voltages (Fig. 4-18c). Besides, the temperature curves during 8 cycles at 2.6 V are nearly identical, verified the stable cyclic electrothermal conversion and storage behavior (Fig. 4-18d). Furthermore, the long-term stability test was performed under the voltage of 2.6V, the saturation temperature around 50 °C can remain constant within 3000 s, exhibiting good heating durability and reliability (Fig. 4-18e).

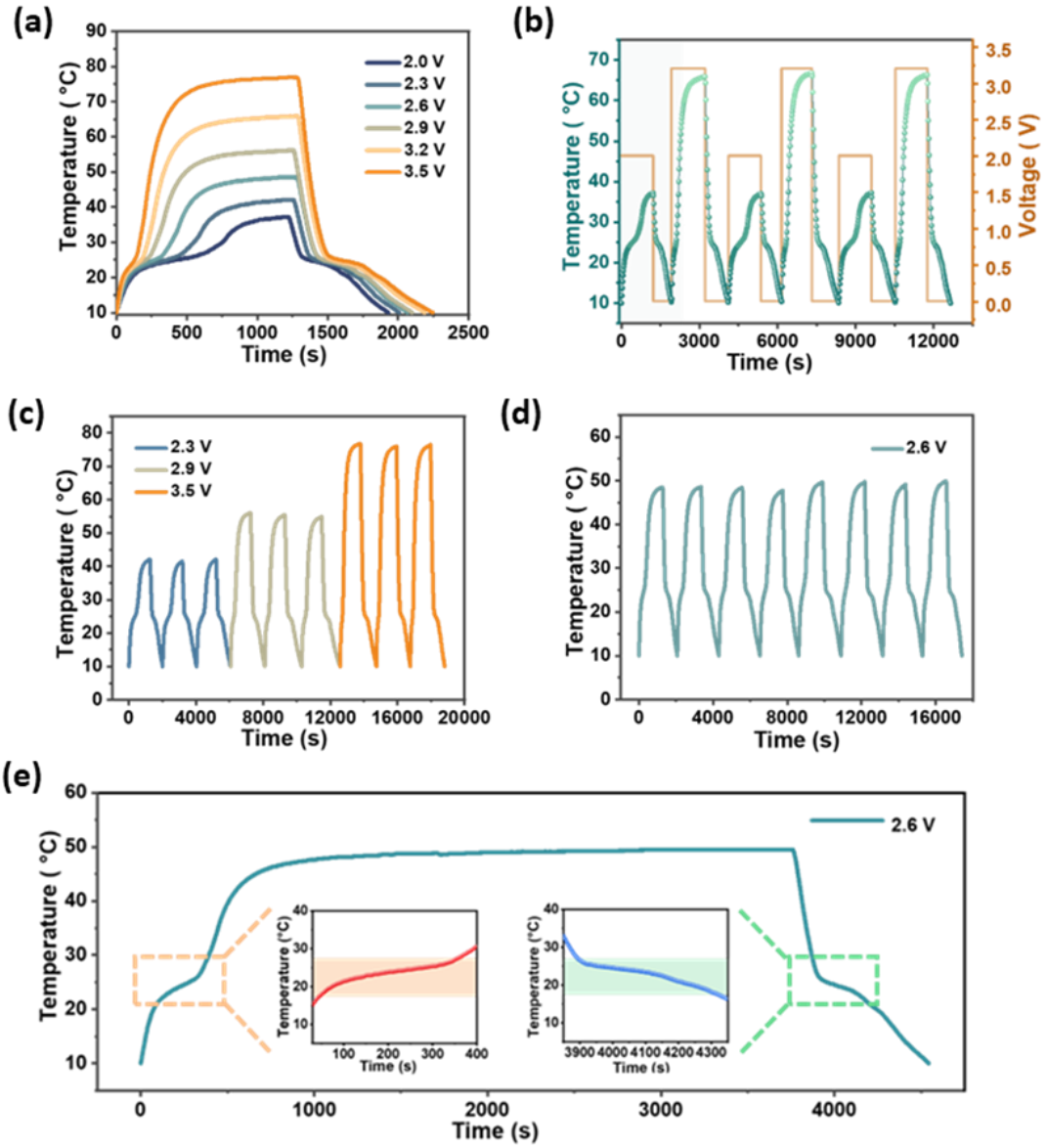

Fig. 4-18. (a) Temperature variation curves of APCF40 at different voltages. (b) Thermal response of APCF40 switching at 2 V and 3.2 V. (c) Heating/cooling cycles in 3 times at 2.3, 2.9, and 3.5 V. (d) Cyclic test at 2.6 V. (e) Long-term test at 2.6 V.

IR camera was used to monitor the surface temperature in real time, the homogeneous temperature distribution in IR images at different voltages revealed the uniform heating behavior (Fig. 4-19a). To validate the conformability of APCF40 on the curved surface of body, the membrane was attached on a finger joint, the surface temperature changed from 40 °C in straight state to 37 °C in bent state, ascribed to the increased electrical resistance (Fig. 4-19b). It is acceptable for the small temperature

variation in the dynamic body movement, which demonstrated the reliable heating performance. A bule thermochromic alphabet pattern was painted on the surface of the membrane for visual temperature detection (Fig. 4-20). The pattern exhibits gradient color change from dark bule (20 °C) to white (35 °C), providing an intuitive way for temperature indicating. Overall, the metallic phase change membranes exhibited excellent mechanical compliance, electrothermal conversion and energy storage capabilities, including a low-voltage safety, decent heating uniformity, sensitive temperature response, bidirectional tunability and operational stability.

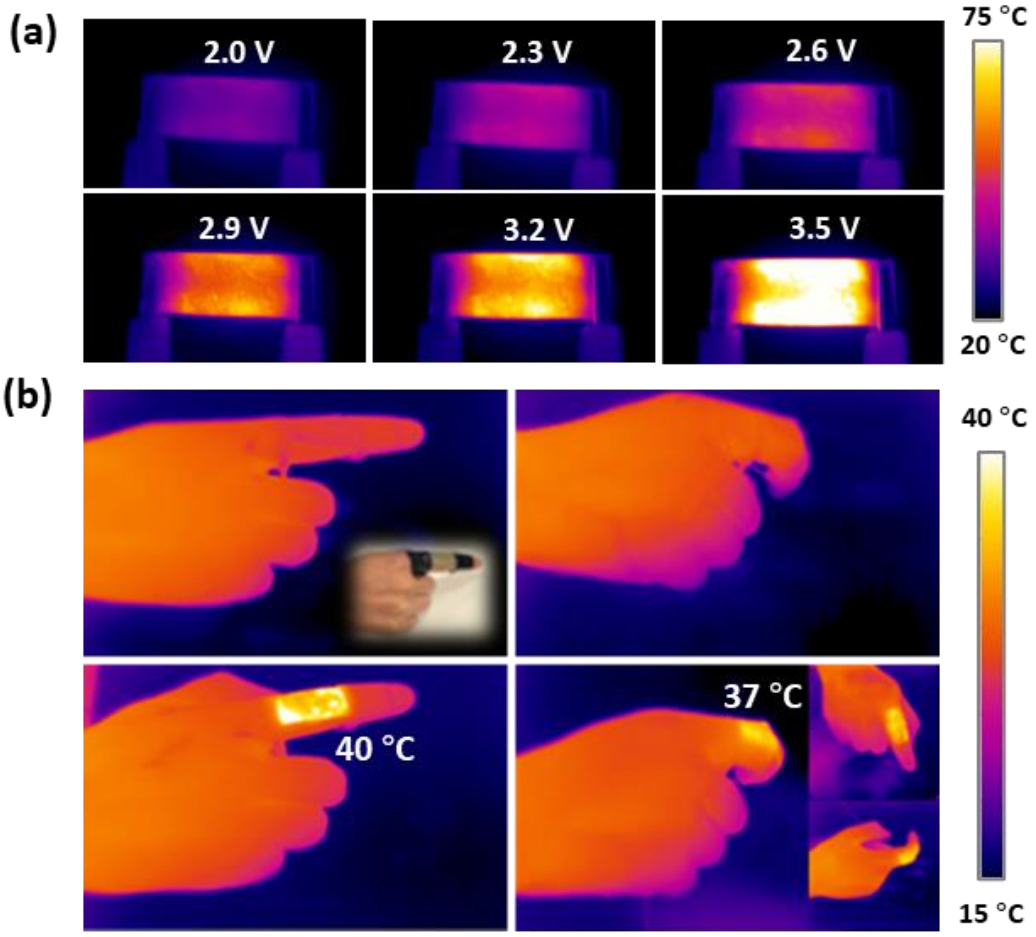

Fig. 4-19. (a) IR thermal images of APCF40 at different voltages. (b) IR thermal images of APCF40 wrapped on the human finger before and after bending.

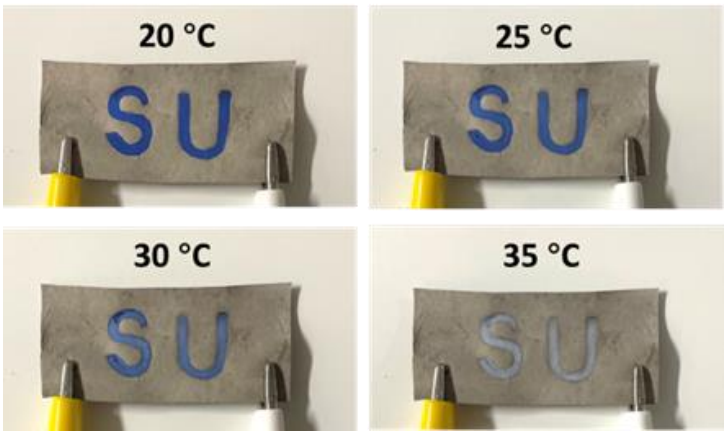

Fig. 4-20. Visual Joule heating performances of APCF40 with a thermochromic pattern.

4.3.5 Electrical stability and breathability

The wearable multifunctional textiles should have favorable flexibility and structural stability, because they are inevitably subjected to complicated deformations in practical applications. It's an important issue to ensure a good adhesion between the conductive metallic sheath and the flexible/stretchable polymer fiber substrate. Therefore, we characterized the normalized electrical resistance changes ($\Delta R/R_0$) of APCF40 under mechanical deformation, such as bending, torsion and stretching, to evaluate its electrical stability and structural robustness. As shown in Fig. 4-21a, the electrical resistance exhibits a small decrease (lower than 5%) under bending, because the conductive layer is compressed and formed a dense conductive path at bent state.[53] In long-term cyclic bending test, the resistance shows a gradual increase at the initial stage, because the irreversible fracture occurred on the weak regions of the conductive pathways.[54] After that, the resistance shows a regular and reversible change and remains stable after bending for 1000 cycles (Fig. 4-21b). In addition, the membrane also shows small changes in resistance under torsion from 0° to 360° (Fig. 4-21a). The light-emitting diode (LED) bulb was light up when the APCF40 membrane was connected in the circuit, and no visible change of the brightness was observed when the membrane was bent and twisted (Fig. 4-21c).

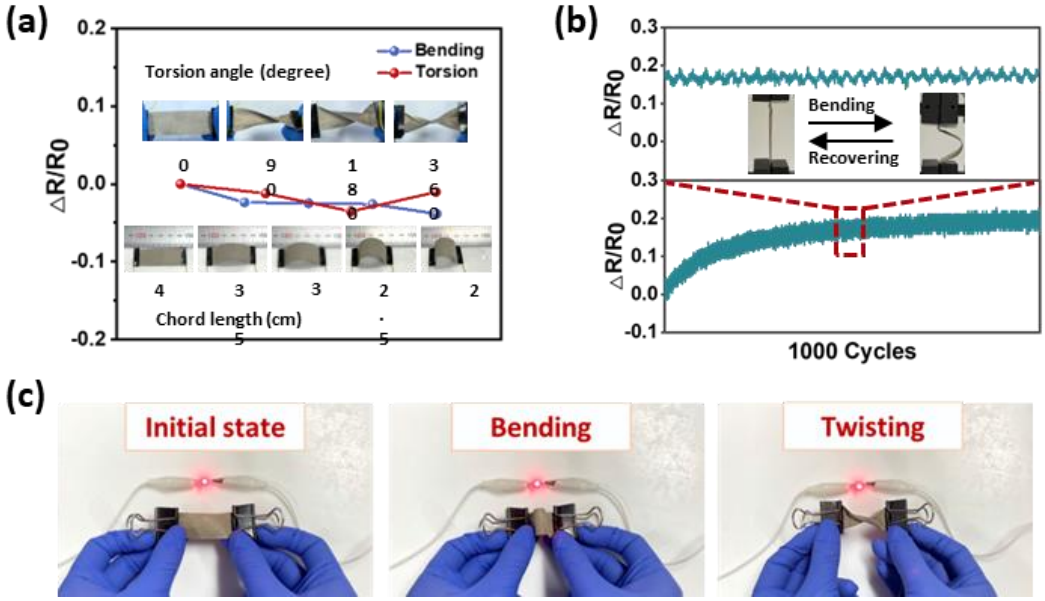

Fig. 4-21. (a) The resistance changes of APCF40 under torsion and bending. (b) Long-term cyclic bending test. (c) Metalized membrane applied as an electrical connector to light an LED bulb under bending and twisting state.

Fig. 4-22 represents the normalized resistance change of APCF40 membrane under 1000 stretch/release cycles from 0% to 10% strain, the stable baseline of the normalized resistance change validated a good resistance recovery and long-term reliability at low strain level.

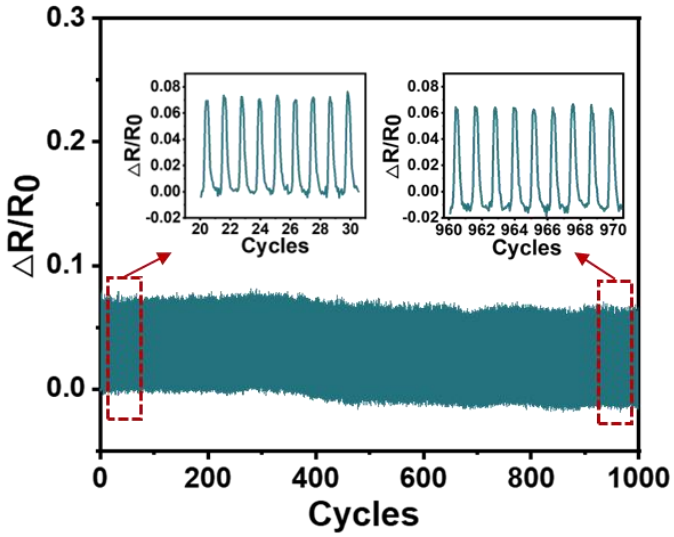

Fig. 4-22. The resistance changes under 1000 stretch/release cycles from 0% to 10% strain.

A larger tensile strain was conducted in Fig.4-23, the electric resistance increased slightly at the low strain (about less than 10%), and gradually increased to 58.29 Ω at a strain of 50%. The low strain endurance was ascribed to the strain dissipation provided by the stretchable fibrous mesh structure, and the degraded conductance at large strains was attributed to the cracking silver shell.

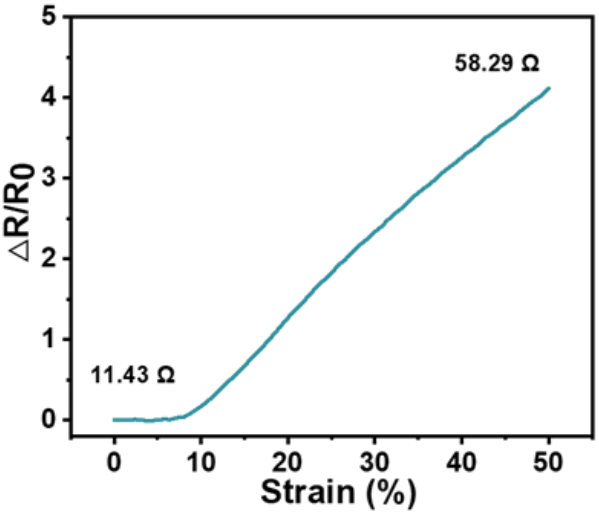

Fig. 4-23. The resistance changes under the uniaxial tensile strain of 50%.

What's more, the metalized membrane was subjected to the ultrasonic washing for 10, 20 and 40 min to examine the adhesion stability of the conductive layer on fibers. The low resistance of the membrane was remained even after ultrasonic washing for 40 min (Fig. 4-24 (a, b)), and the SEM images (Fig. 4-25) revealed that the AgNPs can be stably attached to fibers after long-term washing. The interfacial layer PDA plays a key role for strongly binding the metallic layer and the polymer fiber substrate, which ensures the long-time mechanical durability and electrical stability of the metallized membrane in practical applications.

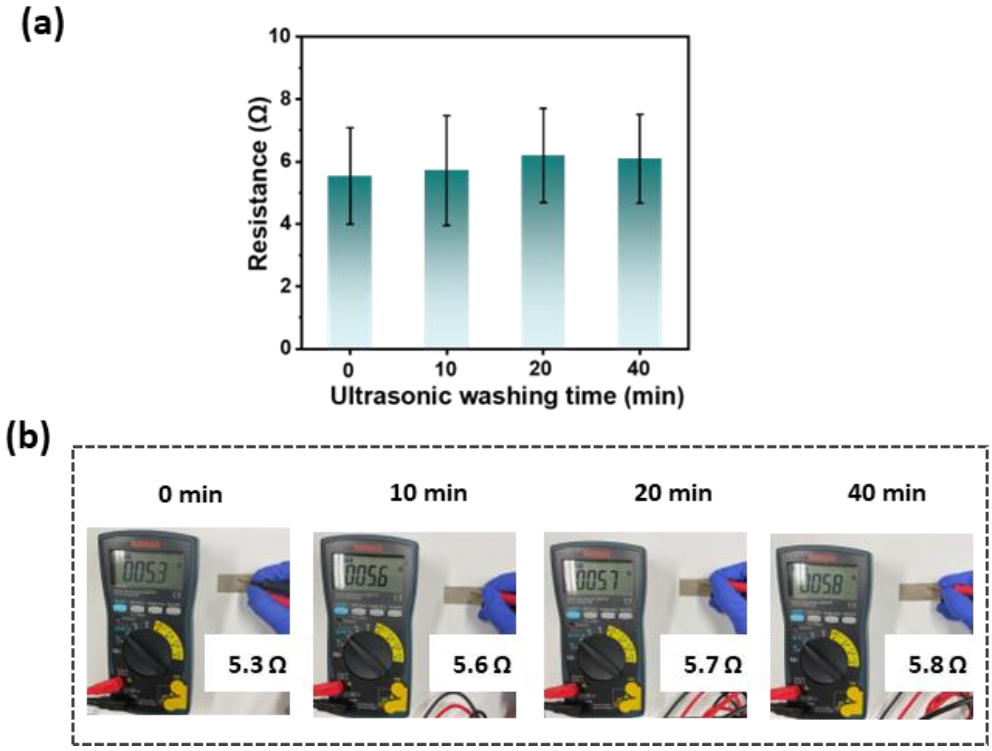

Fig. 4-24. (a, b) The resistance changes of APCF40 before and after ultrasonic washing for 10, 20, and 40 min.

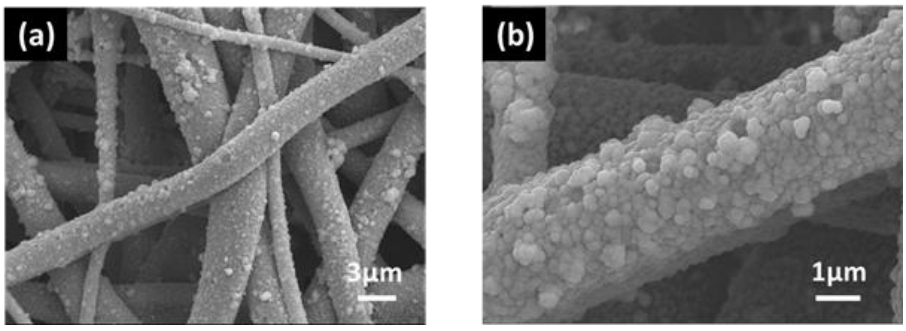

Fig. 4-25. (a-b). SEM images of APCF40 after ultrasonic washing for 40 min.

The permeability of air and moisture is essential for ensuring long-term wearing comfort.[55] Contrast to dense films, fibrous membranes have the advantage of intrinsically permeability ascribed to the interconnected porous structure, and the process of PDA-assisted silver plating could achieve the conformally deposition of AgNPs around the individual fibers, thereby preserving the porous structure of the pristine fibrous membranes (Fig. 4-26a). As proofs of concept for air/moisture

permeability in Fig. 4-26b, a bottle with hydrochloric acid (HCl aq) was covered by the membrane APCF40, when another bottle with aqueous ammonia (NH_3 aq) was moved close to it, the obvious smoke, the reaction products of HCl and NH_3, emerged instantly, which proved good air permeability of the membrane. In Fig. 4-26c, two beakers filled with hot water were covered by the membrane APCF40 and a nonporous PVC film, respectively. The outer large beaker covering the PVC film was clean, while the beaker covering the membrane APCF40 was deposited with dense condensed water droplets, which confirmed a high moisture permeability of APCF40.

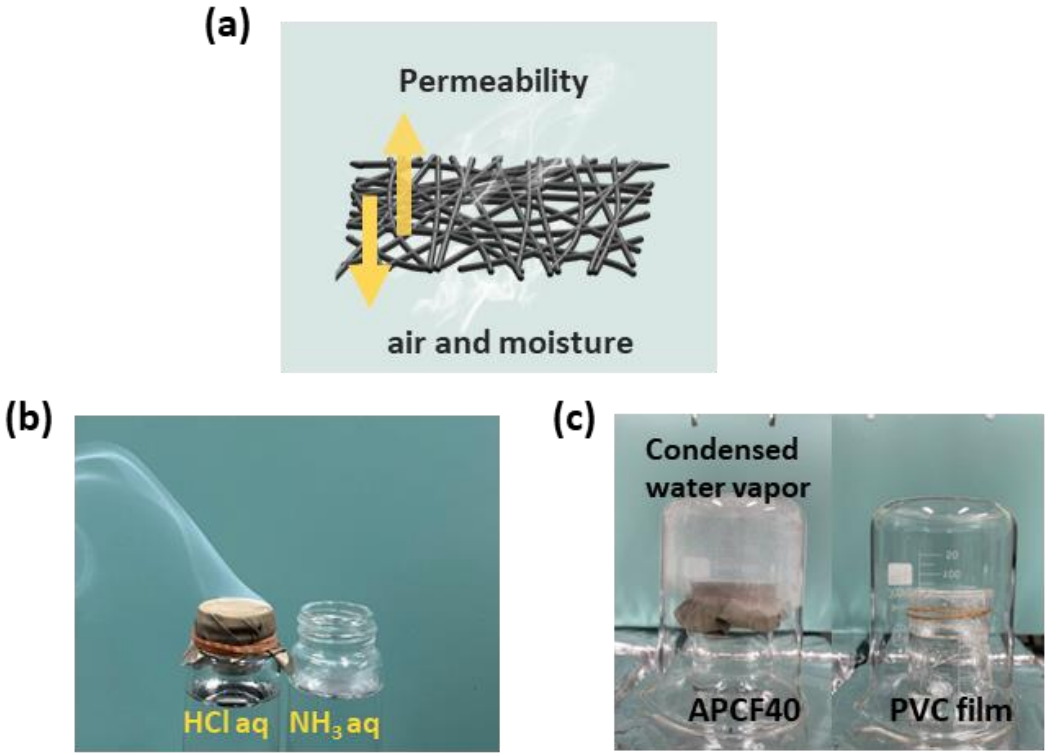

Fig. 4-26. (a) Schematic illustration of the permeability of fibrous membranes. (b) Photos showing the HCl gas permeability of APCF40. (c) Photos showing water vapor transmission performance of APCF40.

We estimated the water vapor transmission rate based on ASTM E96 with modification, through measuring the weight loss of water-filled bottles sealed with fibrous membranes and a nonporous PVC film in an environmental chamber (30 °C, 35%) (Fig. 4-27).[8] The metalized phase change membrane APCF40 showed vapor transmission rate of 80.67 $g/m^2/h$, which is close to that of the pristine phase change

membrane PCF (85.15 g/m^2/h) and much higher than the average rate of insensible perspiration of human skin (20 g/m^2/h),[56] while the nonporous PVC plastic film is completely impermeable, demonstrating that the porous structure allowed water vapor to penetrate through the fibrous membranes for the skin to “breath”, and the porous structure was well remained after metallization.

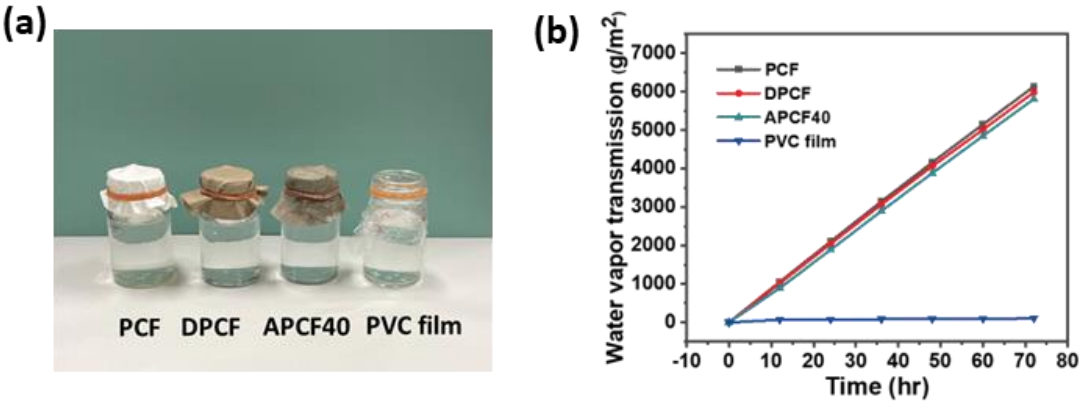

Fig. 4-27. (a) Experimental setup for measuring water vapor transmission rate. (b) Weight loss curves of the water inside the bottles covered with different fibrous membranes and a dense PVC film.

As the Fig. 4-28 and Tab.4-1 shown, most previously reported thermal management composites integrated multi-functions into nonporous films or hydrogels. Alternatively, PCMs were absorbed in porous substrates, such as aerogels, foams, and textiles, thus the original pores were blocked, leading to the limited permeability. On the other hand, the study on combining dual-driven heating functions with thermal energy storage capability into one fiber-based wearable device is rare in previous researches. Our fibrous membrane could simultaneously acquire favorable permeability, flexibility and highly integrated cooperative triple thermal regulating routes, which provides design inspirations for the next-generation personal thermal management (more detailed comparison are listed in Tab.4-1).

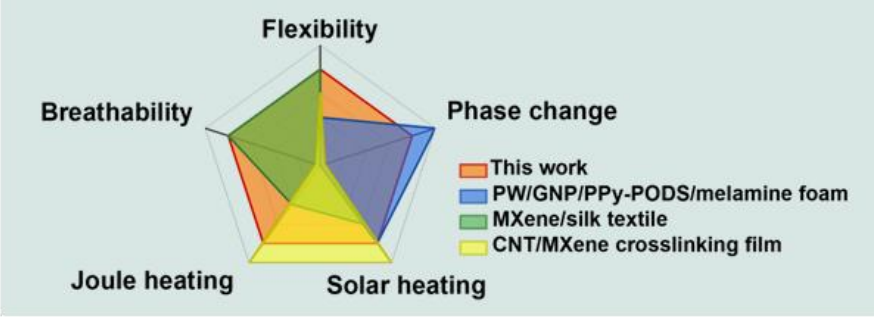

Fig. 4-28. The advantage of the high integration of multi-thermoregulatory routs with breathability compared to previous studies on thermal management.

In addition, with the introduction of abundant polar groups from PDA, the membrane surface changed from hydrophobic (PCF) to hydrophilic (DPCF). While the silver coating converted the surface from hydrophilic to hydrophobic again (Fig. 4-29). In contrast to the moisture sensitivity of many reported conductive materials,[20,21] the inherent waterproof property of the metalized membrane without extra hydrophobic coatings, can improve its stability and reliability in humid working environment.

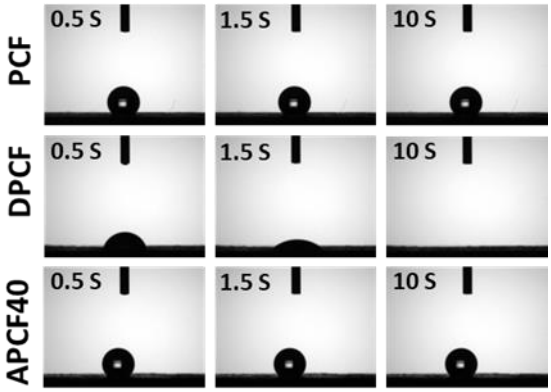

Fig. 4-29. Water contact angle measurements of PCF, DPCF, and APCF40.

Moreover, due to the pure polymer sheathes in the core-sheath structured fibers acting as the elastic supportive scaffolds, the composite phase change membrane PCF inherits the high tensile strain of PU fibrous membranes, with a high breaking elongation of 390% (Fig. 4-30).[57] The modification of PDA has little effect on the elongation at break, but slightly promote the tensile stress as a “nano glue”, which could bond the interlaced fibers. Besides, the silver layer improves the tensile stress at break,

which is ascribed to the thicker sheathes after silver coating and the higher Young's modulus of the metal layer. Meanwhile, the slightly decreased elongation at break results from the low stretchability of metal layer and the strong interfaces between polymer and metal layers which may cause crack growth and propagation in sheathes of fibers under high stress. Overall, the above results indicate that the metalized membrane has robust mechanical and electrical stability, as well as the favorable breathability and stretchability, which ensures broad prospect in practical wearable applications.

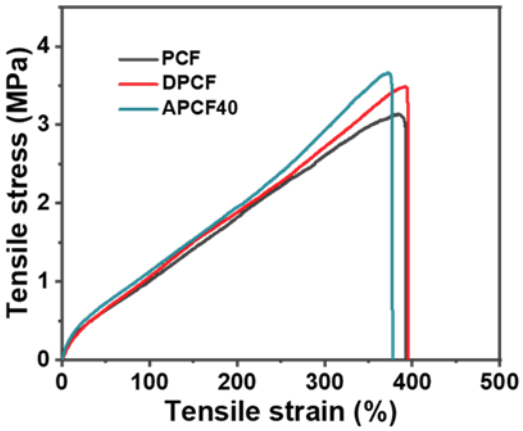

Fig. 4-30. Tensile stress–strain curves.

4.4. Conclusion

In summary, a breathable and thermoregulating fibrous membrane integrated with photo/electrothermal conversion and energy storage/release performance, was successfully prepared through coaxial electrospinning and PDA-assisted silver deposition technique. The complementary relationship between the solar heating and Joule heating effects could overcome the operational limitations of the intermittent availability of single input energy source (e.g., sunlight or electricity). Furthermore, the dual driving heating performance coupled with the thermal energy storage behavior can relieve the mismatch between the energy supply and demand, and expand the application scenarios. This highly integrated multimodal thermoregulating routes rely on the careful design of the hierarchically ordered coaxial architecture of the fibers,

which combines the core PCM, elastic sheath PU, interfacial layer PDA and the outermost layer of AgNPs into an efficient configuration. PDA layer not only facilitates the uniform, dense growth of AgNPs, but also offers an interfacial reinforcement for enhanced mechanical durability of the as-deposited conductive layer. Besides, the porous structure of the pristine phase change membrane is remained, guaranteeing a favorable air permeability and wearing comfort. What's more, the density of the deposited AgNPs can be tuned by controlling the reduction time to customize the light absorbability and electrical conductivity to meet different application requirements. Consequently, the resulting membrane APCF40 achieved the admirable solar-heating effect (up to 63.2 °C at 100 mW/cm^2), and the low voltage-driven Joule heating performance (up to 76.8 °C at 3.5 V), coupled with the thermal energy storage capability with a heat enthalpy of 101.1 J/g. Therefore, the flexible, breathable and synergistic thermoregulating fibrous membrane demonstrates a promising prospect in all-weather, energy saving and personalized thermal management application.

References

[1] T. Tat, G. Chen, X. Zhao, Y. Zhou, J. Xu, J. Chen, Smart Textiles for Healthcare and Sustainability, ACS Nano. 16 (2022) 13301–13313.

[2] Y. Peng, Y. Cui, Advanced Textiles for Personal Thermal Management and Energy, Joule. 4 (2020) 724–742.

[3] Y. Fang, G. Chen, M. Bick, J. Chen, Smart Textiles for Personalized Thermoregulation, Chem. Soc. Rev. 50 (2021) 9357–9374.

[4] H. Wang, Y. Zhang, X. Liang, Y. Zhang, Smart Fibers and Textiles for Personal Health Management, ACS Nano. 15 (2021) 12497–12508.

[5] R. Hu, Y. Liu, S. Shin, S. Huang, X. Ren, W. Shu, J. Cheng, G. Tao, W. Xu, R. Chen, X. Luo, Emerging Materials and Strategies for Personal Thermal Management, Adv. Energy Mater. 10 (2020) 1903921.

[6] Y. Cui, H. Gong, Y. Wang, D. Li, H. Bai, A Thermally Insulating Textile Inspired by Polar Bear Hair, Adv. Mater. 30 (2018) 1706807.

[7] Y. Yu, G. Zheng, K. Dai, W. Zhai, K. Zhou, Y. Jia, G. Zheng, Z. Zhang, C. Liu, C. Shen, Hollow-porous Fibers for Intrinsically Thermally Insulating Textiles and Wearable Electronics with Ultrahigh Working Sensitivity, Mater. Horiz. 8 (2021) 1037–1046.

[8] L. Cai, A.Y. Song, P. Wu, P.-C. Hsu, Y. Peng, J. Chen, C. Liu, P.B. Catrysse, Y. Liu, A. Yang, C. Zhou, C. Zhou, S. Fan, Y. Cui, Warming Up Human Body by Nanoporous Metallized Polyethylene Textile, Nat Commun. 8 (2017) 496.

[9] Y. Zhang, Y. Li, K. Li, Y.S. Kwon, T. Tennakoon, C. Wang, K.C. Chan, S.-C. Fu, B. Huang, C.Y.H. Chao, A Large-area Versatile Textile for Radiative Warming and Biomechanical Energy Harvesting, Nano Energy. 95 (2022) 106996.

[10] X. Li, Y. Yang, Z. Quan, L. Wang, D. Ji, F. Li, X. Qin, J. Yu, S. Ramakrishna, Tailoring Body Surface Infrared Radiation Behavior through Colored Nanofibers for Efficient Passive Radiative Heating Textiles, Chem. Eng. J. 430 (2022) 133093.

[11] X. Fan, Y. Ding, Y. Liu, J. Liang, Y. Chen, Plasmonic Ti_3C_2 T_x MXene Enables Highly Efficient Photothermal Conversion for Healable and Transparent Wearable Device, ACS Nano. 13 (2019) 8124–8134.

[12] Y. Peng, W. Zhao, F. Ni, W. Yu, X. Liu, Forest-like Laser-Induced Graphene Film with Ultrahigh Solar Energy Utilization Efficiency, ACS Nano. 15 (2021) 19490–19502.

[13] L. Wang, X. He, Y. Hao, M. Zheng, R. Wang, J. Yu, X. Qin, Rational Design of Stretchable and Highly Aligned Organic/inorganic Hybrid Nanofiber Films for Multidirectional Strain Sensors and Solar-driven Thermoelectrics, Sci. China Mater. 66 (2023) 707–715.

[14] X. Wu, Y. Wang, P. Wu, J. Zhao, Y. Lu, X. Yang, H. Xu, Dual-Zone Photothermal Evaporator for Antisalt Accumulation and Highly Efficient Solar Steam Generation, Adv. Funct. Mater. 31 (2021) 2102618.

[15] M.O. Faruk, A. Ahmed, M.A. Jalil, M.T. Islam, A.M. Shamim, B. Adak, M.M. Hossain, S. Mukhopadhyay, Functional Textiles and Composite based Wearable Thermal Devices for Joule Heating: Progress and Perspectives, Applied Materials Today. 23 (2021) 101025.

[16] Q. Gao, T. Lauster, B.A.F. Kopera, M. Retsch, S. Agarwal, A. Greiner, Breathable and Flexible Dual-Sided Nonwovens with Adjustable Infrared Optical Performances for Smart Textile, Adv. Funct. Mater. 32 (2022) 2108808.

[17] Z. Ma, X. Xiang, L. Shao, Y. Zhang, J. Gu, Multifunctional Wearable Silver Nanowire Decorated Leather Nanocomposites for Joule Heating, Electromagnetic Interference Shielding and Piezoresistive Sensing, Angewandte Chemie. 134 (2022).

[18] B. Li, Y. Yang, N. Wu, S. Zhao, H. Jin, G. Wang, X. Li, W. Liu, J. Liu, Z. Zeng, Bicontinuous, High-strength, and Multifunctional Chemical-Cross-Linked MXene/Superaligned Carbon Nanotube Film, ACS Nano. (2022) acsnano.2c08678.

[19] Y. Zhang, Z. Ma, K. Ruan, J. Gu, Multifunctional $Ti_3C_2T_x$-(Fe_3O_4/polyimide) Composite Films with Janus Structure for Outstanding Electromagnetic Interference Shielding and Superior Visual Thermal Management, Nano Res. 15 (2022) 5601–5609.

[20] Y. Shi, Z. Xiang, L. Cai, F. Pan, Y. Dong, X. Zhu, J. Cheng, H. Jiang, W. Lu, Multi-interface Assembled N-Doped MXene/HCFG/AgNW Films for Wearable Electromagnetic Shielding Devices with Multimodal Energy Conversion and Healthcare Monitoring Performances, ACS Nano. 16 (2022) 7816–7833.

[21] Z. Zhou, Q. Song, B. Huang, S. Feng, C. Lu, Facile Fabrication of Densely Packed Ti_3C_2 MXene/Nanocellulose Composite Films for Enhancing Electromagnetic Interference Shielding and Electro-/Photothermal Performance, ACS Nano. 15 (2021) 12405–12417.

[22] X. Liu, H. Su, Z. Huang, P. Lin, T. Yin, X. Sheng, Y. Chen, Biomass-based Phase Change Material Gels Demonstrating Solar-thermal Conversion and Thermal Energy Storage for Thermoelectric Power Generation and Personal Thermal Management, Solar Energy. 239 (2022) 307–318.

[23] Z. Tang, H. Gao, X. Chen, Y. Zhang, A. Li, G. Wang, Advanced Multifunctional Composite

Phase Change Materials based on Photo-responsive Materials, Nano Energy. 80 (2021) 105454.
[24] Y. Meng, L. Zhang, M. Peng, D. Shen, C. Zhu, S. Qian, J. Liu, Y. Cao, C. Yan, J. Zhou, T. Qian, Developing Thermoregulatory Hydrogel Electrolyte to Overcome Thermal Runaway in Zinc-Ion Batteries, Adv. Funct. Mater. 32 (2022) 2206653.
[25] J. Wu, M. Wang, L. Dong, C. Zhu, J. Shi, H. Morikawa, Ultraflexible, Breathable, and Form-Stable Phase Change Fibrous Membranes by Green Electrospinning for Personal Thermal Management, ACS Sustainable Chem. Eng. 10 (2022) 7873–7882.
[26] J. Yang, Y. Zhou, L. Yang, C. Feng, L. Bai, M. Yang, W. Yang, Exploring Next-Generation Functional Organic Phase Change Composites, Adv. Funct. Mater. 32 (2022) 2200792.
[27] T. Liu, Y. Zhao, Y. Lei, S. Zhao, L. Jiang, J. Wang, X. Fu, J. Lei, Catalyst-free, Reprocessable, Intrinsic Photothermal Phase Change Materials Networks based on Conjugated Oxime Structure, Chem. Eng. J. 450 (2022) 138144.
[28] X. Hu, C. Zhu, B. Quan, M. Sheng, H. Wu, X. Lu, J. Qu, Engineering Robust Multifunctional Composites with Enhanced Electromagnetic Interference Shielding and All-weather Thermal Management Capability via Simple Layer-by-layer Assembly, Chem. Eng. J. 446 (2022) 137423.
[29] J. Wu, M. Wang, L. Dong, J. Shi, M. Ohyama, Y. Kohsaka, C. Zhu, H. Morikawa, A Trimode Thermoregulatory Flexible Fibrous Membrane Designed with Hierarchical Core–Sheath Fiber Structure for Wearable Personal Thermal Management, ACS Nano. 16 (2022) 12801–12812.
[30] S. Gong, X. Sheng, X. Li, M. Sheng, H. Wu, X. Lu, J. Qu, A Multifunctional Flexible Composite Film with Excellent Multi-Source Driven Thermal Management, Electromagnetic Interference Shielding, and Fire Safety Performance, Inspired by a “Brick–Mortar” Sandwich Structure, Adv. Funct. Mater. 32 (2022) 2200570.
[31] J. Wang, X. Ma, J. Zhou, F. Du, C. Teng, Bioinspired, High-Strength, and Flexible MXene/Aramid Fiber for Electromagnetic Interference Shielding Papers with Joule Heating Performance, ACS Nano. 16 (2022) 6700–6711.
[32] K. Sun, H. Dong, Y. Kou, H. Yang, H. Liu, Y. Li, Q. Shi, Flexible Graphene Aerogel-based Phase Change Film for Solar-thermal Energy Conversion and Storage in Personal Thermal Management Applications, Chem. Eng. J. 419 (2021) 129637.
[33] S. Xiang, J. Tang, L. Yang, Y. Guo, Z. Zhao, W. Zhang, Deep Learning-enabled Real-time Personal Handwriting Electronic Skin with Dynamic Thermoregulating Ability, Npj Flex Electron. 6 (2022) 59.
[34] X. Ji, Y. Jiang, T. Liu, S. Lin, A. Du, MXene Aerogel-based Phase Change Film for Synergistic Thermal Management Inspired by Antifreeze Beetles, Cell Reports Physical Science. 3 (2022) 100815.
[35] Y. Wang, H.-K. Peng, T.-T. Li, B.-C. Shiu, H.-T. Ren, X. Zhang, C.-W. Lou, J.-H. Lin, MXene-Coated Conductive Composite Film with Ultrathin, Flexible, Self-cleaning for High-Performance Electromagnetic Interference Shielding, Chem. Eng. J. 412 (2021) 128681.
[36] Q. Wang, H. Sheng, Y. Lv, J. Liang, Y. Liu, N. Li, E. Xie, Q. Su, F. Ershad, W. Lan, J. Wang, C. Yu, A Skin-Mountable Hyperthermia Patch Based on Metal Nanofiber Network with High Transparency and Low Resistivity toward Subcutaneous Tumor Treatment, Adv. Funct. Mater. 32 (2022) 2111228.
[37] Z. Wang, Y. Zou, Y. Li, Y. Cheng, Metal-Containing Polydopamine Nanomaterials: Catalysis, Energy, and Theranostics, Small. 16 (2020) 1907042.

[38] W. Wei, P. Zhang, F. Cao, J. Liu, K. Qian, D. Pan, Y. Yao, W. Li, Ultrathin Flexible Electrospun EVA Nanofiber Composite with Electrothermally-driven Shape Memory Effect for Electromagnetic Interference Shielding, Chem. Eng. J. 446 (2022) 137135.

[39] Z. Zeng, F. Jiang, Y. Yue, D. Han, L. Lin, S. Zhao, Y. Zhao, Z. Pan, C. Li, G. Nyström, J. Wang, Flexible and Ultrathin Waterproof Cellular Membranes Based on High-Conjunction Metal-Wrapped Polymer Nanofibers for Electromagnetic Interference Shielding, Adv. Mater. 32 (2020) 1908496.

[40] W. Wang, R. Li, M. Tian, L. Liu, H. Zou, X. Zhao, L. Zhang, Surface Silverized *Meta* -Aramid Fibers Prepared by Bio-inspired Poly(dopamine) Functionalization, ACS Appl. Mater. Interfaces. 5 (2013) 2062–2069.

[41] Y. Liu, K. Ai, L. Lu, Polydopamine and Its Derivative Materials: Synthesis and Promising Applications in Energy, Environmental, and Biomedical Fields, Chem. Rev. 114 (2014) 5057–5115.

[42] D.R. Merkel, C.M. Laursen, C.M. Yakacki, R.A. Rorrer, C.P. Frick, Characterization and mechanical testing of polydopamine-adhered electroless copper films, Surface and Coatings Technology. 331 (2017) 211–220.

[43] J. Li, R. Cheng, Z. Cheng, C. Duan, B. Wang, J. Zeng, J. Xu, X. Tian, H. Chen, W. Gao, K. Chen, Silver-Nanoparticle-Embedded Hybrid Nanopaper with Significant Thermal Conductivity Enhancement, ACS Appl. Mater. Interfaces. 13 (2021) 36171–36181.

[44] B. Gu, X. Huang, F. Qiu, D. Yang, T. Zhang, Laminated Cellulose Hybrid Membranes with Triple Thermal Insulation Functions for Personal Thermal Management Application, ACS Sustainable Chem. Eng. 8 (2020) 15936–15945.

[45] Y. Xiao, Y. He, R. Wang, Y. Lei, J. Yang, X. Qi, Y. Wang, Mussel-inspired Strategy to Construct 3D Silver Nanoparticle Network in Flexible Phase Change Composites with Excellent Thermal Energy Management and Electromagnetic Interference Shielding Capabilities, Composites Part B: Engineering. 239 (2022) 109962.

[46] G.-Z. Yin, A. Marta López, X.-M. Yang, X. Ao, J. Hobson, D.-Y. Wang, Polyrotaxane based Leakage-proof and Injectable Phase Change Materials with High Melting Enthalpy and Adjustable Transition Temperature, Chem. Eng. J. 444 (2022) 136421.

[47] X. Lan, Y. Wang, J. Peng, Y. Si, J. Ren, B. Ding, B. Li, Designing Heat Transfer Pathways for Advanced Thermoregulatory Textiles, Materials Today Physics. 17 (2021) 100342.

[48] J. Chen, Z. Ye, F. Yang, Y. Yin, Plasmonic Nanostructures for Photothermal Conversion, Small Science. 1 (2021) 2000055.

[49] H. Gholami Derami, P. Gupta, K. Weng, A. Seth, R. Gupta, J.R. Silva, B. Raman, S. Singamaneni, Reversible Photothermal Modulation of Electrical Activity of Excitable Cells using Polydopamine Nanoparticles, Adv. Mater. 33 (2021) 2008809.

[50] L. Zhou, Y. Tan, D. Ji, B. Zhu, P. Zhang, J. Xu, Q. Gan, Z. Yu, J. Zhu, Self-assembly of Highly Efficient, Broadband Plasmonic Absorbers for Solar Steam Generation, Sci. Adv. 2 (2016) e1501227.

[51] Z. Liu, X. Liu, S. Huang, P. Pan, J. Chen, G. Liu, G. Gu, Automatically Acquired Broadband Plasmonic-Metamaterial Black Absorber during the Metallic Film-Formation, ACS Appl. Mater. Interfaces. 7 (2015) 4962–4968.

[52] J. Lee, B. Llerena Zambrano, J. Woo, K. Yoon, T. Lee, Recent Advances in 1D Stretchable Electrodes and Devices for Textile and Wearable Electronics: Materials, Fabrications, and

Applications, Adv. Mater. 32 (2020) 1902532.
[53] B. Sun, R.N. McCay, S. Goswami, Y. Xu, C. Zhang, Y. Ling, J. Lin, Z. Yan, Gas-Permeable, Multifunctional On-Skin Electronics Based on Laser-Induced Porous Graphene and Sugar-Templated Elastomer Sponges, Adv. Mater. 30 (2018) 1804327.
[54] Q.-W. Wang, H.-B. Zhang, J. Liu, S. Zhao, X. Xie, L. Liu, R. Yang, N. Koratkar, Z.-Z. Yu, Multifunctional and Water-Resistant MXene-Decorated Polyester Textiles with Outstanding Electromagnetic Interference Shielding and Joule Heating Performances, Adv. Funct. Mater. 29 (2019) 1806819.
[55] X. He, J. Shi, Y. Hao, M. He, J. Cai, X. Qin, L. Wang, J. Yu, Highly Stretchable, Durable, and Breathable Thermoelectric Fabrics for Human Body Energy Harvesting and Sensing, Carbon Energy. 4 (2022) 621–632.
[56] Q. Huang, Z. Zheng, Pathway to Developing Permeable Electronics, ACS Nano. 16 (2022) 15537–15544.
[57] X. He, J. Shi, Y. Hao, L. Wang, X. Qin, J. Yu, PEDOT:PSS/CNT Composites based Ultra-Stretchable Thermoelectrics and Their Application as Strain Sensors, Composites Communications. 27 (2021) 100822.

Tab. 4-1. Comparative performance of the thermal regulatory composites in previous literatures

Components and configuration	Solar heating	Joule heating	Heat energy storage	Porous structure/ Permeability	Ref.
CNT/MXene crosslinking film	77°C, 1 sun	81 °C, 1.8 V	×	×	S1
MXene /HCFG/AgNW film	125 °C, 500mW/cm^2 (NIR)	75 °C 1.6 V	×	×	S2
GNP/PU film	×	63 °C 7 V	×	×	S3
AGr/PEG6000 hydrogel	×	×	143.4J/g	×	S4
PW/PVA hydrogel	×	×	126 J/g	×	S5
PEG4000-derived and BQDO-derived crosslinking polyurethane network	120 °C, 2.16 sun	×	85.2 J/g	×	S6
PW absorbed in MXene/BC@MTMS aerogel	45°C, 1 sun	×	93.5 J/g	×	S7
PEG absorbed in MXene/PI aerogel	78°C, 1 sun	×	167.9 J/g	×	S8
PEG4000 absorbed in a MXene/AgNWs coated textile	60 °C, 1 sun	×	181.1 J/g	×	S9
PW/GNP absorbed in melamine foam decorated with PPy-PODS	65 °C, 1 sun	×	130.6 J/g	×	S10
PVA/MXene/PCCs film	√	84 °C, 2.5 V	136.8 J/g	×	S11
CNF/MXene/PEG film	77°C, 1 sun	50 °C, 10 V	136.1 J/g	×	S12
PP/CNT/PW/EPDM film	40 °C, 1 sun	64 °C, 6 V	103.5 J/g	×	S13
TPU/ CWO@PW fiber (textile)	√	×	90.5 J/g	√	S14
MXene/silk textile	44 °C, 1 sun	60 °C, 10 V	×	√	S15
acrylate polymeric @NPCM membrane	×	×	106.2 J/g	√	S16
PAN@PW membrane	×	×	86.7 J/g	√	S17
PEDOT@CSF textile	×	58 °C, 6 V	×	√	S18
AgNPs@PDA@PU@PW	63 °C	77 °C	101.1 J/g	√	**This**

membrane	1 sun	3.5 V			**work**

HCFG: graphene oxide wrapped hollow carbon fiber; AGr: agarose; PEG: polyethylene glycol; BQDO: p-Benzoquinone dioxime; PW: paraffin wax; PVA: polyvinyl alcohol; BC: bacterial cellulose; MTMS: hydrophobic modifier; PI: polyimide; AgNW: silver nanowire; PPy: polypyrrole; PODS: polymerized octadecylsiloxane; GNP: graphene nanoparticle; PCCs: n-octadecane phase change capsules; CNFs: cellulose nanofibrils; PP: polypropylene; EPDM: ethylene propylene diene monomer; CWO: $Cs_{0.33}WO_3$. NPCM: nano-encapsulated phase change materials; CSF: cotton/spandex fabric

Note: (1) 1 sun: a sunlight-like xenon light radiation of 100 mW/cm^2.

(2) In reference [11], the research demonstrated the solar heating performance of the samples under different radiations, but it didn't record the saturation temperatures.

(3) In reference [14], the NIR absorption ability of the prepared phase change fibers was demonstrated, but the detailed saturation temperature under a specific light irradiation was not investigated.

Reference inTab.4-1

[S1] B. Li, Y. Yang, N. Wu, S. Zhao, H. Jin, G. Wang, X. Li, W. Liu, J. Liu, Z. Zeng, Bicontinuous, High-Strength, and Multifunctional Chemical-Cross-Linked MXene/Superaligned Carbon Nanotube Film, ACS Nano. 16 (2022) 19293–19304.

[S2] Y. Shi, Z. Xiang, L. Cai, F. Pan, Y. Dong, X. Zhu, J. Cheng, H. Jiang, W. Lu, Multi-interface Assembled N-Doped MXene/HCFG/AgNW Films for Wearable Electromagnetic Shielding Devices with Multimodal Energy Conversion and Healthcare Monitoring Performances, ACS Nano. 16 (2022) 7816–7833.

[S3] W. Chen, S. Yang, H. Wang, K. Yang, X. Wu, F. Gao, B. Zheng, K. Qian, W. Yao, T. Zhang, B. Zhong, X. Huang, Flexible, stretchable, waterproof (IPX7) electro-thermal films based on graphite nanoplatelets & polyurethane nanocomposites for wearable heaters, Chem. Eng. J. 431 (2022) 133990.

[S4] Y. Meng, L. Zhang, M. Peng, D. Shen, C. Zhu, S. Qian, J. Liu, Y. Cao, C. Yan, J. Zhou, T. Qian, Developing Thermoregulatory Hydrogel Electrolyte to Overcome Thermal Runaway in Zinc-Ion Batteries, Adv Funct Materials. 32 (2022) 2206653.

[S5] Y.-C. Zhou, J. Yang, L. Bai, R.-Y. Bao, M.-B. Yang, W. Yang, Flexible phase change hydrogels for mid-/low-temperature infrared stealth, Chem. Eng. J. 446 (2022) 137463.

[S6] T. Liu, Y. Zhao, Y. Lei, S. Zhao, L. Jiang, J. Wang, X. Fu, J. Lei, Catalyst-free, reprocessable, intrinsic photothermal phase change materials networks based on conjugated oxime structure, Chem. Eng. J. 450 (2022) 138144.

[S7] X. Ji, Y. Jiang, T. Liu, S. Lin, A. Du, MXene aerogel-based phase change film for synergistic thermal management inspired by antifreeze beetles, Cell Reports Physical Science. 3 (2022) 100815.

[S8] Y. Cao, M. Weng, M.H.H. Mahmoud, A.Y. Elnaggar, L. Zhang, I.H. El Azab, Y. Chen, M. Huang, J. Huang, X. Sheng, Flame-retardant and leakage-proof phase change composites based on MXene/polyimide aerogels toward solar thermal energy harvesting, Adv Compos Hybrid Mater. 5 (2022) 1253–1267.

[S9] X. Liu, J. Miao, Q. Fan, W. Zhang, X. Zuo, M. Tian, S. Zhu, X. Zhang, L. Qu, Smart Textile Based on 3D Stretchable Silver Nanowires/MXene Conductive Networks for Personal Healthcare and Thermal Management, ACS Appl. Mater. Interfaces. 13 (2021) 56607–56619.

[S10] W. Cui, X. Li, X. Li, T. Si, L. Lu, T. Ma, Q. Wang, Thermal performance of modified

melamine foam/graphene/paraffin wax composite phase change materials for solar-thermal energy conversion and storage, Journal of Cleaner Production. 367 (2022) 133031.

[S11] S. Gong, X. Sheng, X. Li, M. Sheng, H. Wu, X. Lu, J. Qu, A Multifunctional Flexible Composite Film with Excellent Multi-Source Driven Thermal Management, Electromagnetic Interference Shielding, and Fire Safety Performance, Inspired by a "Brick–Mortar" Sandwich Structure, Adv Funct Materials. 32 (2022) 2200570.

[S12] J. Zhang, J. Mu, S. Chen, F. Xu, Mechanically strong, flexible, and multi-responsive phase change films with a nacre-mimetic structure for wearable thermal management, Journal of Energy Chemistry. 75 (2022) 229–239.

[S13] X. Hu, C. Zhu, B. Quan, M. Sheng, H. Wu, X. Lu, J. Qu, Engineering robust multifunctional composites with enhanced electromagnetic interference shielding and all-weather thermal management capability via simple layer-by-layer assembly, Chem. Eng. J. 446 (2022) 137423.

[S14] X. Li, Q. Li, J. Hu, R. Li, J. Lin, Y. Liu, Core-sheath phase change fibers via coaxial wet spinning for solar energy active storage, Composites Part B: Engineering. 247 (2022) 110346.

[S15] B. Yan, M. Zhou, X. Liao, P. Wang, Y. Yu, J. Yuan, Q. Wang, Developing a Multifunctional Silk Fabric with Dual-Driven Heating and Rapid Photothermal Antibacterial Abilities Using High-Yield MXene Dispersions, ACS Appl. Mater. Interfaces. 13 (2021) 43414–43425.

[S16] Y. Zhang, T. Li, S. Zhang, L. Jiang, J. Xia, J. Xie, K. Chen, L. Bao, J. Lei, J. Wang, Room-temperature, energy storage textile with multicore-sheath structure obtained via in-situ coaxial electrospinning, Chem. Eng. J. 436 (2022) 135226.

[S17] Z. Liu, Q. Hu, S. Guo, L. Yu, X. Hu, Thermoregulating Separators Based on Phase-Change Materials for Safe Lithium-Ion Batteries, Adv. Mater. 33 (2021) 2008088.

[S18] Y. Cui, Z. Jiang, G. Zheng, W. Wang, M. Zhou, P. Wang, Y. Yu, Q. Wang, Green preparation of PEDOT-based composites with outstanding electrothermal heating and durable rapid-response sensing performance for smart healthcare textiles, Chem. Eng. J. 446 (2022) 137189.

Chapter 5
Conclusion and outlook

Chapter 5: Conclusion and outlook

5.1 Conclusion

The traditional space heating and cooling systems result in huge energy consumption, owning to its inefficient use of energy that regulates the temperature of the entire building space. Currently, the energy crisis stimulates intensive efforts to produce next-generation personal thermal management (PTM) textiles, because PTM strategies emphasize thermal management of human body and its local environment in a more energy-saving manner. Phase change materials (PCMs) capable of absorbing and releasing heat energy are attractive for maintaining a constant temperature in the PTM field. A high thermal management efficiency required that the PCMs can be conformed to the curved surface of human skin, and a permeable structure is adorable for wearing comfort. In this regarding, we use electrospinning to fabricate phase change fibers for personal thermal management, because of the inherent flexibility and permeability of fibrous membrane.

As research continues, we found that the single thermal regulating effect based on phase change property can't meet the thermal regulating needs of long-term, multi-function and multi-scenario. Integrating solar and electric heating with phase change property based on photothermal/electrothermal conversion and energy storage is promising in all-weather, on-demand personal thermal management. Thus, we designed the hierarchical core-sheath fiber structure to assemble various functional materials into single fibers and maintain the porous structure of the whole membrane to ensure wearing comfort.

(1) We presented a green strategy to construct an eco-friendly and degradable micro-nanofibrous membranes with responsive reversal thermal regulation properties via electrospinning and surface crosslinking. Biocompatible and biodegradable polymer PVA and PEG were employed as supporting matrix and functional component, respectively, and toxic organic solvent were excepted from electrospinning process, therefore, the issue of poisonous solvent residue or recovery challenges were also

avoided. Subsequently, glutaraldehyde vapor was grafted or crosslinked on the surface of ultrafine fibers to block hydrophilic groups. The mass ratio of PEG can reach to 55 wt% and realized an optimal melting/freezing enthalpy of 60.1/59.1 J/g, which is comparable to these of toxic solvent-based electrospun membranes. Furthermore, high conductive CNTs were integrated into composite fibers to enhance thermal conductivity by 40.4% than the blank one. Besides, the phase change fibrous membranes possessed excellent tensile elongation of 262%, overcoming the intrinsic brittleness of traditional PCMs, and exhibited remarkable shape tailorability and foldability. Considering the favorable flexibility, breathability and reasonable phase change enthalpy, the resultant phase change fibrous membranes exhibit great potential for further application such as personal thermal management textile and thermal-regulated electric system.

(2) We report a fibrous membrane-based textile with tri-mode thermoregulatory performance that includes reversible temperature-responsive phase change property, solar-heating, and Joule heating effects. The integrated multimodal thermal regulating system is attributed to the cooperation between the intrinsic properties of the employed materials and the delicately designed hierarchical core-sheath fiber structure. The favorable thermal storage capability originated from the effective encapsulation of PW through coaxial electrospinning technology, where the plastic elastomer PU, as a protective and supportive shell, assures decent mechanical properties. The introduction of light absorbers of CNTs, PDA, and PEDOT:PSS through various surface modifications achieved a synergistic photothermal conversion, reaching a high saturated temperature of 70.5 °C (1 sun). Owing to the low resistance of PEDOT:PSS, the prepared membrane possessed an favorable electrothermal conversion performance with a high saturated temperature of 73.8 °C (4.2 V). The combination of phase change, solar-heating, and Joule heating effect enables the phase change membrane to be charged by either solar energy or electrical energy, and it provides multiple thermal regulation routes, which presents promising potential for application in wearable personal thermal management.

(3) A breathable and thermoregulating fibrous membrane integrated with photo/electrothermal conversion and energy storage/release performance, was successfully prepared through coaxial electrospinning and PDA-assisted silver deposition technique. The complementary relationship between the solar heating and Joule heating effects could overcome the operational limitations of the intermittent availability of single input energy source (e.g., sunlight or electricity). Furthermore, the dual driving heating performance coupled with the thermal energy storage behavior can relieve the mismatch between the energy supply and demand, and expand the application scenarios. This highly integrated multimodal thermoregulating routes rely on the careful design of the hierarchically ordered coaxial architecture of the fibers, which combines the core PCM, elastic sheath PU, interfacial layer PDA and the outermost layer of AgNPs into an efficient configuration. PDA layer not only facilitates the uniform, dense growth of AgNPs, but also offers an interfacial reinforcement for enhanced mechanical durability of the as-deposited conductive layer. Besides, the porous structure of the pristine phase change membrane is remained, guaranteeing a favorable air permeability and wearing comfort. What's more, the density of the deposited AgNPs can be tuned by controlling the reduction time to customize the light absorbability and electrical conductivity to meet different application requirements. Consequently, the resulting membrane APCF40 achieved the admirable solar-heating effect (up to 63.2 °C at 100 mW/cm^2), and the low voltage-driven Joule heating performance (up to 76.8 °C at 3.5 V), coupled with the thermal energy storage capability with a heat enthalpy of 101.1 J/g. Therefore, the flexible, breathable and synergistic thermoregulating fibrous membrane demonstrates a promising prospect in all-weather, energy saving and personalized thermal management application.

5.2 Outlook

In this work, we designed fibrous membrane-based phase change textile for personal thermal management. We also integrated solar heating and electric heating to the phase change membranes to achieve all-weather personal thermal management through

photo/electro thermal conversion and energy storage. However, some problems need to be optimized and improved:

(1) In chapter 2, although we applied surface crosslinking treatment to improve the water stability of the membrane, and improved their form-stability based on the chemical bonding between PCM chains and supportive polymer chains, the current water stability can not meet the requirement for daily washing. Strong crosslinking will improve the water stability but decrease the heat enthalpy significantly. The trade-off between mechanical property and heat enthalpy is still challenging.

(2) In chapter 3 and 4, we employed coaxial electrospinning to encapsulate the PCMs, but the opened ends of the core-sheath fiber face the leaking threats in long-term using, such as squeezing, pressing and washing. Thus, the membrane edges needed to be sealed in real application for better using stability.

(3) Investigation of smart thermoregulatory textiles under synergistic parameters is required, and the wearability requirements such as washability, breathability, and biocompatibility, as well as the large-scale production capacity of smart thermoregulatory textiles for sustainable development are essential and needed to be taken into consideration.

(4) It is necessary to establish a universally accepted set of criteria for the standardization community to evaluate smart thermoregulatory textiles using various experimental equipment, parameters, and control methods.

(5) In addition, to enhance the thermoregulation capacity of smart thermoregulatory textiles from principles, a multi objective optimization model of heat and mass transfer that could coordinate passive and active thermoregulation strategies in response to microenvironmental and macroenvironmental changes is required.

Published papers

The dissertation based on the following papers:

[1] **Jiajia Wu**, Mingxu Wang, Li Dong, Chunhong Zhu*, Jian Shi, and Hideaki Morikawa*, Ultraflexible, Breathable, and Form-Stable Phase Change Fibrous Membranes by Green Electrospinning for Personal Thermal Management, *ACS Sustainable Chemistry & Engineering*, 2022, 10, 24, 7873-7882.

[2] **Jiajia Wu**, Mingxu Wang, Li Dong, Jian Shi, Masatoshi Ohyama, Yasuhiro Kohsaka, Chunhong Zhu*, and Hideaki Morikawa*, A Trimode Thermoregulatory Flexible Fibrous Membrane Designed with Hierarchical Core–Sheath Fiber Structure for Wearable Personal Thermal Management, *ACS Nano*, 2022, 16, 8, 12801-12812.

[3] **Jiajia Wu**, Mingxu Wang, Li Dong, Yi Zhang, Jian Shi, Masatoshi Ohyama, Yasuhiro Kohsaka, Chunhong*, Hideaki Morikawa*, Highly integrated, breathable, metalized phase change fibrous membranes based on hierarchical coaxial fiber structure for multimodal personal thermal management, *Chemical Engineering Journal*, 2023, 457, 141164.

Conference:

[1] **Jiajia WU**, Chunhong Zhu, Hideaki Morikawa. “Phase change fibrous membranes by electrospinning for personal thermal management”, 2022 Annual Conference of the Textile Society of Japan (June 2022, Tokyo, Japan). (Oral presentation)

Acknowledgments

Over the course of my researching and writing this paper, I would like to express my thanks to all those who have helped me.

First of all, I would like to express my gratitude to my supervisor Prof. Morikawa for his great support on my project. Thanks for giving me the opportunity to study in Japan. In addition to academic guidance, the charming personality of diligence and humility of Prof. Morikawa has deeply affected me and will always encourage me in future. Then, I would like to thank Prof. Zhu. Thank you for giving me a chance to restart my study three years ago. Thank you for your careful guidance and help. You always push me at the right time, especially when I'm not confident. Besides, I would like to thanks all the administrative and technical teachers in Shinshu university for the help in the study of courses and instrument operation.

I also would like to thank all the people I met in Japan, especially the members of Morikawa & Zhu lab. I'd like to thank Wang Mingxu and Dong Li. We have studied together and gone through the most difficult and happiest times. I'd like to thank Zhang Yi, Cai Yingying for your kindness and warmth. I also would like to thank Yu Yongtao, Yan Jiawei and many other members. Then I'd like to thank Wang hao, Weng kai and Li fang, it's precious to share this journey with you.

At last, I would like to thank my family. Thank you for supporting and believing me at any time. I am so happy and lucky to be surrounded by your love.